

Stromatolite-rimmed thrombolite columns and domes constructed by microstromatolites, calcimicrobes and sponges in late Cambrian biostromes, Texas, USA

JEONG-HYUN LEE*  and ROBERT RIDING†

*Department of Geological Sciences, Chungnam National University, Daejeon, 34134, Korea
(E-mail: jeonghyunlee@cnu.ac.kr)

†Department of Earth and Planetary Sciences, University of Tennessee, Knoxville, TN, 37996, USA

Associate Editor – Ying Zhou

ABSTRACT

Microbial carbonates formed stromatolitic, thrombolitic, dendrolitic and maceriate (mazelike) fabrics in shallow marine Cambrian–Early Ordovician carbonates encircling Laurentia. However, poor preservation often hinders recognition of their specific components. Well-preserved examples of normal shallow marine limestones in the ca 490 Ma upper Cambrian Point Peak Member, Wilberns Formation, central Texas, include stromatolitic cones, steep-sided laminated rimmed columns with grainy interiors, and laminated and maceriate domes. Together these form decimetre to metre-thick biostromes. In these examples, a single component, microstromatolite, on its own or with minor calcimicrobes, creates macroscopic stromatolitic, dendrolitic, thrombolitic and maceriate fabrics. Microstromatolites constructed upward widening stromatolitic cones that developed into columns with laminated rims surrounding slightly depressed interiors. These columns accumulated allochthonous sediment by a ‘bucket effect’. Their interiors contain either clusters of dendrolitic microstromatolite or ragged columns of laminated stromatolite–sponge biolithite, and are often characterized by a ‘mottled’ fabric that superficially resembles thrombolite. This mottling was formed by localized dolomitization around millimetric burrows that otherwise do not appear to have significantly influenced the biolithite fabric. Calcimicrobes, including cyanobacteria (*Razumovskia*) and microproblematica (*Renalcis* and *Tarthinia*), impart a mesoscopic clotted appearance to maceriate fabric, and locally to column rims, both of which are dominated by microstromatolite. Similar component-fabric relationships should be recognizable in rimmed columns and domes that were locally abundant elsewhere in Cambrian–Early Ordovician shallow carbonate seas.

Keywords Cambrian, dendrolite, maceriate, microbial carbonate, microstromatolite, stromatolite, thrombolite.

INTRODUCTION

Although small organisms form benthic microbial carbonates, they can create large and diverse sedimentary structures, ranging from domes, columns and cones to sheetlike, branched and maceriate forms (Grey & Awramik, 2020, fig. 14e). These are conventionally subdivided by their internal

structure, evident to the naked eye, variously termed *fabric* (Monty, 1976), *mesostructure* (Kennard & James, 1986; Shapiro, 2000), *mesofabric* (Fagerstrom, 1987) or *macrofabric* (Riding, 1991a, 2000). Widely recognized microbial macrofabric-based categories include stromatolite (laminated), dendrolite (dendritic), thrombolite (clotted) and leiolite (aphanitic) (Riding, 1991a; Riding &

Awramik, 2000; Grey & Awramik, 2020; Shapiro & Wilmeth, 2020). Of these, stromatolite and thrombolite are the more widely reported.

Thrombolites are described from the early (Kah & Grotzinger, 1992; Barlow *et al.*, 2016) and middle (Tang *et al.*, 2013) Proterozoic, and from the early Neoproterozoic (Turner *et al.*, 2000), but are most conspicuous in the late Ediacaran (Grotzinger & James, 2000; Li *et al.*, 2021) and Cambrian (Kennard & James, 1986, fig. 8). The term thrombolite is based on middle and late Cambrian examples (Aitken, 1967). Thrombolites, like stromatolites, are widely regarded as essentially microbial, but there have been persistent suggestions that their diagnostic macro-clotted fabric might also reflect remodelling of precursor fabrics by bioturbation (Walter & Heys, 1985; Glumac & Walker, 1997) and early diagenesis (Planavsky & Ginsburg, 2009; Riding, 2011b; Harwood Theisen & Sumner, 2016; Zhang *et al.*, 2021). These widespread and overlapping effects have tended to confuse not only recognition and interpretation of thrombolites and associated non-laminated microbial fabrics, but also definition of the term thrombolite (Riding, 2000, 2011b). Improved understanding of thrombolites, as well as other microbial carbonates, requires detailed microfabric studies.

This study focuses on well-preserved, and locally well-exposed, upper Cambrian stromatolitic, thrombolitic and dendrolitic fabrics with a long history of research, in the *ca* 490 Ma Point Peak Member of the Wilberns Formation, central Texas, USA (Ahr, 1971; Chafetz, 1973; Portnoy, 1987; Ruppel & Kerans, 1987; Proctor *et al.*, 2019; Khanna *et al.*, 2020a,b; Lehrmann *et al.*, 2020). It is shown herein that microstromatolite – alone or with minor amounts of calcimicrobes – is a key component of stromatolite cones, column rims, column interior dendrolite and maceriate dome fabric. In overall shape, some large circular to elongate Point Peak columns resemble present-day, shallow marine, current moulded Bahamian and Shark Bay columns (Khanna *et al.*, 2020b), but they differ in fabric and often also in the presence of well-developed rims. Point Peak columns could shed light on widely reported late Cambrian examples that, in the field, appear to consist of stromatolitic rims and thrombolitic (mottled or ‘burrowed’) cores (e.g. Pratt & James, 1982, fig. 8a; Griffin, 1988; de Freitas & Mayr, 1995; Lee *et al.*, 2010; Riding, 2011b, fig. 7; Miller *et al.*, 2012, fig. 93; Coulson, 2016; Proctor *et al.*, 2019; Khanna *et al.*, 2020a; Lehrmann *et al.*, 2020, fig. 13c).

GEOLOGICAL SETTING

Late Cambrian of the Llano uplift

Laurentia was located in the tropics during the late Cambrian (Cocks & Torsvik, 2011; Álvaro *et al.*, 2013). Early Palaeozoic flooding – the Sauk transgression (Sloss, 1963) – began in the Ediacaran and continued to the Ordovician (Taylor *et al.*, 2012), reaching the continental interior in the mid–late Cambrian (Peters & Gaines, 2012; Spencer *et al.*, 2014; Alsalem *et al.*, 2018; Karlstrom *et al.*, 2018, 2020). In the Llano Uplift, central Texas, upper Cambrian shallow marine sediments unconformably overlie *ca* 1.4 to 1.0 Ga metamorphic and granitic Grenville rocks (Walker, 1992; Mosher, 1998; Mosher *et al.*, 2008). In the study area, north and west of the Llano Uplift, more than 900 m of Cambrian–Early Ordovician siliciclastic and carbonate sediments, divisible into the Moore Hollow and Ellenburger groups (Cloud *et al.*, 1945; Crowley & Hendricks, 1945; Bridge *et al.*, 1947; Cloud & Barnes, 1948; Ross, 1976; Barnes & Bell, 1977; Ruppel & Kerans, 1987; Kerans, 1990; Loucks, 2003; Morgan, 2012; Miller *et al.*, 2012), continue north and north-eastward into the mainly peritidal Arbuckle Group (Donovan & Ragland, 1986; Fritz *et al.*, 2012) of Oklahoma. The Cambrian–Ordovician boundary is located in the uppermost part of the Moore Hollow Group (Barnes & Bell, 1977; Miller *et al.*, 2012) (Figs 1 and 2). The Moore Hollow Group is divided into the lower, more siliciclastic, Riley Formation and the upper, more carbonate, Wilberns Formation (Barnes & Bell, 1977). In central Texas, the Wilberns is divided into the Welge, Morgan Creek, Point Peak and San Saba members (Dake & Bridge, 1932; Romberg & Barnes, 1944; Bridge *et al.*, 1947; Barnes & Bell, 1977) (Fig. 2). Overall, the Wilberns thins northward from *ca* 180 m in the Honey Creek area to *ca* 150 m near San Saba Bridge (see *Localities*, below, and Appendix S1).

Microbial carbonates

In the first detailed study of Wilberns stromatolites and thrombolites, Ahr (1971) described examples south of the Llano River in southern Mason County and part of northern Gillespie County. Ahr (1971) recognized dendritic, digitate and clotted microfibrils, and identified *Girvanella*, together with *Renalcis*, as their main components. Chafetz (1973) compared clotted

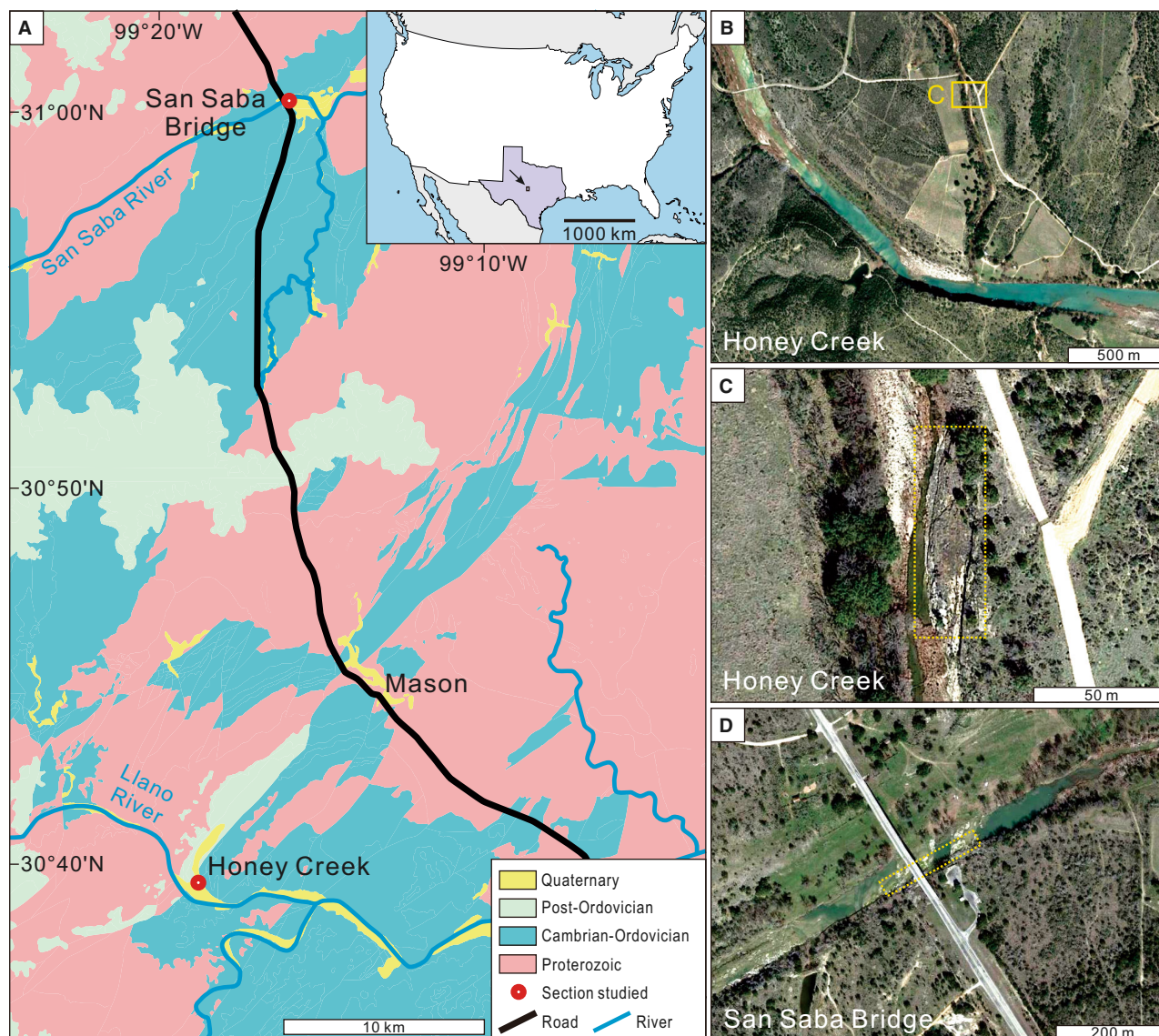


Fig. 1. (A) Geological map of the study area, adapted from USGS map (<https://txpub.usgs.gov/txgeology/>), showing Honey Creek and San Saba Bridge sections. Inset shows location in central Texas, USA. (B) General location of Honey Creek section, 1 km north of the Llano River. (C) Detail of (B) showing the area studied (outlined) immediately east of Honey Creek. (D) San Saba Bridge section, showing the outcrop (outlined) on the southern bank of the San Saba River at the Highway 87 bridge. (B) to (D) from Google Maps.

micritic stromatolitic mounds, associated with tidal channels and edgewise conglomerates in the Morgan Creek Member along the Pedernales River near Johnson City, Texas, with present-day stromatolite reefs at Shark Bay, Australia. Ruppel & Kerans (1987, p. 19) suggested that stromatolitic bioherms, at their Stop 4 on the Llano River, had up to 5 m of primary synoptic relief. At the San Saba Bridge section, Portnoy (1987, fig. 10) and Ruppel & Kerans (1987, fig. 13) described stromatolitic

biostromes and bioherms associated with carbonate sand channels. At Honey Creek, Portnoy (1987, fig. 26) noted columnar stromatolites in a shallow water grainy environment. Crinoids, bivalves, gastropods, ostracodes, trilobites and conodonts associated with the microbial carbonates at San Saba Bridge and Honey Creek indicate normal marine conditions (Portnoy, 1987, p. 109, 119). Johns *et al.* (2007) reported the lithistid sponge *Wilbernicyathus donegani* Wilson, 1950 from “sponge-microbial and

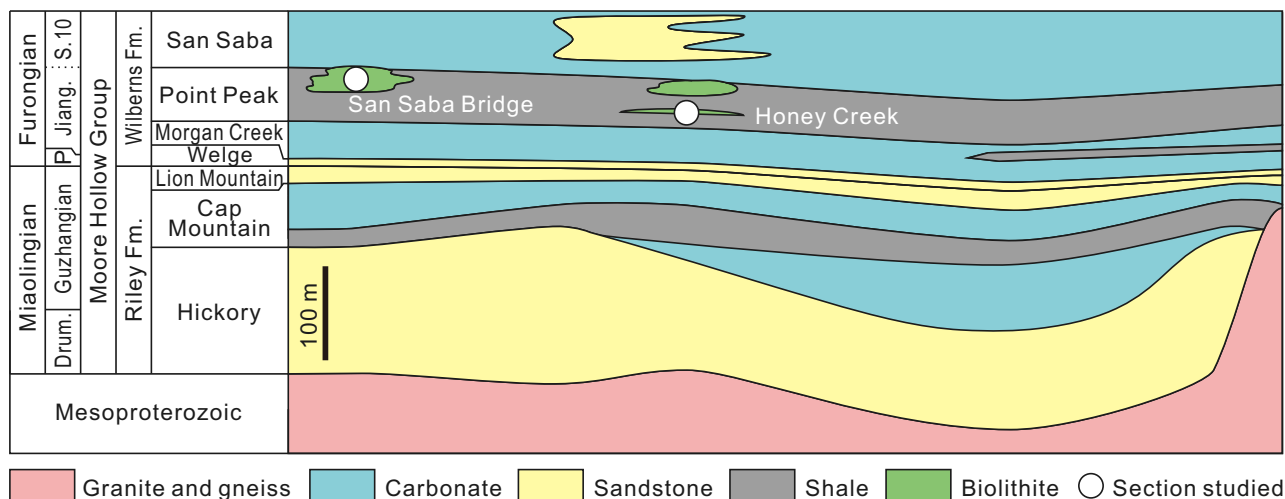


Fig. 2. Schematic stratigraphy of Cambrian sedimentary units overlying Proterozoic igneous and metamorphic rocks in Mason and adjacent counties, central Texas (modified after Barnes & Bell, 1977, fig. 1; Miller *et al.*, 2012). Biolithite units (green) within the Point Peak Member were studied at Honey Creek and San Saba Bridge (white circles). Section shown is approximately 450 m thick and 75 km from west–east. Drum., Drumian; P., Paibian; Jiang., Jiangshanian; S.10, Series 10.

stromatolitic reefs” that include the San Saba Bridge locality (CSS in Johns *et al.*, 2007, fig. 1, although they regarded this as within the San Saba rather than the Point Peak Member), and noted its close association with calcimicrobes.

A series of significant studies (Proctor *et al.*, 2019; Khanna *et al.*, 2020a,b; Lehrmann *et al.*, 2020) documented details of the facies, sedimentation and micromorphology of Point Peak carbonates in outcrops along the Llano River, Mill Creek and James River, 1 to 3 km south-east of the Honey Creek section in southern Mason County. They suggested tidal influence and morphological comparisons with Exuma and Shark Bay stromatolites. Detailed mapping of extensive river cliff and pavement exposures (Khanna *et al.*, 2020a,b; Lehrmann *et al.*, 2020) revealed the morphological architecture and spatial distribution of Point Peak microbial buildups and their key components, including calcimicrobes (*Girvanella*, *Epiphyton* and *Renalcis*) and the lithistid sponge *Wilbernicyathus*, together with mesoscale stromatolite, leiolite and thrombolite fabrics, and macroscale microbial mounds encapsulated by stromatolitic or micritic rinds.

LOCALITIES

This study examined *ca* 490 Ma microbial carbonates in the upper Cambrian Point Peak Member of the Wilberns Formation west of the Llano

Uplift in central Texas at two locations: (i) Honey Creek (Mason County, Texas) (not to be confused with Honey Creek, Llano County, *ca* 18 km south-east of Llano, Texas); and (ii) San Saba Bridge section at Highway 87 bridge on the San Saba River north of Camp San Saba (McCulloch County, Texas) (Fig. 1).

Honey Creek

Stream section 13 km south-west of Mason, 1 km east of White’s Crossing, and 1 km north of the classic bioherm at the top of the Point Peak Shale Member in the southern cliff of the Llano River (Cloud & Barnes, 1948, pl. 19a; Ahr, 1971, fig. 1a; Khanna *et al.*, 2020a, fig. 5) (30°39′28″N 99°18′47″W). In 2020, a subhorizontal *ca* 3 m thick succession *ca* 20 m east–west and *ca* 100 m north–south could be observed in outcrop along the eastern side of Honey Creek. The stratigraphically lower part of the section, nearest the creek, contains thin beds with cones, domes and rimmed columns. These are overlain by coarse carbonates that form a broad limestone pavement, overlain to the east by a low cliff of first shaly and then well-bedded limestones with thin laterally connected metre-scale lenticular bioherms.

San Saba Bridge

Section on the southern bank of the San Saba River at the Highway 87 bridge (31°00′14″N

99°16'9"W), 2 km north-west of Camp San Saba Cemetery, and ca 28 km north of Mason, Texas (Fig. 1). In 2020, from the bridge, the outcrop extended ca 100+ m both WSW and NNE along the shoreline and, depending on seasonal water level, for similar distances in the riverbed. Sub-horizontal bedding plane surfaces display ca 5 m of microbial biostrome complexes and associated carbonates (Ruppel & Kerans, 1987, fig. 13). At this location, Portnoy (1987, figs 10, 11) recognized eight thin carbonate units with a total thickness of 5.4 m. From base to top these are: SS1 (domal stromatolites, 0.5 m +); SS2 to SS4 (mounds with laterally equivalent packstones, 2 m); SS5 (stromatolites, 1 m); SS6 (wackestone, 0.4 m); SS7 (stromatolites, 2 m +); and SS8 (calcareous arenite). Portnoy (1987) considered the base of SS5 to be unconformable. The present work refers to the units SS2 to SS4 of Portnoy (1987) as the Lower Biostrome and laterally equivalent packstones, and to the immediately overlying Unit SS5 as the Upper Biostrome. These respectively conform to the lower and upper units discerned by Ruppel & Kerans (1987, fig. 13). Other units of Portnoy (1987) were not observed. The ca 2 m of Lower Biostrome contains aligned rimmed columns that are either juxtaposed or separated by narrow interspaces containing burrowed sediment. Beneath the bridge, this succession is sharply overlain by the ca 1 m thick Upper Biostrome which consists of low domes, each ca 50 cm across and 30 cm thick.

In addition to Portnoy (1987) and Ruppel & Kerans (1987), stromatolite mounds in this vicinity were reported by Comstock (1889, p. 301) and Dake & Bridge (1932, p. 726–727) (see Appendix S1). This section was also described by Cloud & Barnes (1948, p. 136, 146–147), mentioned by Johns *et al.* (2007), and figured by Shapiro & Awramik (2000, fig. 2a) and Rowland & Shapiro (2002, fig. 7b).

Overall stratigraphic correlation and age

The Honey Creek section is regarded as being within the Point Peak Member (<https://txpub.usgs.gov/txgeology/>), and the biostrome complex exposed at the San Saba Bridge locality as top-most Point Peak Member (Cloud & Barnes, 1948, p. 136), consistent with correlation of these areas by Cloud & Barnes (1948, pl. 14). In this assessment, the Honey Creek section occurs in the middle Point Peak Member, whereas both the Llano River bioherms (e.g. Barnes & Bell,

1977; Khanna *et al.*, 2020a) and the San Saba Bridge/Camp San Saba biostrome complex are stratigraphically correlative with one another, near the top of the Point Peak Member (see Appendix S1) (Fig. 2).

Late Cambrian stratigraphy continues to develop (Geyer, 2019; Peng *et al.*, 2020). According to Johns *et al.* (2007, figs 1, 2), the San Saba Bridge locality is within the lower part of the *Saukia* (trilobite) Zone. According to Miller *et al.* (2012, fig. 5) the middle part of the Point Peak Member (which likely includes the Honey Creek section) belongs to the *Ellipsocephaloides* (trilobite) Zone, immediately prior to the *Saukia* Zone. According to Peng *et al.* (2020, fig. 12.2) the *Ellipsocephaloides* Zone is ca 493 to 492 Ma (mid-Jiangshanian) and the lower part of the *Saukia* Zone is ca 492 to 491 Ma (late Jiangshanian), or possibly earliest Age 10 (ca 491–490 Ma). On this basis, both the Honey Creek and San Saba Bridge localities appear to be within the ca 493 to 490 Ma (mid-Furongian, latest Cambrian) age range, with the Honey Creek section being the slightly older of the two (Fig. 2).

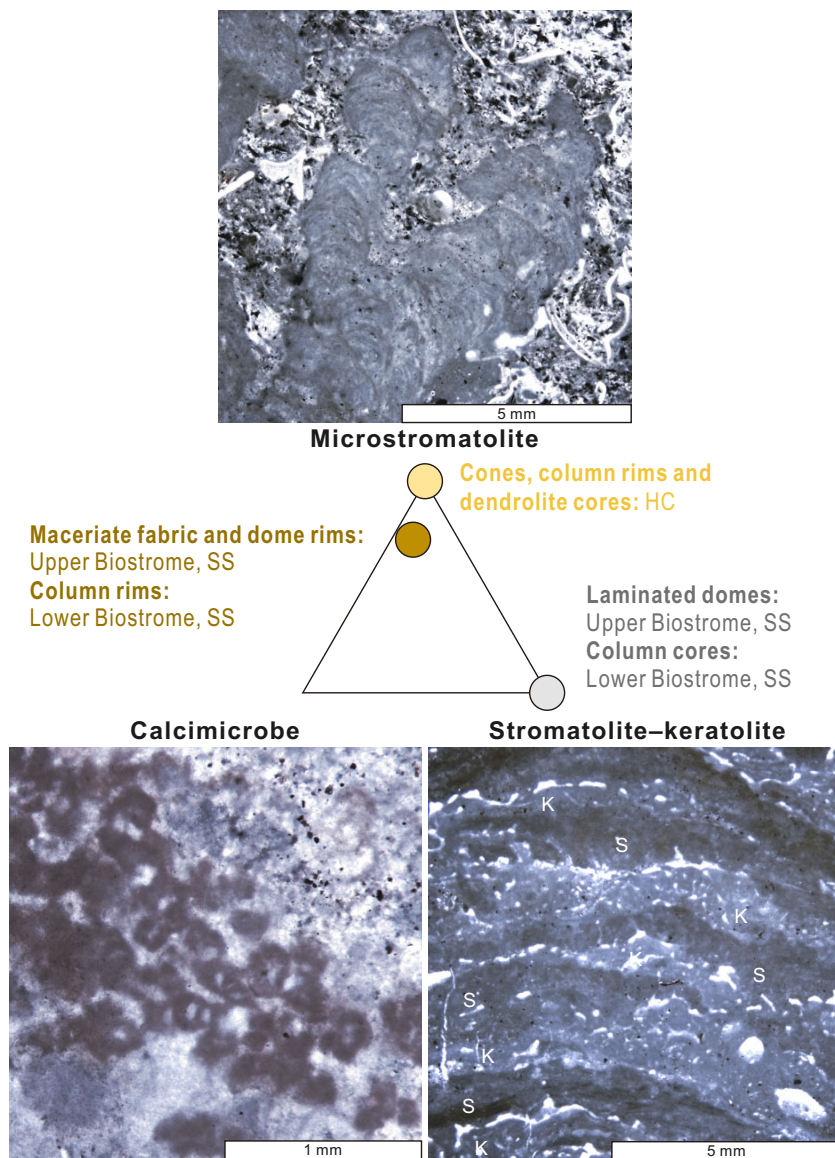
LITHOLOGICAL DESCRIPTIONS

Components

In our samples, the main components of Point Peak column rims and cores are microstromatolite, together with calcimicrobes (*Razumovskia*, *Renalcis* and *Tarthinia*) and stromatolite–keratolite (Fig. 3). Lithistid sponges are locally present. Matrix between and within columns includes bioclasts, for example, trilobites, brachiopods, crinoids, gastropods, sponge spicules (mostly monaxon), small reworked flakes that include *Razumovskia* fragments, as well as glauconite and minor quartz.

Microstromatolite

Microstromatolite is the key component of the rims of Honey Creek and San Saba Bridge Lower Biostrome columns (Fig. 3). It also forms Honey Creek cones, as well as column interior dendrolite, and dominates Upper Biostrome macerate structure. Individual microstromatolites are layered, fine-grained, sub-centimetric columns with parallel or upward-widening sides, and a width to height ratio ranging 3:1 to 1:3. Margins of adjacent microstromatolites often appear diffuse, but are distinct when surrounded by matrix. Occasionally, microstromatolite growth



is locally delimited by trilobite fragments, and sub-millimetric microcavities can occur between microstromatolite columns. Microstromatolites often branch and also merge. Vertically elongate microstromatolites are often laterally aligned, and subvertical to horizontal examples can also occur. Microstromatolites commonly consist of thin indistinct laminae that partially or completely envelop the microstromatolite column, being vertical to overhanging on column margins. Laminae are typically sub-millimetric (*ca* 100 μm thick) fine-grained darker and lighter layers, that appear essentially micritic but can also be irregularly microclotted or very finely peloidal, although this might reflect diagenetic alteration. Microstromatolites only occasionally

contain coarse detrital sediment. Calcimicrobes locally co-occur with microstromatolite.

Calcimicrobes

'Calcimicrobe' (James & Gravestock, 1990, p. 460) is a general term for a variety of microfossils with calcareous walls, common in Cambrian and Early Ordovician biolithites and often of uncertain affinity (e.g. Pratt & James, 1982; Pratt, 1984; Riding & Voronova, 1985). In this usage, they can include *Epiphyton* (Bornemann, 1886), *Nuia* (Maslov, 1954), *Renalcis* (Vologdin, 1932), *Tarthinia* (Drosdova, 1975) and similar taxa (Riding, 1991b, 2001; Zhuravlev, 2001), as well as forms which resemble cyanobacteria such as *Angusticellularia*

(Vologdin, 1962), *Girvanella* (Nicholson & Etheridge, 1878) and *Razumovskia* (Krasnopeeva, 1937). Kennard & James (1986) suggested that Cambrian 'calcareous microbes' may have contributed to the rise of thrombolites. In addition to being common in the Cambrian and Early Ordovician, calcimicrobes recur at intervals until the Early Cretaceous, for example, Silurian, Late Devonian, Early Carboniferous, Permian–Triassic boundary and Late Jurassic (Sāsāran *et al.*, 2014). Calcimicrobes that are common in our Point Peak samples include the microproblematica *Renalcis* and *Tarthinia* and the cyanobacterium *Razumovskia*. These are mainly minor components within rim-forming microstromatolite at Honey Creek and in the Lower Biostrome, but are also conspicuous, again in microstromatolite, in Upper Biostrome maceriate fabric (Fig. 3) where they are mesoscopically evident in slabs and thin-sections as small areas of clotted fabric.

Razumovskia, a calcified tubiform microfossil reminiscent of small *Girvanella*, was described from the Lower Cambrian (Botomian) of the Kuznetsky Alatau in southern Siberia (Krasnopeeva, 1937, p. 19; Vologdin, 1939, p. 216). It is characterized by narrow filaments arranged in felted layers and has been suggested to be a calcified cyanobacterium (Luchinina, 1975).

Renalcis, a calcified botryoidal microfossil described from the Lower Cambrian (Toyonian) of the Gorny Altay in southern Siberia (Vologdin, 1932, p. 15) is characterized by clusters of densely micritic thick walled lunate chambers. It has been compared with algae (Vologdin, 1932) and cyanobacteria (Korde, 1958). The authors consider its affinities to be uncertain.

Tarthinia, originally described as a species of *Renalcis*, from the Lower Cambrian (Atdabanian) of western Mongolia (Drosdova, 1975) is distinguished by its very thick and typically diffuse light-coloured microsparitic wall. It has been compared with algae and cyanobacteria (Riding & Voronova, 1985). The authors consider its affinities to be uncertain.

Ahr (1971, fig. 4) recognized *Girvanella*, *Renalcis*, *Nuia* and *Epiphyton* in the Wilberns Formation of the Llano region, but did not specify horizons or locations. At localities south of Honey Creek, Lehrmann *et al.* (2020, fig. 14f, g) identified *Girvanella* and *Tarthinia*. *Epiphyton* reported by Khanna *et al.* (2020a, fig. 11e) may be *Girvanella*. The authors have not observed *Epiphyton* or *Girvanella* in the studied samples.

Stromatolite–keratolite

At San Saba Bridge, thin, irregularly alternating layers of stromatolite and what appears to be keratolite form ragged laminated branching columns in the cores of Lower Biostrome rimmed columns, and laminated domes in the Upper Biostrome. The stromatolite consists of dark grey micrite with crudely laminated, chaotic to microclotted fabric that often contains very fine, sand-sized, orange euhedral dolomite crystals of secondary origin (Fig. 3). Keratolite (defined by Lee & Riding, 2021a) is characterized by a vermiform fabric of thin sparry branching to anastomosing tubules in micritic matrix. Tubules are interpreted as the calcified remains of the originally proteinaceous spongin network of keratosan demosponges, based on size and structural similarities between the three-dimensional arrangement of vermiform fabric and present-day spongin fibres (Luo & Reitner, 2014). The vermiform tubules in our samples show differing degrees of diagenetic enlargement and are *ca* 20 to 40 µm wide and 100 to 500 µm long (Fig. 3). Although these fabrics are often not distinct in our samples, anastomose tubules of relatively uniform thickness and with delimited distribution, characteristic of keratolite (Lee & Riding, 2021a, 2022; Luo *et al.*, 2022), are locally evident (see *Sponges*, below).

Other invertebrates

Johns *et al.* (2007) reported the lithistid sponge *Wilbernicyathus* from San Saba Bridge. In the Lower Biostrome at this locality numerous cone-like, tube-like, plate-like and bowl-like structures filled with spar cement that appear to be lithistid sponges were observed, together with a poorly preserved example identifiable as *Wilbernicyathus* (see *Lower Biostrome Unit*, below). Crinoid stem fragments are locally common in the surrounding sediments, but have not been observed in the columns.

Grains

At Honey Creek, the main grain components are fine to coarse sand-size bioclasts of trilobites, brachiopods, gastropods and echinoderms, together with abundant glauconite and minor quartz, forming packstone and grainstone. These sediments, which overlie and underlie the biostromes and occupy intercolumn spaces, are locally crudely cross-laminated and also dolomitized. At San Saba Bridge, the matrix composition ranges from bioclastic wackestone with

abundant sponge spicules (mostly monaxons) and trilobite/gastropod fragments, to grainstone with micritic flakes. Some of the micritic flakes could be poorly preserved *Razumovskia*. These fabrics in general are commonly bioturbated.

Rimmed microbial columns and biostromes

Honey Creek locality

Thin biostromes exposed on the eastern bank of Honey Creek (Fig. 4) contain two types of microbial carbonate column:

1 Cones: Narrow rimless steep-sided stromatolite columns that are circular in plan, with inverted conical bases and convex-up lamination, up to 50 cm (typically 5–10 cm) wide, and separated by narrow (*ca* 5 cm wide) interspaces filled by bioclastic grainstone (Fig. 4C and D).

2 Rimmed Columns: Drum-like columns, mostly 10 to 60 cm in diameter, each with distinct pale grey laminated rims typically 2 to 5 cm thick, around complex mottled cores with centimetric clusters of dendritic biolithite, in coarse, mostly bioclastic (for example, trilobite), light brown, matrix with abundant glauconite (Figs 4B, 4E and 5A to C). In plan view, column interior dendrolite fabric resembles thrombolite and can form rounded and invaginated lobate patterns within the associated wackestone–packstone matrix (Fig. 4G and H).

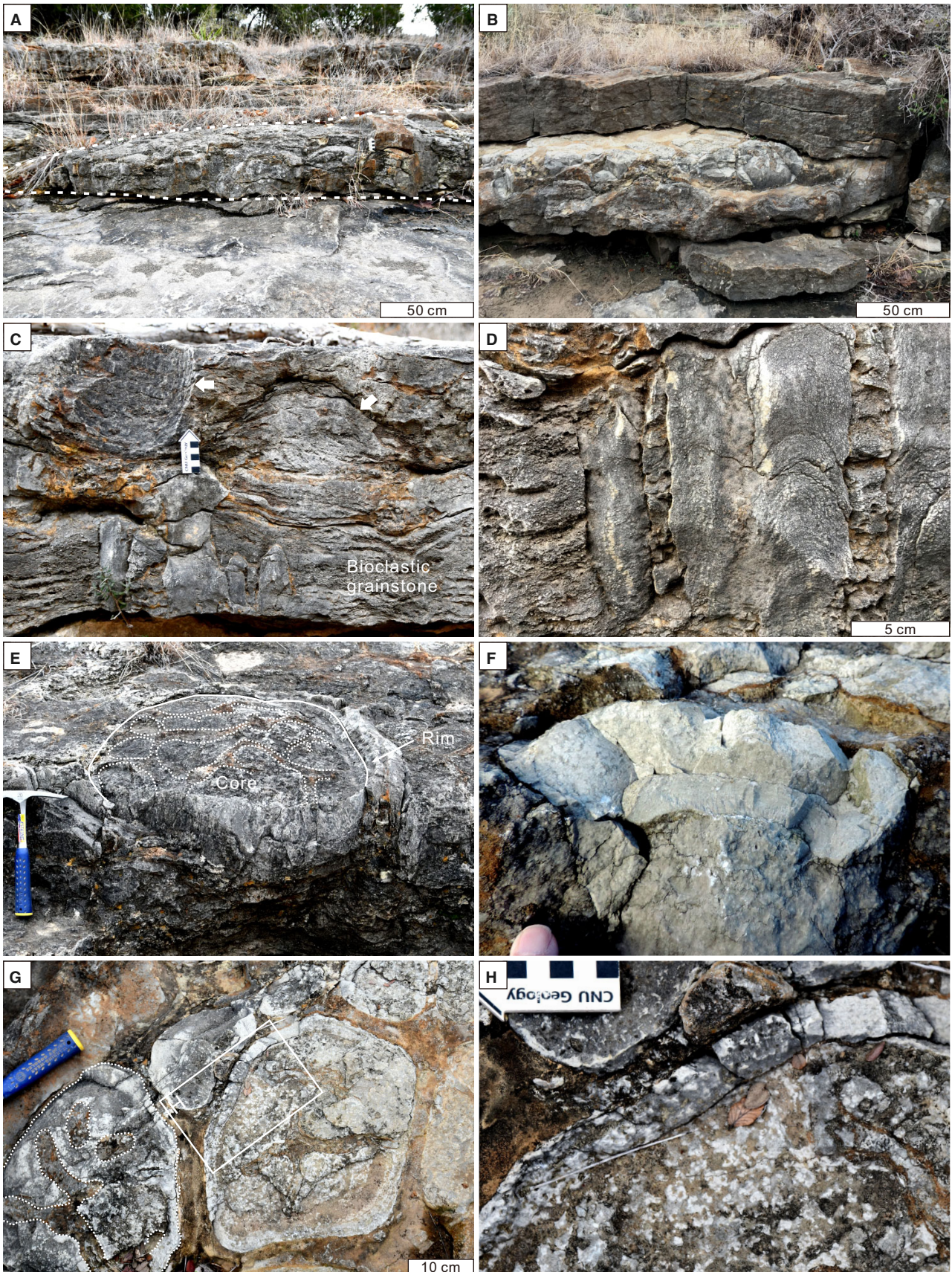
Cones and rimmed columns both form low-relief biostromes in moderately coarse matrix that are up to *ca* 60 cm thick, and at least several tens of metres in lateral extent, underlain and overlain by bedded coarse glauconitic bioclastic packstone–grainstones (Figs 4A, 4B and 6H). Elsewhere, flat pebble conglomerate substrates have been noted (Ahr, 1971; Khanna *et al.*, 2020a; Lehrmann *et al.*, 2020). The larger drum-shaped columns in these biostromes are

either mutually juxtaposed (Fig. 4B and E) or separated by thin grainstone fills (Fig. 4G and H). Similar, probably approximately coeval, rimmed columns with identical thrombolitic fabrics occur in the lower Point Peak Member at the Shepard Pavement section on the Llano River, *ca* 2 km south-east of the Honey Creek section (Lehrmann *et al.*, 2020, fig. 12c–e). Stromatolite–keratolite and calcimicrobes, which are common at San Saba Bridge, have not been observed in Honey Creek cones and columns which, apart from grainy fill sediment, appear to be exclusively dominated by microstromatolite (Fig. 6). Individual microstromatolites range in shape from tall and narrow to short and stubby (Fig. 6). Mutual orientation of microstromatolites gives column bases and rims a macroscopic layered appearance, that is steep at the margins and low domical in the interior (Fig. 5D and E). Juxtaposed laterally aligned microstromatolites form convex-up layers at the bases of the columns. The column interiors exhibit a vertically dendritic (dendrolite) fabric consisting of digitate microstromatolite clusters surrounded by bioclastic matrix (Fig. 5A and C). This has a clotted (thrombolite) appearance in plan view (Fig. 4H). In contrast, the column margins have macroscale laminated (stromatolite) fabric produced by innumerable densely packed subvertical microstromatolites arranged in steeply angled layers (Figs 5B, 5D, 5E, 6B and 6C). Consequently, the microstromatolite rims of these columns have a mesoscopic stromatolite fabric, whereas microstromatolite clusters surrounded by matrix within the column interior are dendritic (dendrolite) in vertical section and clotted (thrombolite) in plan view.

San Saba Bridge locality

At this well-exposed section along the south bank of the San Saba River, large steep-sided

Fig. 4. Honey Creek section. Views (A) to (F) are to the east; (G) and (H) from above. (A) Columns forming thin biostrome (outlined) that tapers to the left. (B) Biostrome of drum-shaped columns with planar tops, underlain and overlain by crudely cross-stratified glauconitic bioclastic packstone–grainstone. (C) Small stromatolite cones (bottom) and larger rimmed columns (top, arrowed), in bioclastic grainstone. (D) Steep-sided stromatolite cones/columns composed of microstromatolite layers with convex-up lamination, in coarse bioclastic grainstone. (E) Drum-like column with narrow microstromatolite rim (inner boundary indicated by a solid line) and a core patterned by dendrolite clusters (dotted outlines) in grainy matrix. (F) Upward expanding biolithite column core showing thickly layered dendrolitic microfabric formed by microstromatolites. (G) Drum-like ovoid and rounded polygonal columns in plan view, showing ‘fitted’ outlines, narrow rims, and internal lobate patterning (dotted lines, lower left) formed by microstromatolite biolithite in grainy matrix. (H) Detail of (G), showing column rim enclosing thrombolite core in plan view, produced by cross-sections of dendrolite. Centimetre scale in (C) and (H). Hammer in (E) is 28 cm long.



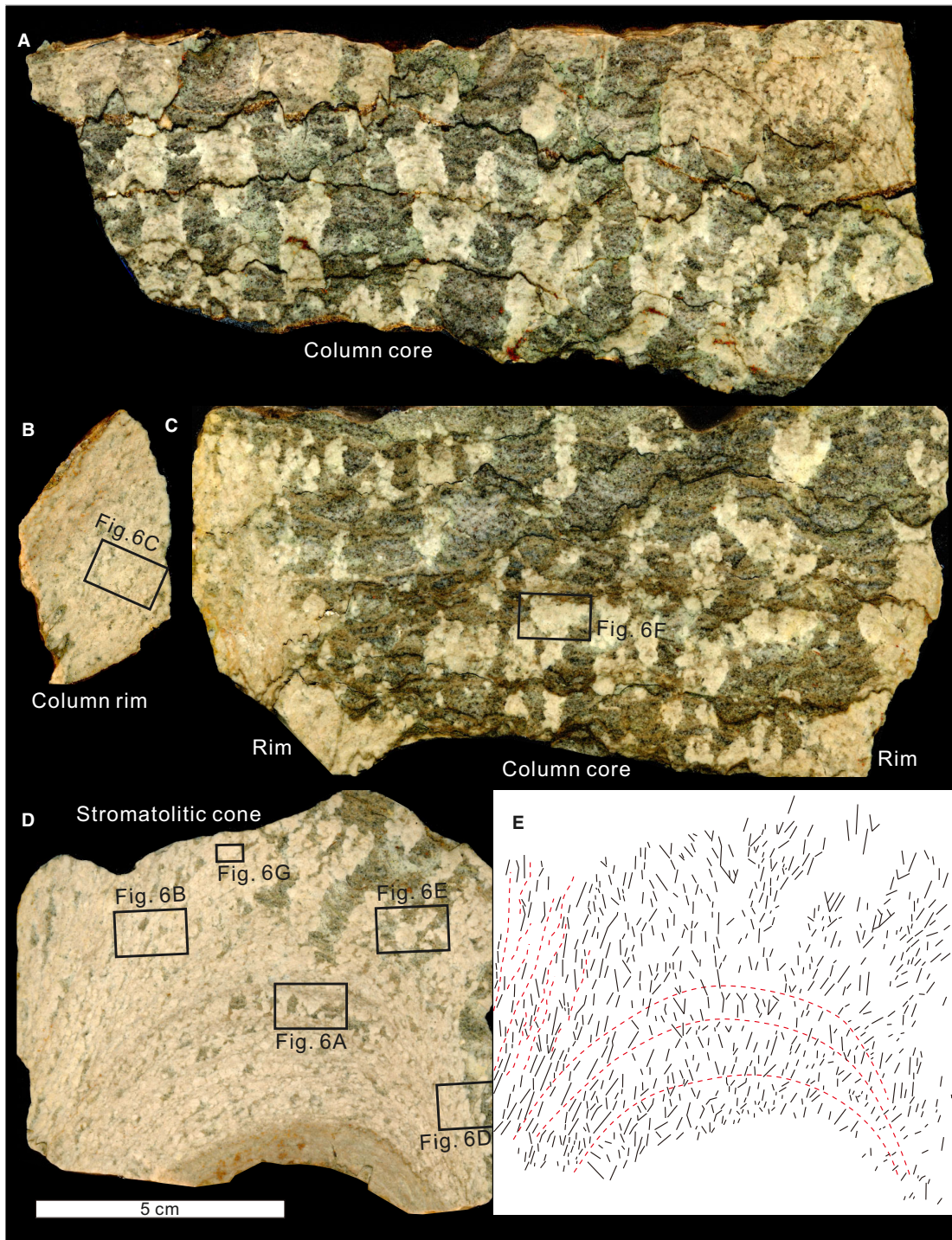


Fig. 5. Honey Creek microstromatolite cones and rimmed columns in vertical slabs. (A) Interior of rimmed column with pale microstromatolite dendrolite in dark poorly sorted grainy matrix. (B) Microstromatolite column rim with crude sub-vertical lamination. (C) Section through a small rimmed column showing stromatolitic rims (formed by microstromatolite) on either side, and interior dendrolite (also formed by microstromatolite) in grainy matrix. (D) Lower part of stromatolite cone with pale-coloured laminated microstromatolite fabric becoming dendrolitic upward by admixture with dark grainy matrix. Macrolamination is visible towards the lower left. (E) Sketch of (D), each small line shows the growth direction of an individual microstromatolite; red dashed lines indicate macrolamination.

rimmed columns form a 2 m thick Lower Biostrome Unit (Figs 7 and 8). A 20 m wide channel (Portnoy, 1987; Ruppel & Kerans, 1987) between the biostromes east of the bridge contains bioclastic wackestone (Fig. 7A), locally traversed by horizontal *Palaeophycus*-like burrows with passive infill that are up to 1 cm wide and more than 20 cm long (Fig. 7B). The Lower Biostrome Unit is irregularly overlain by the 1 m thick Upper Biostrome Unit consisting of lenticular low-relief rimless domes, each up to 50 cm wide and *ca* 30 cm high.

The Lower Biostrome Unit consists of elongate to sinuous, locally conjoined, rimmed steep-sided columns, up to 60 cm wide, 1.5 m or more long, and at least 1 m high, narrowly separated by moderately coarse matrix (Fig. 8). Each column possesses a well-defined grey-coloured laminated rim (2–8 cm wide) (Figs 8A to 8E and 9A) that can be locally complex, thick and invaginated due to coalescence of adjacent columns (Fig. 9B). Tangential vertical sections of the margins can produce cone-like stromatolitic appearance (Fig. 8G). In slabs and thin-sections, the main rim components are dense associations of microstromatolite and calcimicrobes (for example, *Tarthinia* and *Razumovskia*), almost devoid of detrital sediment (Figs 10 and 11C to E). In vertical section, column interiors contain ragged irregular to slightly sinuous, crudely layered grey cores of interlayered stromatolite–keratolite (Figs 8G, 8H, 9E, 10A, 12 and 13A to C) in a mottled matrix of grey bioclastic wackestone and orange dolomite (Figs 12, 13D and 13E). In transverse section, these macrofabrics create distinctive mottled to polygonal netlike patterns (Figs 8B to 8D, 9C, 12 and 13). Stromatolite fabric appears to have been more prone to dolomitization than keratolite (Figs 12B and 13A to C), and orange patches of preferentially dolomitized poorly sorted bioclastic grainstone (*Razumovskia* flakes, trilobite fragments and monaxon sponge spicules) are also common within the matrix (Fig. 13D and E). Very small horizontal to subhorizontal spar-filled burrows (<1 mm in diameter and up to 10 mm long) in the matrix are often surrounded by zones of orange dolomite, up to three times wider than the burrow diameter (see also *Upper Biostrome*) (Fig. 13D). Similar burrows have been figured from Mill Creek by Lehrmann *et al.* (2020, fig. 14d). This patchy dolomitization contributes to colouration that complicates the appearance of column interiors in plan view (Fig. 12A).

Margins of adjacent columns locally merge, creating complex interlocking invaginated patterns in plan view (Fig. 9B). In addition, columns separated by bioturbated muddy matrix are locally connected by bridges that appear to be composed of column-rim material (Fig. 9A). Thin tube-shaped to cone-shaped sparry fossils, probably including the lithistid sponge *Wilberniocyathus*, locally occur in column interiors and rarely in column margins (Johns *et al.*, 2007) (Figs 8G, 9C, 9E, 9F, 11F and 13F). Column tops were sometimes capped by stromatolite overgrowth (Fig. 9D). The authors have not observed the bases of Lower Biostrome columns. Column elongation can exhibit generally north-east/south-west orientation (Portnoy, 1987; Ruppel & Kerans, 1987, fig. 13) (Fig. 8A), indicating sustained wave and current influence.

The Upper Biostrome Unit contains closely spaced low-relief grey domes, 20 to 100 cm wide (Fig. 14B and C), and appears to disconformably overlie the Lower Biostrome Unit (Fig. 14A and B). In contrast to the tall columns separated by grain-filled interspaces that characterize the Lower Biostrome, the Upper Biostrome is relatively grain-poor and the domes consist either of: (i) convex-up laminated stromatolite–keratolite fabric (Figs 15 and 16); or (ii) ragged *ca* 1 to 3 cm wide columns of irregularly branching macerate fabric (Figs 17 and 18).

In slabs (Fig. 15B) and thin sections (Fig. 16A), the convex-up laminated fabric consists of stromatolite–keratolite, similar to that in the Lower Biostrome (Figs 11A and 13A to C) but with less dolomitization, and the stromatolitic fabric consists of crudely layered, grumous, dark-coloured micrite with rare *Razumovskia* (Fig. 16A). Both keratolite and stromatolite layers are laterally discontinuous and variable in thickness. Microstromatolite–calcimicrobe biolithite locally rims the stromatolite–keratolite domes (Figs 15B, 16C and 16D). Wackestone sediment, between domes cored by stromatolite–keratolite and rimmed by microstromatolite–calcimicrobes, contains sponge spicules and trilobite fragments. It often contains burrows that locally have central areas filled by spar cement (Fig. 16B) and resemble those observed in the Lower Biostrome (Fig. 13D). These interstitial grainy fabrics are only slightly dolomitized (Fig. 14B); much less so than in the Lower Biostrome.

Macerate fabric is relatively inconspicuous in the field, but evident in slabs (Fig. 17). It consists of pale pink biolithite at least several

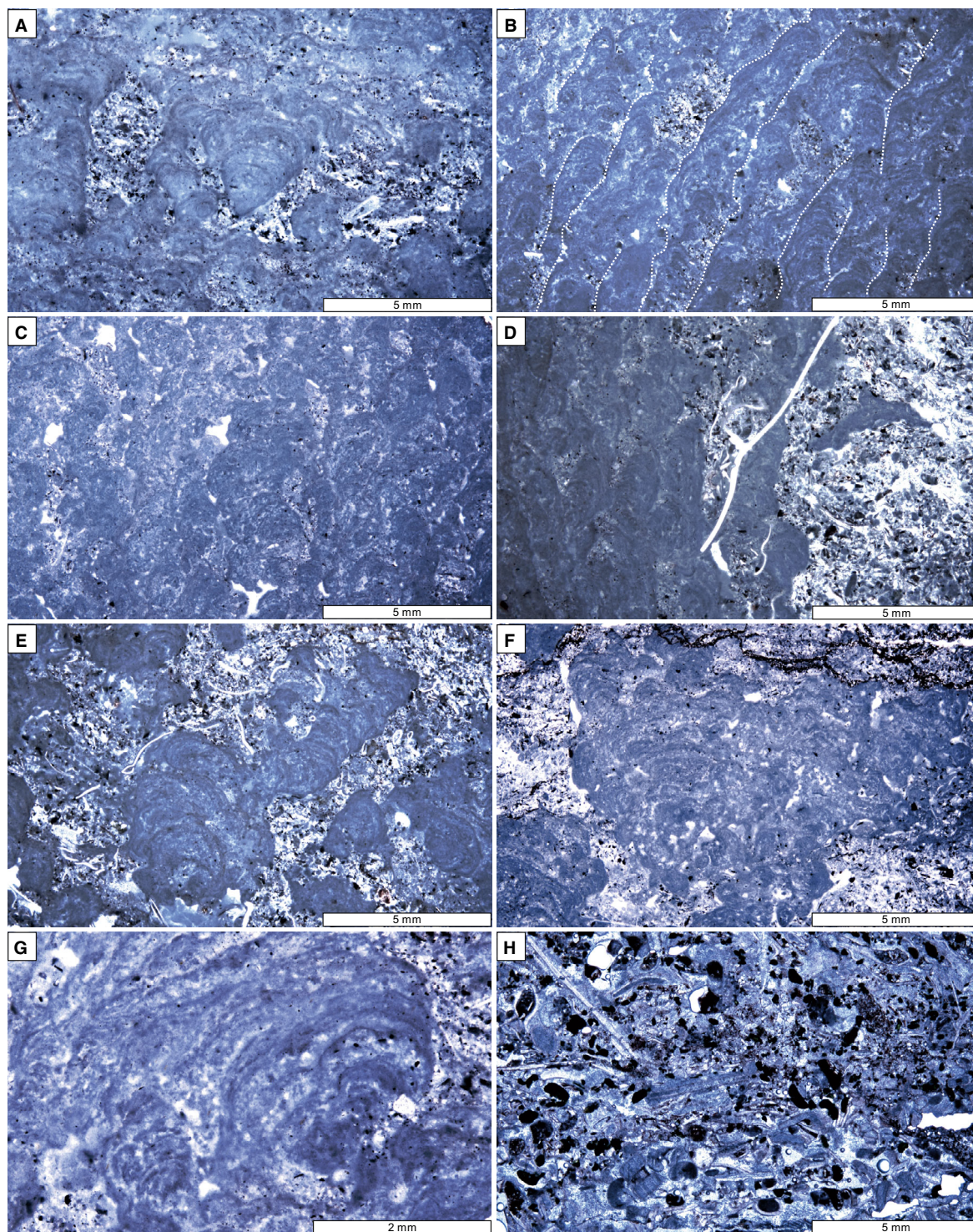


Fig. 6. (A) to (G). Details of the Honey Creek fabrics shown in Fig. 5B to D. (A) Microstromatolite biolithite with grainy interspaces. (B) Steep-sided overlapping (macro)stromatolitic lamination (white dotted lines) formed by mutually encrusting subvertical microstromatolites. (C) Column rim composed almost entirely of microstromatolite with minor spar-filled cavities. (D) Microstromatolite layers (left and centre) incorporating a trilobite fragment (white), beside grain-filled interspace (right). (E) and (F) Irregularly branched and amalgamate microstromatolite dendrolites in bioclastic matrix. (G) Upward amalgamation of unevenly laminated and locally microclotted microstromatolite columns. (H) Glauconitic bioclastic packstone overlying the biostrome.



Fig. 7. (A) San Saba Bridge section from the east, showing grainstone-filled channel traversing the Lower Biostrome. Each span of the bridge is about 25 m in length. (B) *Palaeophycus*-like horizontal burrow systems in channel sediment.

decimetres thick (Fig. 17C to F), composed of light-coloured microstromatolite (Fig. 18A to D) with local clusters of dark-coloured calcimicrobes (*Renalcis* and *Tarthinia*) (Fig. 18E to G) and minor keratolite and *Razumovskia* (Fig. 18B and H). Overall, biolithite (*ca* 80% microstromatolite, *ca* 20% calcimicrobe) occupies *ca* 65 to 75% of the structure. Interspaces between maceriae are occupied by pale yellow wackestone–packstone matrix (*ca* 25–35% of the volume) (Fig. 17C to F).

In vertical section, the maceriae show irregular upward branching and recombination (Fig. 17E and F), and in cross-section are characteristically mazelike (Fig. 17B to D). The microstromatolite framework that forms the maceriae is crudely layered (Fig. 18A to D) and contains conspicuous brownish calcimicrobe clusters (Fig. 18E to G) that locally impart a small-scale clotted appearance. This fabric is similar to that of Lehrmann *et al.* (2020, fig. 14e) from Mill Creek. Overall, the maceriate fabric is a complex centimetric meshwork of subvertical anastomose columns separated by narrow irregular matrix-filled interspaces and does not, in these examples, show diagenetic destruction or enhancement.

Fabric interpretation

Honey Creek

Honey Creek columns commenced as cones, formed by densely layered accumulations of microstromatolites (Figs 19 and 20), colonizing sand-gravel substrates. Low-angle layers at the

bases of cones and columns consist of palisade-like layers of adjacent individual millimetric microstromatolites, whereas high-angle layers forming the column rims consist of subvertical mutually attached microstromatolite (Fig. 5A and B). Consequently, cones and column rims are macroscopically laminated throughout, creating a fabric that can be described as stromatolite composed of mutually aligned microstromatolites (Fig. 20). The authors envisage that, as these microstromatolite cones accreted, their broadening tops became prone to accumulation of allochthonous sediment, whereas rim accretion was relatively unaffected. This is supported by very little evidence of sediment incorporation within the rims (Figs 5B, 5C and 6C). If the rims were slightly elevated, then preferential accumulation of sediment in the column interior could be described as a ‘bucket effect’. The accumulated allochthonous matrix would have progressively surrounded and isolated the microstromatolite clusters, creating a vertically oriented dendrolite fabric of digitate microstromatolite clusters, typically one to a few centimetres in size (Fig. 5A and C). Whereas microstromatolite rims are macroscopically stromatolitic (Fig. 5B), the microstromatolite clusters in column interior matrix are dendrolitic in vertical section (Fig. 5A and C) and – in detail – resemble thrombolite in plan view (Fig. 4G and H). In this way, a single component, microstromatolite, depending on spacing and orientation, could create stromatolite, dendrolite and thrombolite fabrics (Fig. 20).

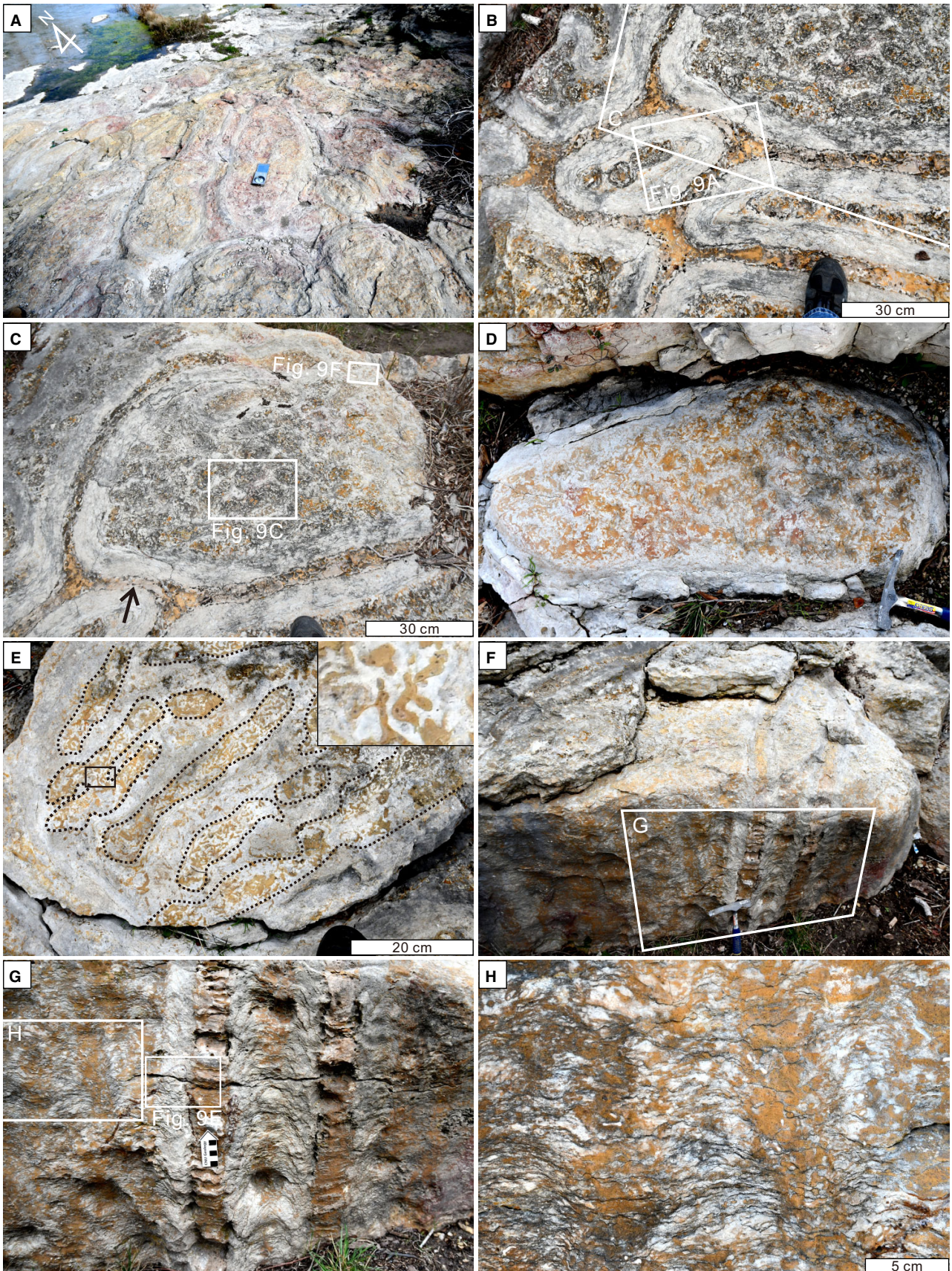


Fig. 8. Lower Biostrome columns, San Saba Bridge section. (A) Juxtaposed north-east/south-west elongate rimmed columns in oblique plan view. Compass is 17.5 cm long. (B) and (C) Closely spaced rimmed columns of various sizes and shapes in plan view, showing net-like patterned interiors. Inter-column bridge material arrowed in (C). (D) Plan view of large rimmed column with netlike interior colour-mottled by orange dolomite. (E) Complex amalgamate rimmed column with elongate interiors (dotted) patterned by tan-coloured burrow systems (inset). (F) Oblique view of wide (to left) and narrower elongate (to right) rimmed columns. (G) Side view of (F) showing vertical section of narrow (centre) rimmed column between broader columns. The centimetre scale is on the narrow interspace between two columns. Tangential section of the laminated rim of the narrow column (centre) has a coniform appearance. Scale in centimetres. (H) Close up of (G), showing ragged crudely layered stromatolite–keratolite and partly dolomitized orange matrix, in the column interior. Hammer head in (D) and (F) is 17 cm long.

These Honey Creek columns developed on grainy, wave-swept substrates in a shallow marine environment. Commonly associated trilobite, and occasional crinoid, fragments suggest normal marine salinity. Essentially rounded, rather than elongate, outlines of the columns in plan view (Fig. 4E and G) suggest multidirectional current activity. The relative thinness of these biostromes (typically <60 cm) (Fig. 4A and B), and apparent lack of lateral column amalgamation, suggests limited upward growth in comparison with larger and often laterally amalgamated Lower Biostrome columns at San Saba Bridge. No column displacement was observed, suggesting firm substrate attachment despite, or perhaps because of, relatively rapid accumulation of grainy substrate that stabilized the bases of these initially narrow columns.

San Saba Bridge, Lower Biostrome

Lower Biostrome columns have microstromatolite rims with some calcimicrobes, and cores of stromatolite–keratolite biolithite in grainy sediment (Fig. 21). The generally well-preserved fabrics show that the distinctively patterned interiors are essentially constructional products of irregular ragged stromatolite–keratolite, together with secondary dolomitic colour patterning. Thick biolithite column margins of dense microstromatolite with minor calcimicrobes suggest persistent exposure to current influence during formation. Although the column bases were not observed, similar examples from the Shepard Pavement section on the Llano River suggest that the mound could have initiated on skeletal grainstone hardgrounds encrusted by eocrinoid holdfasts (Lehrmann *et al.*, 2020, fig. 13a, b). As at Honey Creek, upwardly expanding column rims appear to have accumulated poorly sorted current-borne sediment (skeletal flakestone–wackestone–packstone) in the column interior. The authors envisage that column interior accretion was

mediated by the interaction of *in situ* stromatolite–keratolite biolithite and irregularly distributed current-sourced allochthonous sediment. This created a centimetre/decimetre-scale polygonal netlike pattern in plan view. Small (*ca* 1–2 mm) burrows in these sediments appear to have affected rock colour more than sediment texture, by localizing secondary orange dolomitization that contrasts with the otherwise grey matrix and contributes to an irregular netlike pattern (Figs 8, 12A, 13D and 13E). The mottled appearance of these column interiors therefore likely reflects two effects: (i) primary stromatolite–keratolite arrangement; and (ii) secondary dolomitization localized by very small burrow systems and grainstone patches (Fig. 22). Better preserved layered stromatolite–keratolite dome fabrics in the Upper Biostrome support this interpretation. Overall, however, these diagenetic effects complicate but do not remove the primary patterns of column interior biolithite and matrix.

The relatively large size of San Saba Bridge Lower Biostrome columns may reflect deeper and more offshore conditions than at Honey Creek. Similarly, the presence of calcimicrobes as an additional rim component at San Saba Bridge, albeit minor relative to microstromatolite, as well as keratosan and lithistid sponges, might indicate less stressful conditions with respect to factors such as fluctuations in salinity, temperature and water movement. Although the bases of Lower Biostrome columns have not been observed, the dominant presence of microstromatolites in rim construction suggests, as at Honey Creek, that microstromatolites were substrate colonizers that initiated column formation (Fig. 21). The relatively finer grained intercolumn sediment in comparison to Honey Creek may be due to large, closely clustered, columns that limited sediment sorting. As at Honey Creek, the apparent absence of toppled columns in the Lower Biostrome suggests firm substrate

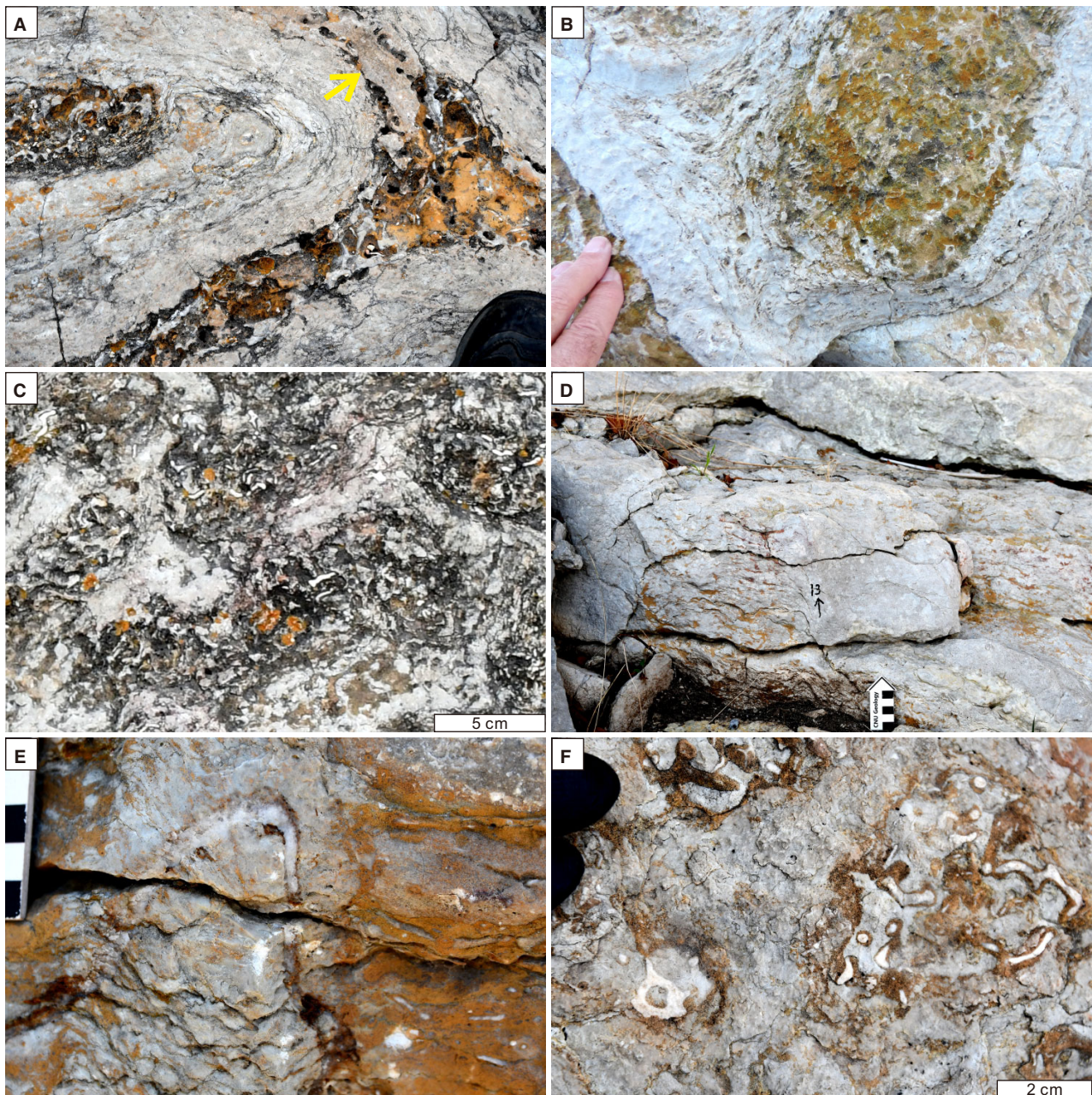


Fig. 9. Lower Biostrome columns and domes, San Saba Bridge section. (A) Plan view of thickly rimmed columns separated by muddy dolomitized matrix with localized biolithite ‘bridge’ (yellow arrow) between adjacent columns. (B) Complex locally thickened rims formed by coalescence of adjacent columns. (C) Netlike pattern of partly dolomitized stromatolite–keratolite column interior in plan view, with numerous small sinuous white skeletons (probably the lithistid sponge *Wilbernicyathus*). Lichen obscures the orange coloured matrix. (D) Top of column, showing pale grey column rim enveloping mottled column interior (see also Fig. 14A). (E) Inverted bowl-shaped fossil, probably the lithistid sponge *Wilbernicyathus*, embedded in column rim (detail of Fig. 8C). Scale in centimetres. (F) White cone-like, tube-like and plate-like fossils (probably the lithistid sponge *Wilbernicyathus*) in a column interior.

attachment. In their overall appearance, Lower Biostrome columns broadly resemble some present-day examples in the Exuma Cays (e.g. Shapiro, 1991; Shapiro *et al.*, 1995, fig. 13) and

their alignment, and association with channel-like sand bodies, suggest tidal current influence (Portnoy, 1987). As these complex rimmed columns enlarged, they provided substrates for

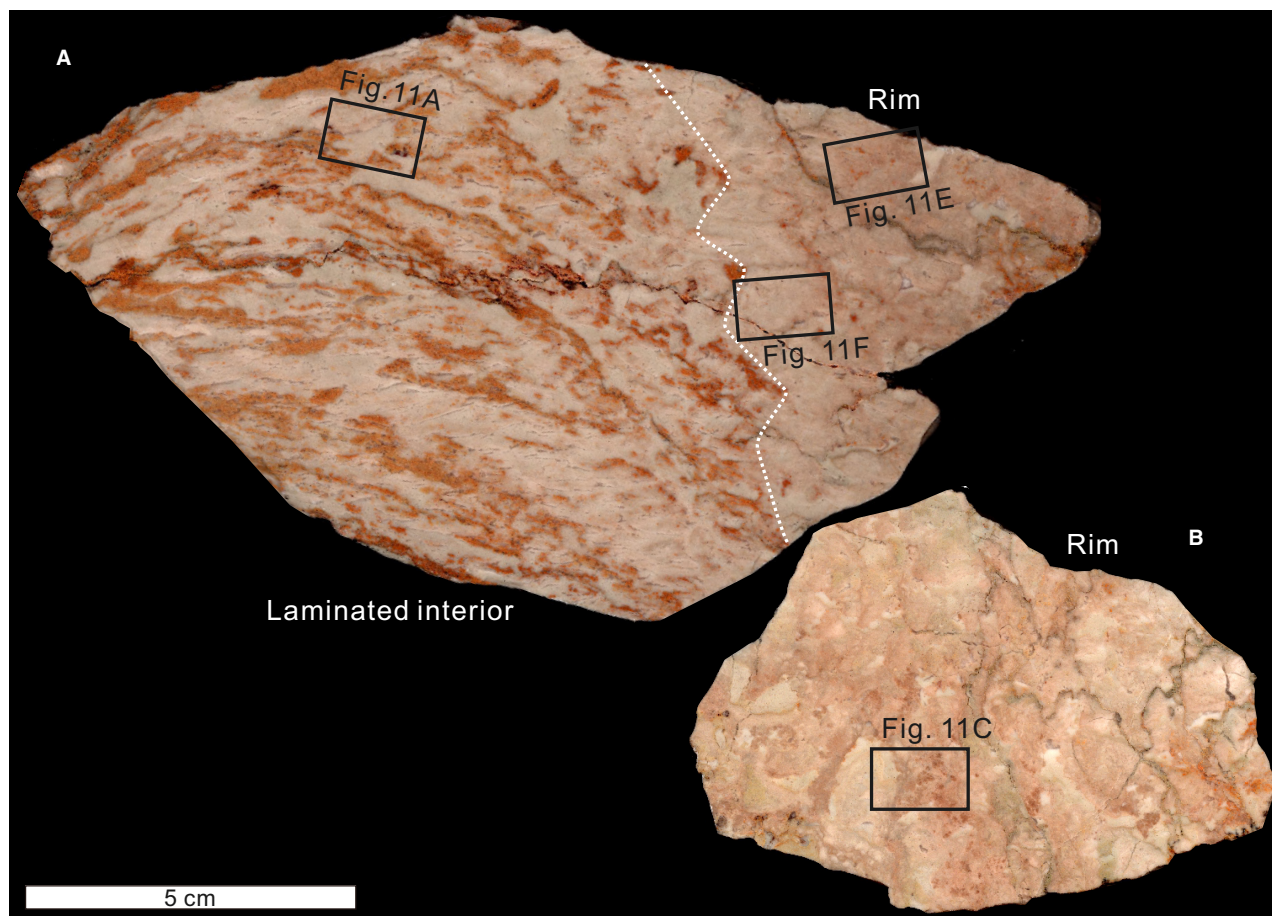


Fig. 10. Slabs of Lower Biostrome rimmed column. (A) Laminated interior to left, with crude convex-up layering of pink biolithite emphasized by orange dolomite, contrasts with more massive rim to right. (B) Complex biolithite rim.

sponge and crinoid attachment in relatively high-energy channel shoal environments, as can occur on present-day microbial columns (for example, *Siderastrea* in the Exuma Cays; Riding *et al.*, 1991, p. 230). Khanna *et al.* (2020a, fig. 8) inferred tidal current influences on similar column morphologies in the Point Peak Member on the James River, south of Honey Creek.

San Saba Bridge, Upper Biostrome

The Upper Biostrome consists of low relief juxtaposed and overlapping domes, formed either by layered stromatolite–keratolite or by macerate microstromatolite–calcimicrobe biolithite, with grainy matrix (Figs 19 and 23). The stromatolite–keratolite domes broadly resemble those in the cores of Lower Biostrome rimmed columns. Keratolite sponge vermiform fabric locally resembling ‘birdseye’ structure appears to occur in the field (Fig. 15C and D), underscoring the

difficulty of distinguishing keratolite and stromatolite (Luo & Reitner, 2016; Lee & Riding, 2021a, b). ‘Birdseye’ structure was described by Ham (1952) from the Ordovician of southern Oklahoma, and interpreted as “irregular spaces within the calcite precipitated as encrustations of blue-green algae (family *Spongiostroma*)”. Illing (1959) suggested that this fabric was most likely produced by gas bubbles and shrinkage. Shinn (1968) agreed and suggested that millimetric ‘birdseye’ structures could be indicators of intertidal, and especially supratidal, deposition. However, in the Upper Biostrome this fabric appears to be formed by keratolite sponges and is relatively large, resembling the original ‘birdseyes’ of Ham (1952, fig. 1). The distinctive triactine branching typical of vermiform fabric is locally observed, but is complicated by the presence of small lensoid geopetal fabrics (Figs 15D and 16A) (see *Sponges*, below).

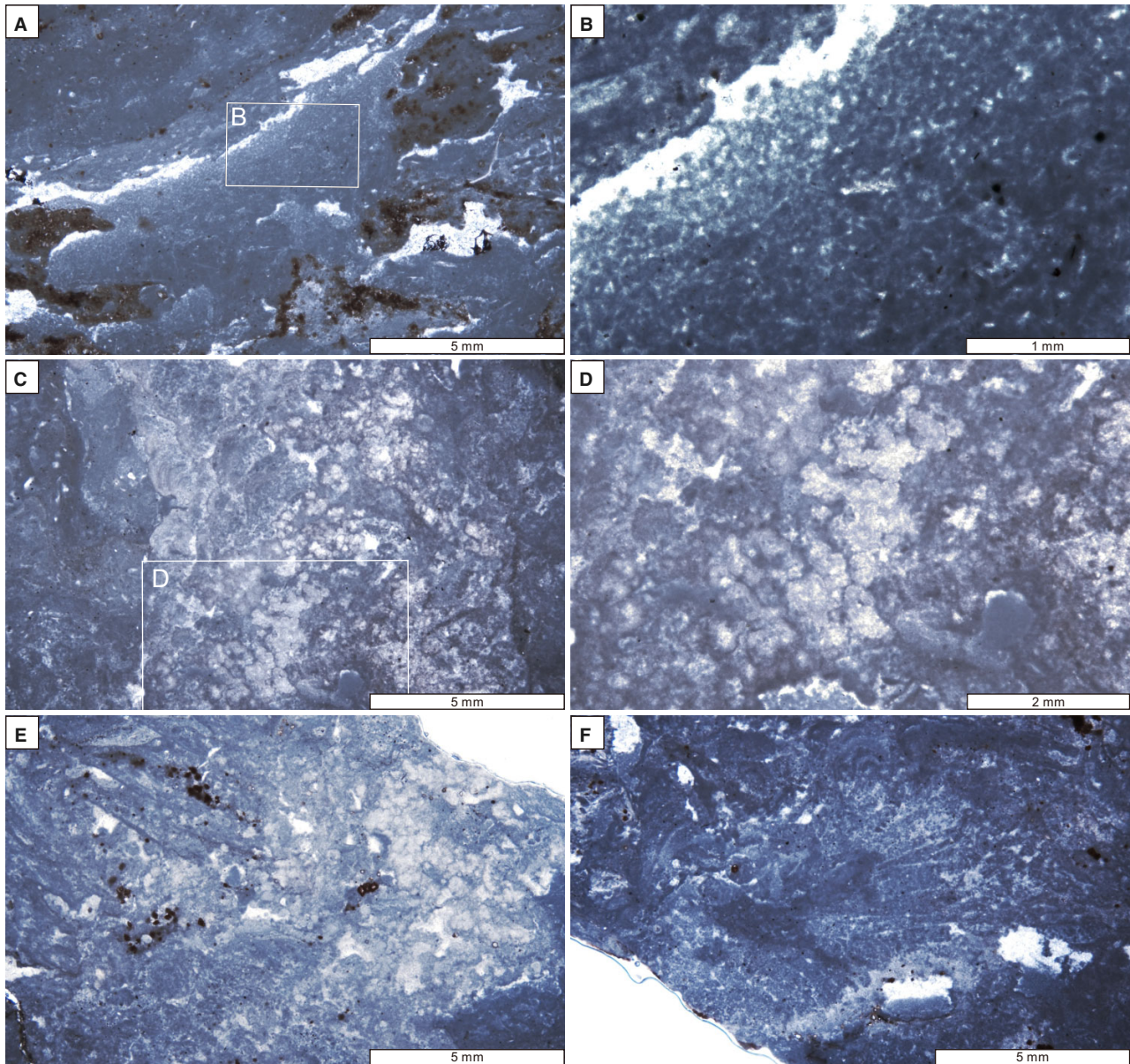


Fig. 11. Photomicrographs of Lower Biostrome rimmed column. (A) Column interior showing partly microbial mudstone-wackestone, keratolite and irregular geopetal cavity floored by peloids. (B) Detail of (A), showing cavity roof, possibly formed by *Razumovskia* crust, overlying geopetal cavity with peloidal fill (centre) and a diffuse contact with keratolite (lower right). (C) Column margin formed by microstromatolite (left upper centre) and clusters of the calcimicrobe *Tarthinia* (bottom). (D) Close up of (C) showing *Tarthinia*. (E) Complex column framework with *Razumovskia* (upper left), *Tarthinia* (right), and indistinct microstromatolite (lower left). (F) Transverse section of the lithistid sponge *Wilbernicyathus* (centre) encrusted by microstromatolite.

Upward accretion of microstromatolite/calcimicrobe biolithite, together with continued sedimentation that filled the intermaceral spaces, resulted in ragged anastomose columns with maceriate fabric (Fig. 23) reminiscent of *Favosmaceria* (Shapiro & Awramik, 2006; Lee *et al.*, 2010). In contrast to relatively high relief columns

at Honey Creek, and especially in the Lower Biostrome, both of which have microstromatolite rims and formed in wave and current-swept grainy sediment, the lenticular maceriate domes of the Upper Biostrome are unrimmed and have less surrounding sediment (Fig. 19), suggesting formation in less energetic conditions.

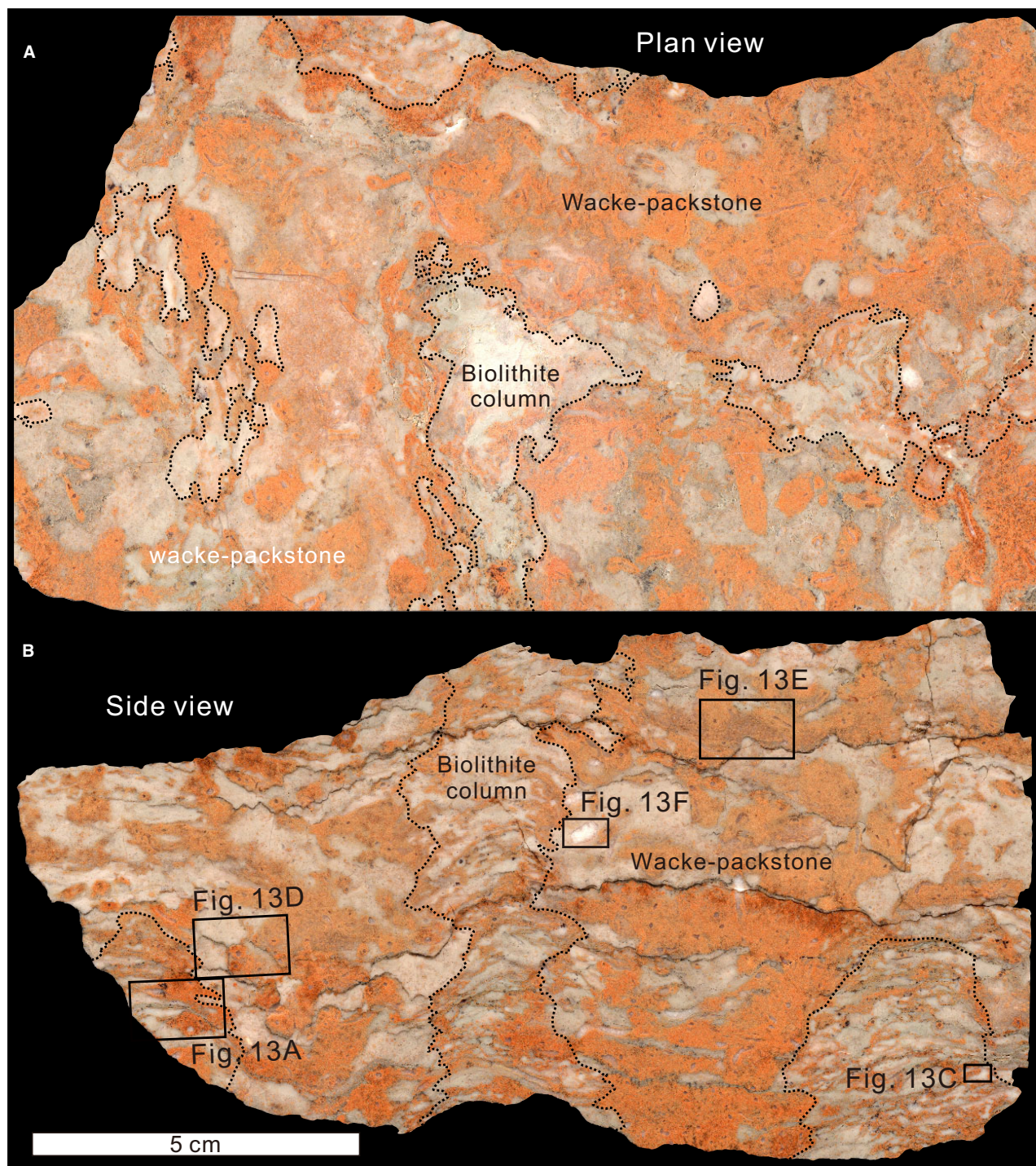


Fig. 12. Transverse (A) and vertical (B) slab sections of Lower Biostrome rimmed column interior. Ragged sub-polygonal columns of stromatolite–keratolite biolithite (outlined) in patchily dolomitized (orange) wackestone–packstone matrix, create a diffusely irregular netlike pattern in plan view.

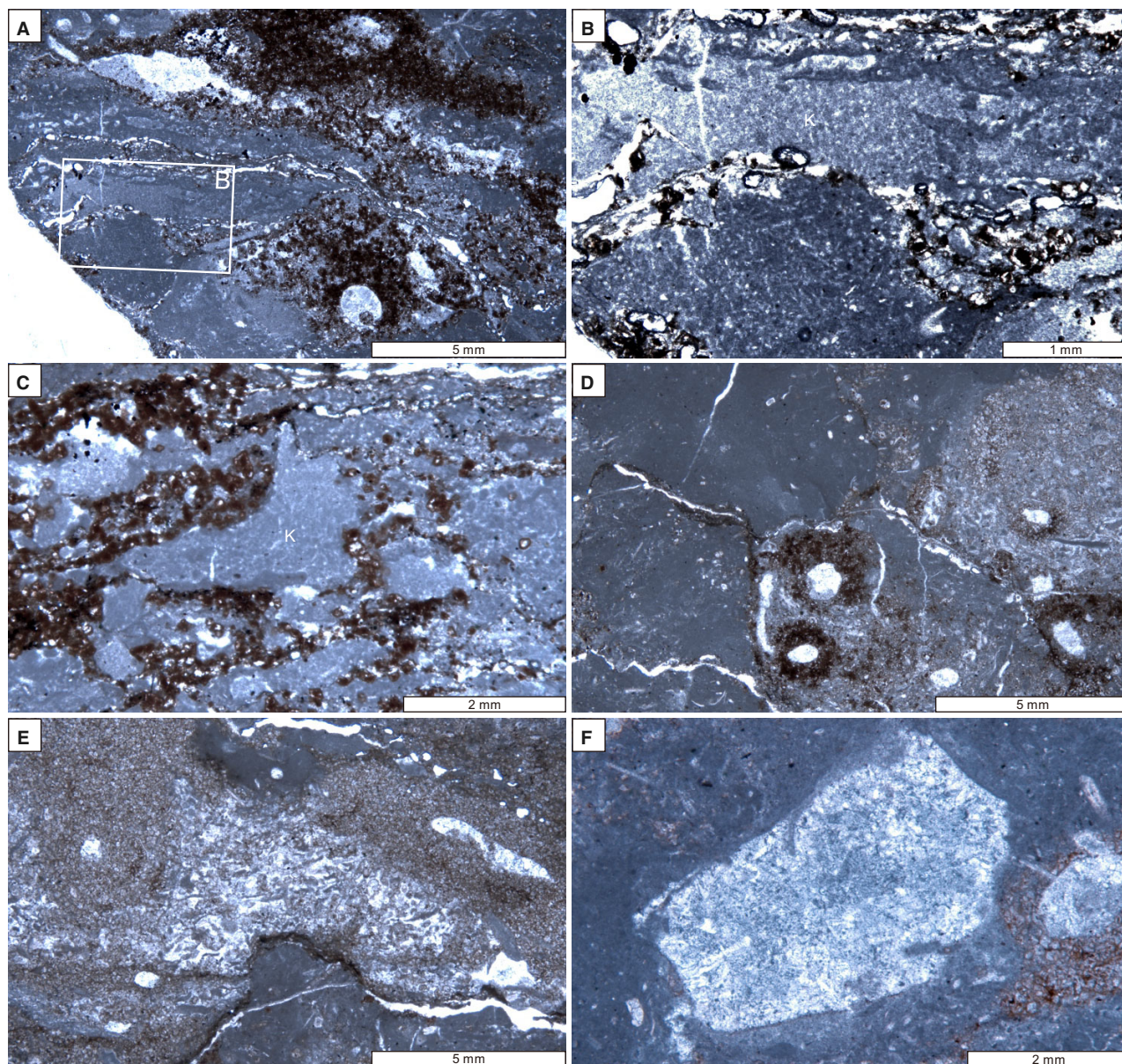


Fig. 13. Photomicrographs of Lower Biostrome rimmed column interior fabrics (see Fig. 12B). (A) Patchily dolomitized (dark colour) stromatolite–keratolite biolithite. (B) Close up of (A), showing keratolite layers with characteristic delicate anastomosing sparry network. (C) Areas of keratolite in dolomitized (dark crystals) matrix. (D) Intracolumn wackestone matrix and grainy areas penetrated by spar-filled burrows that localized dolomitization (lower centre, lower right). (E) Grainstone (mainly micritic flakes, possibly *Razumovskia*) selectively dolomitized around burrows to left and right. (F) Possible lithistid sponge fragment.

DISCUSSION

Rimmed columns with patterned interiors

In the 1800s, Cambrian and Ordovician carbonate domes and columns attracted attention in North America as the search for evidence of early life progressed (Schopf, 2000; Riding,

2011a, p. 32–35). In Texas, thick masses of ‘cabbage-head’ structures, such as at the San Saba Bridge locality, were described as *Stromatocentrum*, *Stromatopora* and *Cryptozoön* (Comstock, 1889; Dake & Bridge, 1932). Detailed mapping subsequently linked these to large ‘stromatolitic bioherms’, impressively exposed further south along the Llano River east of

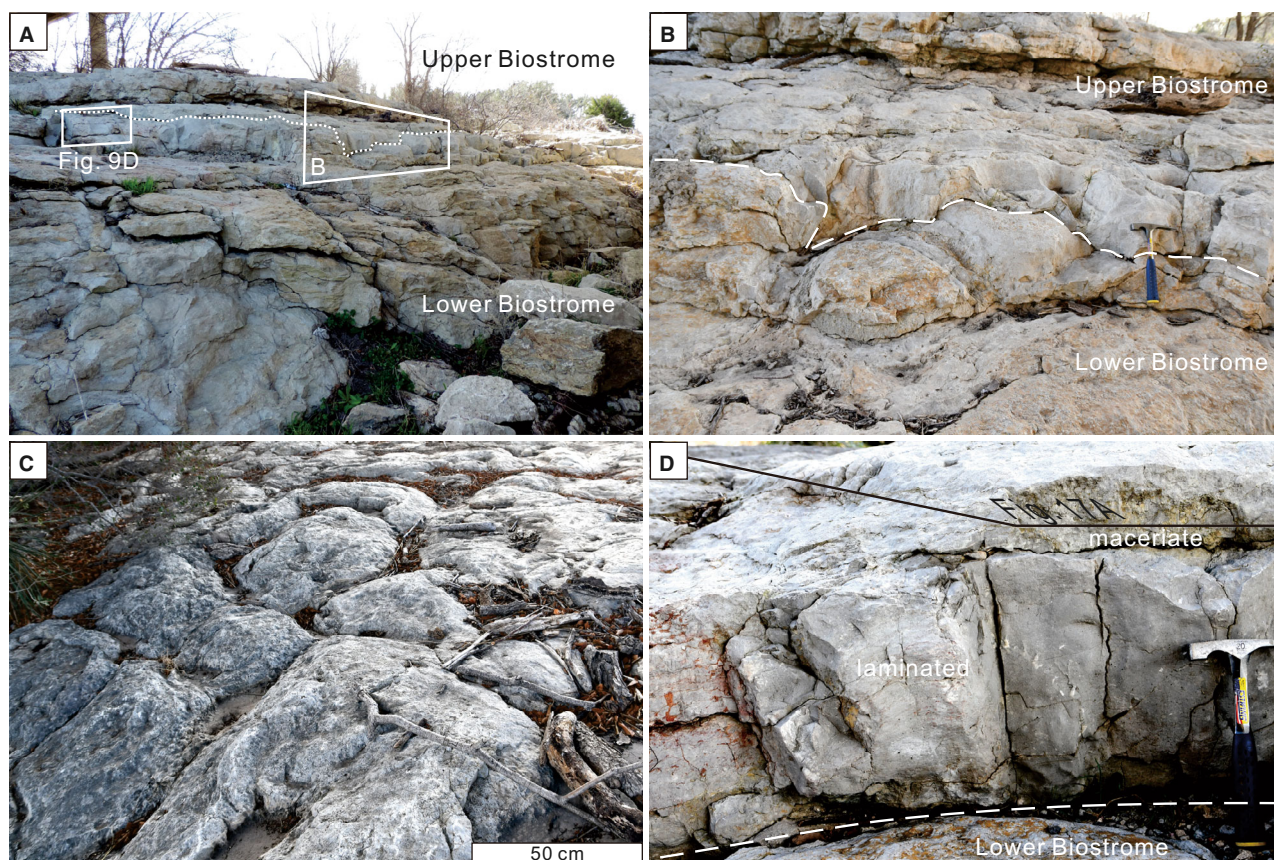


Fig. 14. Lower and Upper biostromes, San Saba Bridge section. (A) The Upper Biostrome irregularly overlying the Lower Biostrome (dotted line). (B) Irregular contact (dashed line) between the Lower Biostrome with rimmed columns (for example, centre left) and Upper Biostrome. (C) Bedding surface of the Upper Biostrome showing numerous domes largely devoid of inter-dome sediments. (D) Base of the Upper Biostrome showing laminated fabric (lower left) and maceriate dome (upper right, see Fig. 17A). Hammer in (B) and (D) is 28 cm long.

White's Crossing (Cloud & Barnes, 1948, p. 155, pl. 18). Whereas structures like *Cryptozoön* are generally distinctly layered throughout (Lee & Riding, 2021b), the Point Peak deposits include columns with complex patterned interiors and well-defined rims (Portnoy, 1987; Ruppel & Kerans, 1987, fig. 14; Khanna *et al.*, 2020a; Lehrmann *et al.*, 2020). These distinctive and well-preserved fabrics shed light on the origins of structures of similar age and appearance that are widely distributed around North America (Shapiro & Awramik, 2006, and references therein) and are also well-known in Argentina (Armella, 1994; Raviolo *et al.*, 2010) and China (Lee *et al.*, 2010, 2014, 2016; Chen *et al.*, 2014).

Rimmed columns

Present-day stromatolite and thrombolite columns in the Exumas and Shark Bay have been compared with elongate Notch Peak (Coulson,

2016) and Point Peak (Khanna *et al.*, 2020a,b) examples. However, present-day marine columns appear to differ significantly in components and degree of rim development from Cambrian examples. Columns with well-developed rim/sinter veneers are known in lacustrine carbonates (Riding, 1979; Straccia *et al.*, 1990; Arp, 1995; Newell *et al.*, 2017), but distinct rims do not appear to occur in present day Bahamian (Planavsky & Ginsburg, 2009) and Shark Bay (Jahnert & Collins, 2012) marine columns, even though these can be very well-lithified. Well-known columnar stromatolites, including Proterozoic as well as present-day Exuma and Shark Bay examples, generally appear to range from well to poorly laminated throughout (Walter, 1972), and marine examples with distinct rims appear to be rare except in the Cambrian/Ordovician (e.g. Runnegar *et al.*, 1979; Hintze *et al.*, 1988; Shapiro *et al.*, 1992;

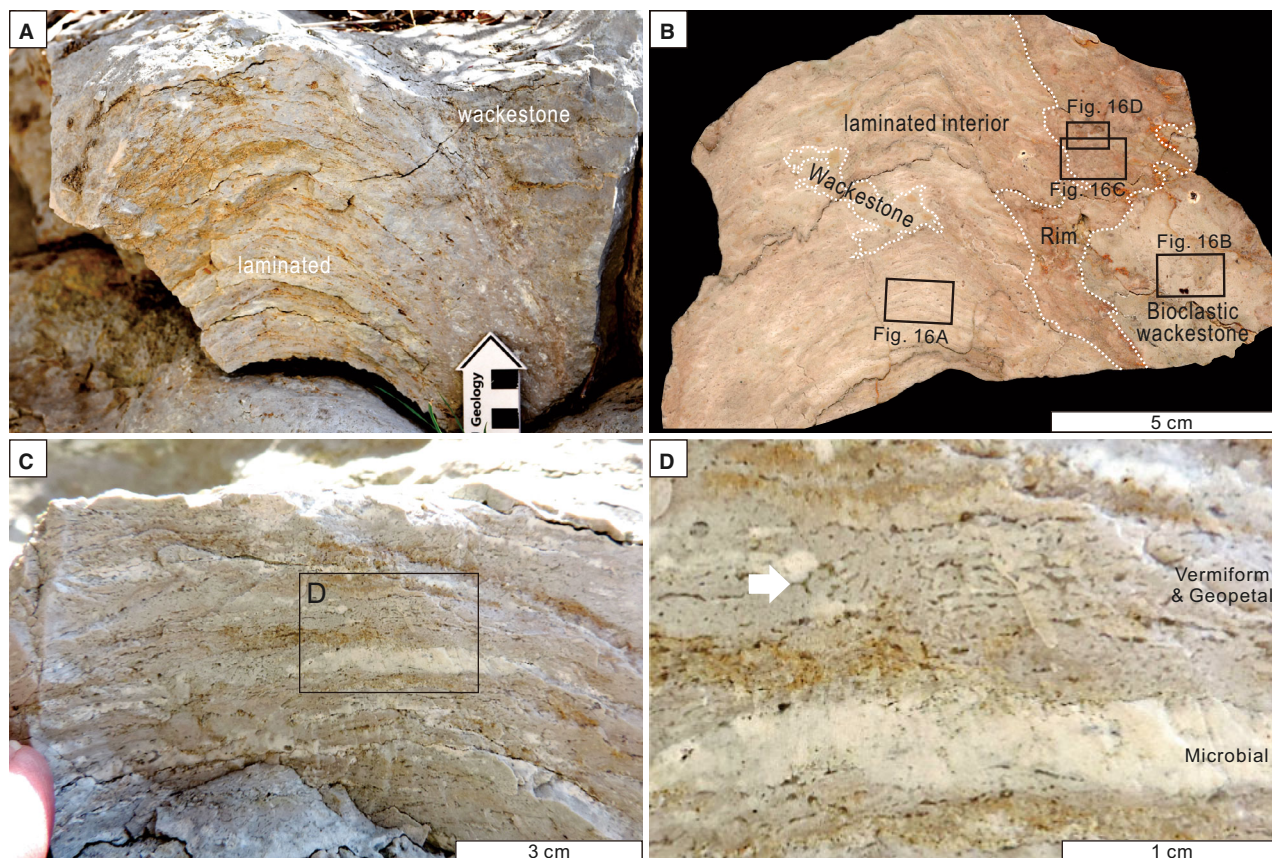


Fig. 15. Field photographs (A), (C) and (D) and slab (B) showing Upper Biostrome laminated dome fabrics, superficially resembling stromatolite but composed of intimately interlayered stromatolite–keratolite. (A) Laminated dome with possible rimmed margin (above scale). (B) Laminated dome with pink microstromatolite–calcimicrobe rim. (C) and (D) Detail of keratolite layer (keratosan sponge) showing vermiform fabric that resembles fenestral ‘birdseye’ structure. Arrow in (D) points to triactine-like shape.

Awramik *et al.*, 1994, p. 28–29; de Freitas & Mayr, 1995; Middleton, 2001; Rowland & Shapiro, 2002; Lee *et al.*, 2010, 2016; Miller *et al.*, 2012, fig. 93; Coulson, 2016; Harwood Theisen & Sumner, 2016).

In Ordovician examples from Newfoundland, Pratt & James (1982, p. 550) suggested that “the poorly laminated or thrombolitic axial zones probably resulted from uneven sediment coating, irregular algal mat surface texture and sporadic burrowing”. Subsequently, from the same location, they figured “cerebral-like weathering pattern ... caused by partial dolomitization” formed by “irregularly interconnected thrombolite heads, each up to 0.2 m across, encrusted by dense *Renalcis* masses up to about 3 cm thick” (Pratt & James, 1989, fig. 6B). In Cambrian examples from Shandong, Lee *et al.* (2010) recognized maceriate fabric with structureless outer rims and coarse-grained

intercolumnar sediments. In Cambrian Hellmarmaria columns in Utah, Coulson (2016, figs 5, 6) and Coulson & Brand (2016, fig. 4) recognized stromatolite columns with mini-stromatolite cores. In Cambrian Wilberns examples from Texas, Lehrmann *et al.* (2020, fig. 12e) drew attention to ‘micritic rind’ at the edges which is described herein as rimmed columns.

In our examples, column rims are mainly formed by distinctive time-limited communities of heavily calcified microstromatolites and calcimicrobes that surround column interiors mainly occupied by microstromatolite (Honey Creek) or stromatolite–keratolite (Lower Biostrome) in micritic and grainy matrix. Point Peak column fabrics show the most complexity in their interiors, where both microbial (microstromatolite and stromatolite) and sponge (keratolite, as well as locally lithistid) biolithite accumulated in poorly sorted grainy sediment. This arrangement

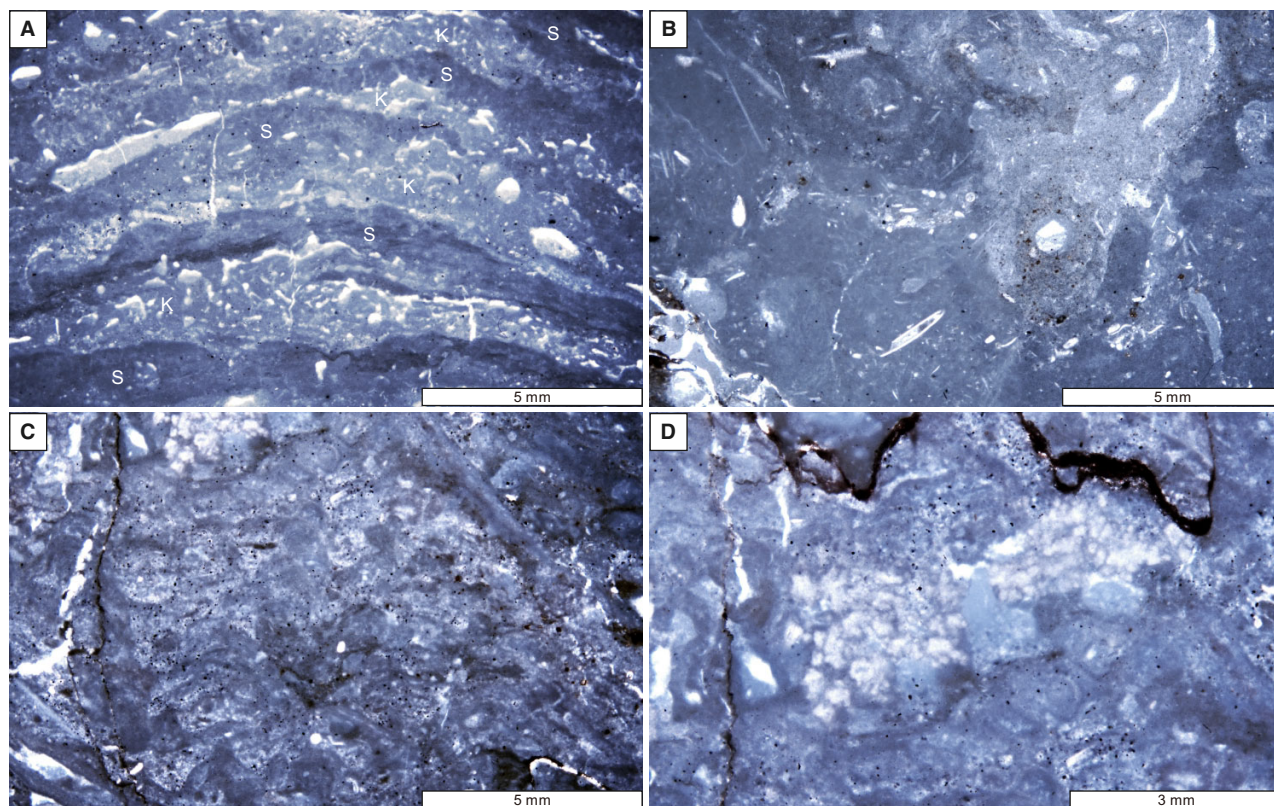


Fig. 16. Photomicrographs of the Upper Biostrome laminated dome. (A) Alternating layers of stromatolite (dark grey; S) and possible keratolite (light grey vermiform fabric; K). Geopetal fabrics occur between some layers (for example, upper left) and within rounded burrows. (B) Interdome bioclastic wackestone with scattered monaxon (thin, straight) sponge spicules and trilobite fragments. Dolomitization, scarce in the wackestone, preferentially occurs around spar-filled burrows (for example, centre right). (C) Rim fabric dominated by microstromatolite. (D) *Tarthinia* (lighter areas) in the rim.

somewhat resembles present-day shallow-water scleractinian coral microatolls that were first described as ‘miniature atolls’ (Guppy, 1886). Essentially, these “coral colonies with dead, flat tops and living perimeters, result from a restriction of upward growth by the air/water interface” (Scoffin & Stoddart, 1978). The term microatoll has also, more broadly, been applied to larger slightly submerged coral accumulations with raised rims and sand-filled centres below the air–water interface (e.g. Kornicker & Boyd, 1962; Scoffin & Stoddart, 1978). Present-day Lake Clifton thrombolite domes that accrete to sea-level in very shallow water have been compared with microatolls (Burne & Moore, 1993). Many Honey Creek columns have planar tops (Fig. 4B). However, there is no direct evidence of contemporaneous erosion, or that sea-level was sufficiently shallow to expose the columns. It remains to be seen whether Point Peak

column growth and height may in some cases be related to water–air exposure during accretion.

Mottled fabrics and burrowing in thrombolites Garrett (1970) suggested that Phanerozoic decline in stromatolite abundance might be attributable to the evolution and diversification of animals that grazed microbial mats and destroyed sedimentary lamination. Data compiled by Awramik (1971) suggested long-term increase in columnar stromatolite variety during the Proterozoic, followed by Ediacaran and early Cambrian decline due to the appearance of metazoans. Monty (1973) doubted that there was evidence to support the view that “stromatolites were eliminated by the rising metazoans which burrowed them and fed upon them”. Nonetheless, Aitken (1967) had noted common occurrence of burrows in thrombolites and Walter & Heys (1985) suggested that “early Palaeozoic

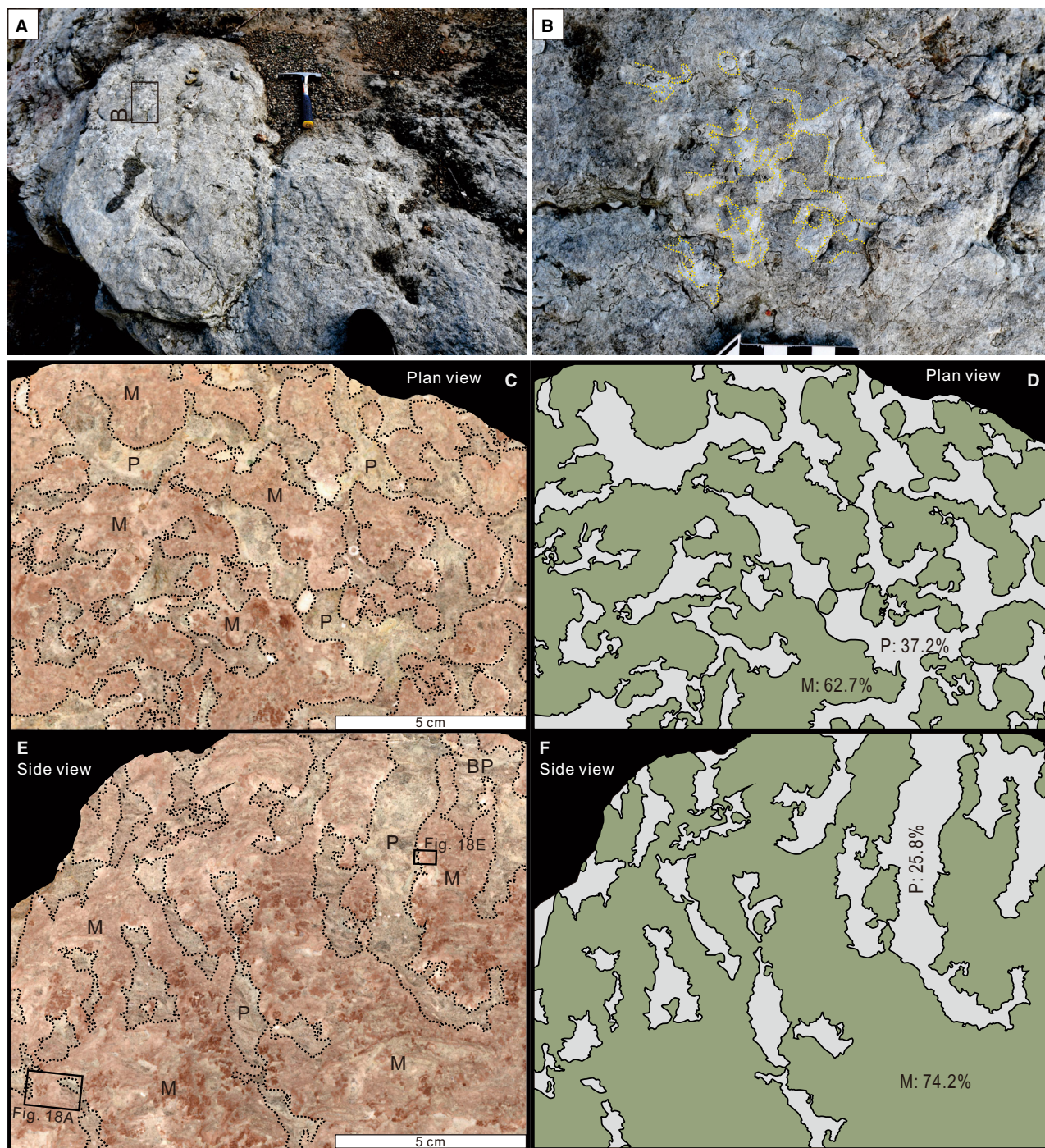


Fig. 17. Maceriate domes in the Upper Biostrome. (A) Surface view of ellipsoidal maceriate domes. Hammer is 28 cm long. (B) Close up of (A), with maceriate structure outlined by dashed yellow lines. Centimetre scale. (C) Transverse slab section showing irregularly meandriform (maceriate) pink microstromatolite biolithite (M) with bioclastic packstone (P) fill. (D) Line drawing of (C) showing irregular maceriate structure. (E) Vertical slab section of pink anastomose microstromatolite biolithite with brown calcimicrobe clusters. (F) Line drawing of (E) showing irregularly anastomose branching of the biolithite.

‘thrombolites’ ... are stromatolites that have been burrowed and bored”. Awramik *et al.* (1994, p. 28–29) compared columns with

stromatolitic margins and coarse clotted cores in the Nopah Formation at Dry Mountain, California, and in the Notch Peak Formation, Utah,

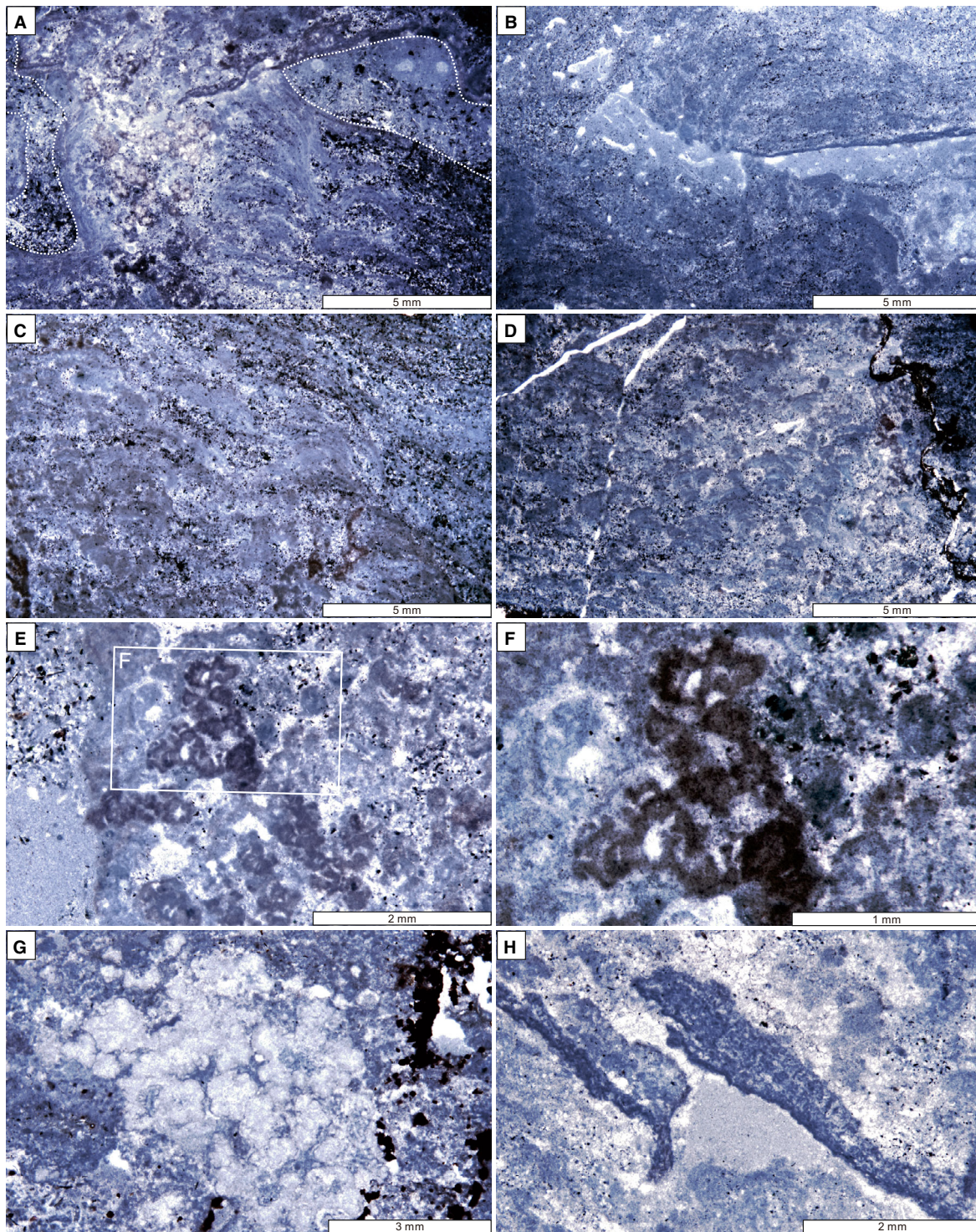


Fig. 18. Photomicrographs of maceriate dome fabrics in the Upper Biostrome. (A) Maceriate biolithite formed by microstromatolite (for example, centre) and calcimicrobes (*Razumovskia*, *Renalcis*, *Tarthinia*) (for example, centre left). Packstone matrix (outlined by white dotted lines) occupies intermacerial spaces. (B) A rare example of keralolite (light grey layer) overlying microstromatolite and overlain by thin *Razumovskia* (dark grey layer), and then by more microstromatolite. (C) Microstromatolite interlayered with abundant detrital sediment. (D) Relatively small microstromatolite clusters forming clotted texture. (E) and (F) *Renalcis*, characterized by distinct walls and lunate chambers. (G) *Tarthinia*, with thick, light coloured diffuse walls and indistinct chambers. (H) Two small flakes formed by *Razumovskia* crust (very small irregular tubules) overlain by patterned fabric of uncertain origin.

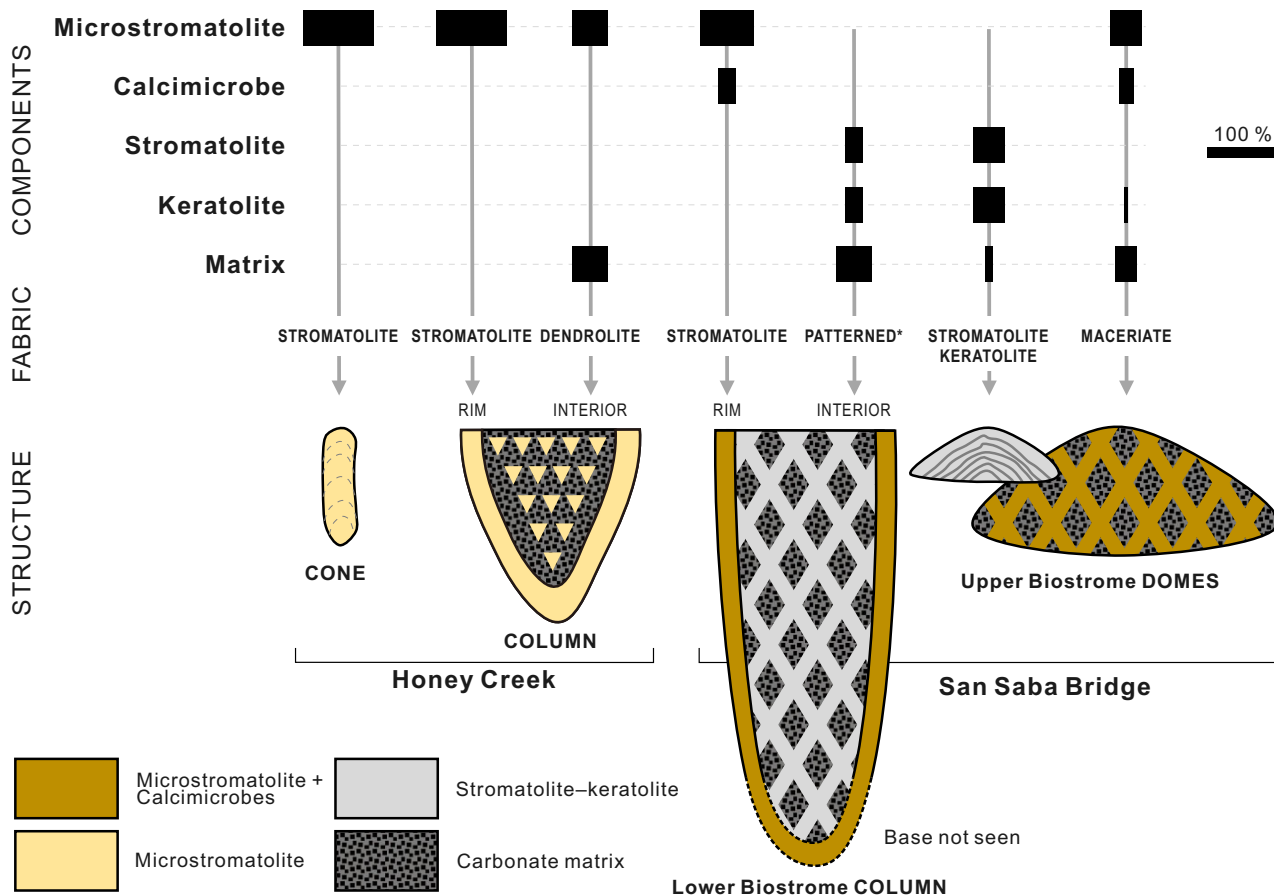


Fig. 19. Approximate relative abundances of macrofabric components in Honey Creek and San Saba Bridge cones, columns and domes. Relatively greater complexity of San Saba Bridge structures reflects the presence of stromatolite–keratolite and calcimicrobes, in addition to microstromatolite which is the sole biolithite component in Honey Creek cones and columns. Patterned* fabric in Lower Biostrome column interiors represents ragged stromatolite–keratolite columns and partly dolomitized matrix that create irregular polygonal networks in cross-section.

with present-day Exuma stromatolites, and suggested that “the thrombolitic texture probably represents bioturbation” (Awramik *et al.*, 1994, p. 29). Similarly, maceriate column cores in the Hellnmaria Member, Utah, have been described as ‘burrowed stromatolites’ (Miller *et al.*, 2012, fig. 93), and in a comprehensive study of upper Cambrian thrombolites in the Great Basin, Harwood Theisen & Sumner (2016) found that “clotted or patchy textures of at least some ancient thrombolites reflect bioturbation of a microbial growth structure”. Xiao *et al.* (2019) attributed the formation of Lower Ordovician ‘reticulated thrombolites’ in Hubei, China to bioturbation.

Bioturbation, in general, significantly increased in the early Cambrian (Boyle *et al.*, 2014), although it has also been argued that bioturbation “remained limited until at least the

late Silurian” (Tarhan *et al.*, 2015). Studies of present-day stromatolites support the view that even quite small mobile organisms such as Foraminifera “may have been responsible for observed changes to microbialite microfabric in the late Precambrian” (Bernhard *et al.*, 2013). On the other hand, it has been pointed out that “well-laminated structures ... coexist with dense and diverse infaunal and epifaunal metazoan communities” in some present-day normal marine microbialites in the Exuma Cays (Tarhan *et al.*, 2013). In the geological record, thrombolite fabrics have been reported from Palaeoproterozoic rocks (e.g. Kah & Grotzinger, 1992; Nomchong & Van Kranendonk, 2020) and became more widespread in the Neoproterozoic (e.g. Aitken & Narbonne, 1989; Turner *et al.*, 1993; Grotzinger *et al.*, 2000; Turner *et al.*, 2000; Oliver & Rowland, 2002; Harwood & Sumner,

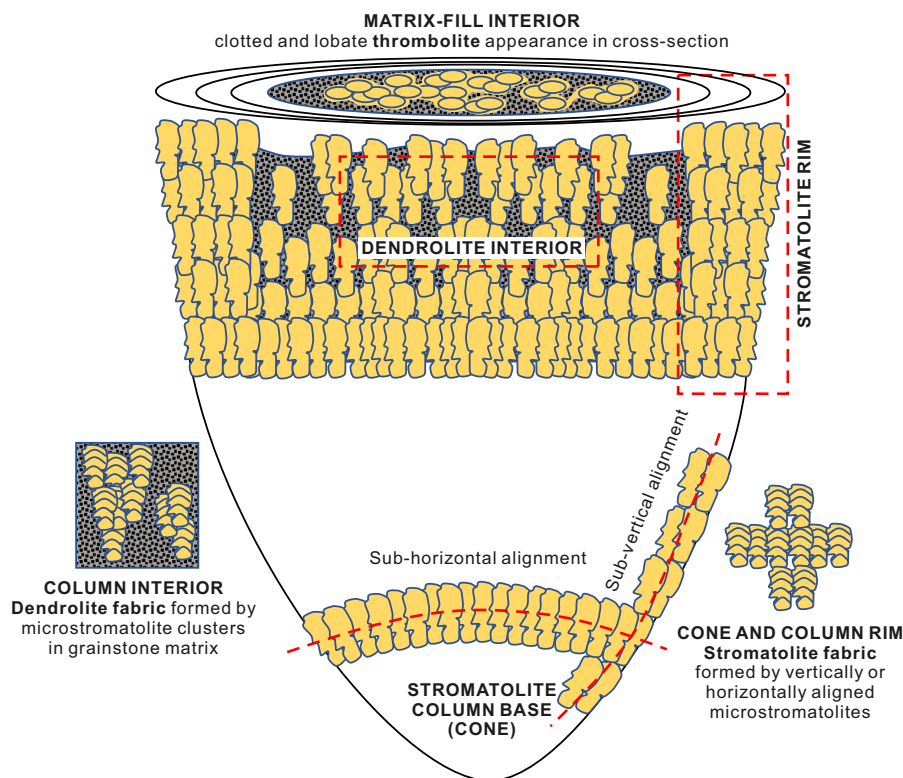


Fig. 20. Model of stromatolite, dendrolite and thrombolite fabric development in a Honey Creek cone/rimmed column. Vertically and horizontally aligned microstromatolites form the base of a stromatolitic cone/column. During upward growth and expansion, development of a stromatolite rim (composed of microstromatolites) leads to accumulation of allochthonous carbonate sediment in the column interior where numerous microstromatolite clusters create vertical dendrolite fabric. In plan view, the latter appears thrombolitic. In this way, a single biolithite component (in this case, microstromatolite) can create a variety of fabrics and structures.

2012). These observations question links between thrombolites and bioturbation.

In the Lower Biostrome columns that were studied herein, small burrows localized dolomitization that contributed to colour contrasts in the column interiors; but on its own this does not appear to have significantly affected primary column fabric, as demonstrated in better preserved Upper Biostrome laminated domes. Nonetheless, it remains possible that a relationship between burrowing, dolomitization and column interior mottling could help to account for reports of burrowed column interiors elsewhere (Walter & Heys, 1985; Armella, 1994; Harwood Theisen & Sumner, 2016; Xiao *et al.*, 2019; Kröger & Penny, 2020). Without this effect, column interiors would likely appear relatively evenly tan-coloured, in contrast to grey column rims. Overall, the patterned interiors of Lower Biostrome columns are products of both: (i) complex primary stromatolite–keratolite (sponge)

biolithite fabrics; and (ii) selective dolomitization localized by small burrows and grainy matrix. These examples may shed light on: (i) the origins of late Cambrian and Early Ordovician columns with stromatolite rims and mottled interiors; and (ii) confusion between mottled interiors and maceriate fabric (see next section).

Maceriate fabric

In addition to well-known microbial carbonate morphologies, such as domes and columns, Shapiro & Awramik (2006) proposed the term ‘maceriate’ (from Latin *maceria*: a brick or clay wall, such as around a garden) to describe the labyrinthine mazelike pattern in plan view of the thrombolite *Favosamaceria*, based on late Cambrian type-specimens from the Nopah Formation (Smoky Formation) at Mohawk Hill, California (see also Grey & Awramik, 2020,

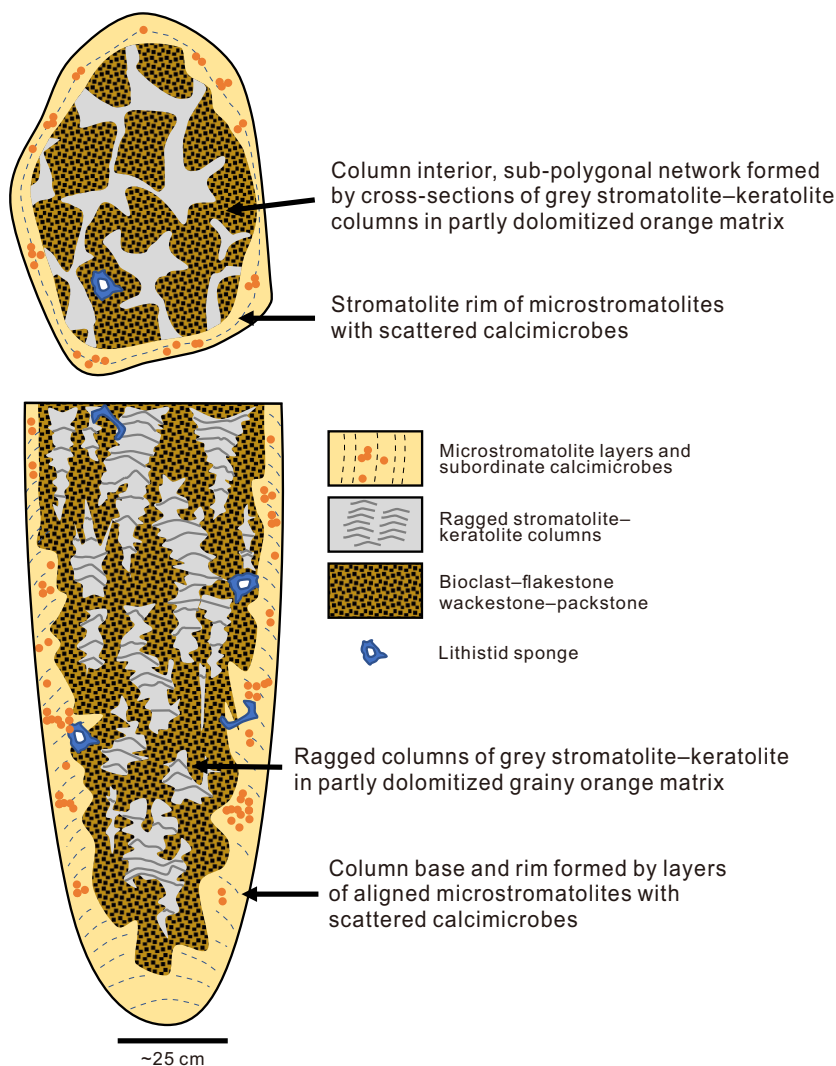


Fig. 21. Fabrics of elongate columns in the Lower Biostrome at San Saba Bridge. As in Honey Creek rimmed columns, microstromatolites (here together with calcimicrobes) form stromatolitic column bases. These grow upward and expand into column rims surrounding poorly sorted grainy column interior sediment colonized by stromatolite-keratolite consortia. In vertical section, the latter form ragged, irregular, discontinuous columns. In horizontal section, they appear as complex column-fill with irregular netlike patterns, further complicated by selective dolomitization localized around small burrows. Both column rims and interiors are locally colonized by lithistid sponges.

fig. 41b). Similar forms have been recognized in Pleistocene tufa from Lake Lahontan, Nevada (Grey & Awramik, 2020, fig. 41a). Whereas most microbial carbonate fabrics, for example, in stromatolites, are traditionally described in vertical section (e.g. Hofmann, 1969b; Walter, 1972; Semikhatov & Raaben, 2000), the maceriate fabric characteristic of *Favosamaceria* is only evident in plan view and often appears cerebroid (Grey & Awramik, 2020, p. 63, 221, 226, figs 51g, 57a, b), with labyrinthine “convoluted ridges separated by mazelike interspaces” (Grey & Awramik, 2020, p. 214). In vertical section it can appear irregularly branched and anastomose (Shapiro & Awramik, 2006, figs 5, 6; Grey & Awramik, 2020, fig. 57a, b). Shapiro & Awramik (2006, p. 415) noted that maceria margins are parallel and often ragged, with low synoptic relief, and suggested that *Favosamaceria*

occurs widely throughout Laurentia. Coulson (2016, fig. 4e) noted upper Cambrian ‘mazelike structures’ in column interiors in Utah. *Favosamaceria* has also been described from Argentina (Raviolo *et al.*, 2010), and similar fabrics have been described from various localities in North China (Lee *et al.*, 2010, 2014, 2016) where Chen *et al.* (2014, p. 250) noted that “The deposition rate of inter-macerial sediment was most likely balanced with the growth rate of maceriae, sustaining a low synoptic relief”.

Point Peak Upper Biostrome maceriate fabric (Fig. 17), macroscopically comparable with *Favosamaceria* (Shapiro & Awramik, 2006, fig. 6), largely consists of microstromatolite. It accreted in grainy sediment under relatively low energy conditions, as low synoptic relief biolithite ridges that are vertically anastomose and meandriform in plan view. Neomorphism and dolomitization

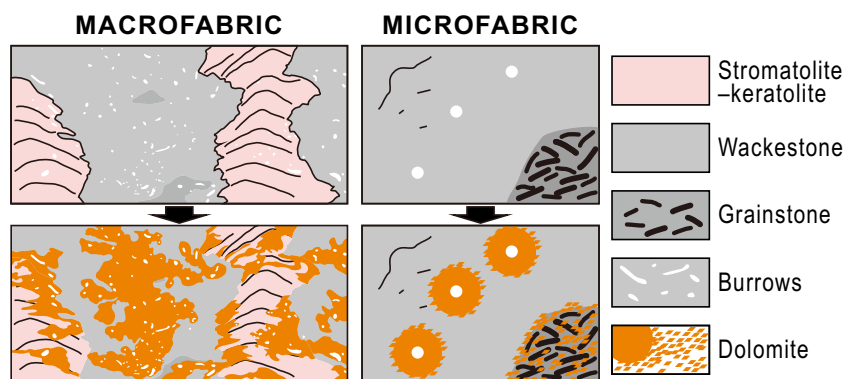


Fig. 22. Diagrammatic interpretation of the effect of localized micro-mesoscale dolomitization on San Saba Bridge Lower Biostrome column interior fabrics. Primary fabrics illustrated at the top become modified below by patchy secondary dolomite (shown in orange). Dolomitization, which partially affects both matrix and stromatolite-keratolite biolithite, is often preferentially localized around small burrows. This alteration and its associated colour changes tend to obscure the primary structure (*cf.* Figs 12 and 13).

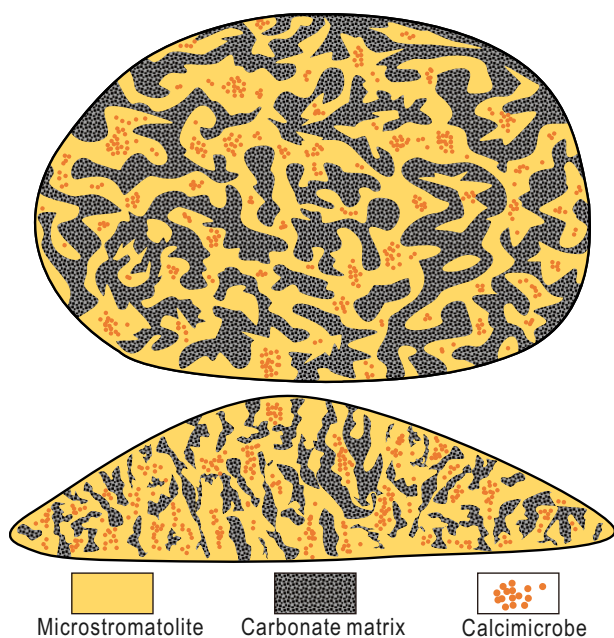


Fig. 23. Maceriate dome structure and composition in the San Saba Bridge Upper Biostrome. Microstromatolite, locally containing clusters of calcimicrobes, forms intricately anastomose biolithite that is maceriate in plan view and crudely radially anastomose in vertical section. Interspaces were progressively infilled by poorly sorted carbonate matrix.

in the type-material of *Favosamaceria* (Shapiro & Awramik, 2006) hinder microfabric recognition and comparisons. Relatively good preservation of Upper Biostrome domes shows that their maceriate fabric is primary, and largely consists of microstromatolite biolithite, locally with clusters

of *Renalcis*, *Tarthinia* and minor *Razumovskia*, and minor amounts of keratolite. In contrast, some other reported maceriate fabrics that are more conspicuous in the field may, as in thrombolite fabrics, have been secondarily enhanced or even, in some cases, superficially created by processes such as dolomitization that alter colour or textural contrast (Shapiro & Awramik, 2006; Lee *et al.*, 2010).

Lee *et al.* (2014) reported upper Cambrian maceriate fabrics composed of microstromatolite, keratosan sponges (identified as ‘siliceous sponges’) and minor calcimicrobes (*Tarthinia* and *Razumovskia*), similar to those described here in the Upper Biostrome. In these examples, microstromatolite and keratolite each constitute up to half of the maceriae volume (Lee *et al.*, 2014). Microstromatolite and keratolite also occur in maceriate fabrics in the upper Cambrian near Beijing (Chen *et al.*, 2014) and in the middle Cambrian of Inner Mongolia (Lee *et al.*, 2016). Keratolite in upper Cambrian maceriate fabrics in Utah was mistaken for lithistid sponge (Coulson & Brand, 2016; see Lee & Riding, 2021a, table 1). It therefore appears that well-preserved *Favosamaceria*-like forms may be constructed either by microstromatolite with minor calcimicrobes (as in our Point Peak examples) or by microstromatolite and keratolite (as in Chinese examples). In contrast, Raviolo *et al.* (2010) reported only clotted micrite and minor filamentous calcimicrobes from upper Cambrian *Favosamaceria* in the eastern Precordillera, Argentina. It remains to be seen how other examples of *Favosamaceria*-like forms developed.

Thrombolite fabric recognition

Based on Cambrian and Ordovician examples, mainly from the Canadian Rockies, Aitken (1967, p. 1164) proposed thrombolite as a parallel term to stromatolite, defining thrombolites as “cryptalgal structures related to stromatolites, but lacking lamination and characterized by a macroscopic clotted fabric”. This drew attention to an important category of microbial carbonate that ranges from Proterozoic (Aitken & Narbonne, 1989; Kah & Grotzinger, 1992; Turner *et al.*, 2000; Tang *et al.*, 2013; Barlow *et al.*, 2016) to late Cenozoic, including present-day columns (Riding *et al.*, 1991; Reid *et al.*, 1995; Macintyre *et al.*, 1996; Feldmann & McKenzie, 1997, 1998; Jahnert & Collins, 2012). As with stromatolites, thrombolites differ widely in origin and formation, as shown by the contrasts between calcified microbial, coarse agglutinated and arborescent forms (Riding, 2000, p. 193–194).

Application of the terminology from Aitken (1967) and that definition of thrombolite have been widely discussed (Pratt & James, 1982; Kennard & James, 1986; Shapiro, 2000; Shapiro & Awramik, 2006; Riding, 2011b; Grey & Awramik, 2020; Shapiro & Wilmeth, 2020). Key points that have attracted attention are: (i) the contrast between stromatolite lamination, which is essentially a primary fabric, and thrombolite clots that may variously be primary, syngenic and/or diagenetic (Riding, 2000, p. 192–194); and (ii) the distinction between thrombolite as a whole and its component clots (Shapiro, 2000).

1 Stromatolites, although diverse in shape and composition, are united in having laminated fabric (Kalkowsky, 1908). Early studies of present-day laminated microbial deposits related layering to seasonal variations in growth and calcification (Roddy, 1915), and to the size of trapped grains and alternation of sediment-rich and organic-rich layers (Black, 1933). Further work over subsequent decades supported and extended these interpretations, and it is now widely accepted that stromatolite lamination reflects episodic, in some cases iterative, changes in accretion variously related to variations in microbial growth and calcification, inorganic precipitation and grain trapping (e.g. Cloud, 1942; Ginsburg & Lowenstam, 1958; Logan, 1961; Hofmann, 1973; Doemel & Brock, 1974; Monty, 1976; Hofmann, 1977). Although

lamination can be created secondarily by metamorphism, and this can obstruct stromatolite recognition in some examples (Allwood *et al.*, 2018), it is unlikely to be secondarily produced by the low temperature/pressure diagenetic processes common in relatively well-preserved carbonate sediments. As a result, the uncertainties that surround stromatolite recognition have tended to focus more on questions of biogenicity than on the origins of the lamination (Buick *et al.*, 1981; Riding, 2008; Riding & Virgone, 2020).

Thrombolite recognition centres on whether clots are primary, or are secondary products of neomorphism or dolomitization. Thrombolite clots can be surrounded by matrix (Aitken & Narbonne, 1989), and this heterogeneity makes the fabric prone to alteration, including dolomitization. In some cases this may enhance primary fabric, but it can also create secondary fabrics that are often difficult to interpret (Harwood Theisen & Sumner, 2016). Consequently, clots may not only have a primary origin, such as *in situ* growth of clusters of calcified microbes, but can also be developed by syngenic disturbance such as bioturbation, and through diagenetic processes of neomorphism and dolomitization that are common in carbonates (Aitken, 1967; Kennard & James, 1986; Burne & Moore, 1993; Riding, 2000; Shapiro, 2000; Tosti & Riding, 2014). Relatively good fabric preservation, as in Point Peak examples, is essential for microbial carbonate interpretation in general, and for thrombolite recognition in particular. In our samples, burrowing is present but does not appear to have significantly affected the macrofabric. This would support the view that bioturbation should not become a default explanation for thrombolite fabric, especially if the components and fabrics are not readily discernible (see *Mottled fabrics and burrowing in thrombolites*, above). It remains to be seen how far Point Peak microbial carbonates may be comparable with thrombolite and dendrolite fabrics elsewhere.

2 Clot definition has been debated. Pratt & James (1982, p. 545) suggested that the clots are the thrombolite; but this amendment was abandoned by Kennard & James (1986, p. 492–493) who took the view that thrombolites “have a distinct internal mesoscopic structure (mesostructure) consisting of millimetre and centimetre-size clots separated by patches of mud and sand-size sediment or sparry carbonate ... The

individual clots within thrombolites are here designated mesoclots ...". This was supported by Shapiro (2000) who noted that Aitken (1967) had referred to both small mesostructural clots and larger 'clots' that represent sections through thrombolite columns. Accordingly, Shapiro (2000, p. 166) wrote: "Mesoclots are generally polymorphic millimetre to centimetre-sized objects whereas columns, which may also be polymorphic, are one to several orders of magnitude larger". Thus, although Aitken (1967, p. 1164) proposed thrombolite as a parallel term to stromatolite, with stromatolites being laminated and thrombolites clotted, these fabrics are not directly comparable because stromatolite lamination is primary and pervasive, whereas thrombolite fabric often consists of clots within matrix. In addition, some thrombolites can solely be formed by calcimicrobes without significant matrix, as in the early Cambrian of Shandong, China, where *Epiphyton* forms dendritic mesoclots (Riding, 2000, figs 12, 13) and *Tarthinia* occupies interspace between the mesoclots (Lee *et al.*, 2014, figs 5, 7). To define thrombolite, the authors rephrase the suggestion by Riding (2011b, p. 642) that "thrombolites can generally be regarded as benthic microbial carbonates with macroclotted fabric", by defining thrombolite as a *macroscopically clotted benthic microbial deposit*. This parallels a definition proposed for stromatolite as a "macroscopically laminated benthic microbial deposit" (Riding, 1999, p. 321).

Microstromatolites

Very small, often millimetric, stromatolite columns, that are widespread and locally abundant in Proterozoic carbonates (Riding, 2008), have variously been termed digitate stromatolite (Donaldson, 1963), microstromatolite (Hofmann, 1969a, p. 15; Raaben, 1980; Lanier, 1986), 'tiny arborescent stromatolite' (Hofmann, 1975), microdigitate stromatolite (Hoffman, 1972; Grotzinger & Read, 1983) and ministromatolite (Hofmann & Jackson, 1987). Their fabrics range from irregularly laminated and peloidal to evenly layered and radially fibrous, and have variously been interpreted as biogenic (Grey & Thorne, 1985) or abiotic (Grotzinger, 1986), and they have often been described from restricted nearshore environments (Hofmann, 1975).

Microstromatolites similar, but not identical, to those of the Proterozoic, are also locally abundant in Cambrian and Early Ordovician reefs. In

addition to the Point Peak examples described here, they have been identified in thrombolite mesoclots (with lamination that is imperceptible to the naked eye) in the middle Cambrian of Inner Mongolia (Lee *et al.*, 2016, fig. 3), and are common but relatively inconspicuous components in late Cambrian maceriate domes and columns in Shandong, China (Lee *et al.*, 2014, figs 4–6). Microstromatolite also forms thrombolitic crusts in late Cambrian (Lee *et al.*, 2019) and Early Ordovician (Adachi *et al.*, 2009; Hong *et al.*, 2015; Pham *et al.*, 2021) microbial–lithistid sponge reefs. Microstromatolites of this type appear to have played a key role in the construction of a wide variety of stromatolite, thrombolite, dendrolite and maceriate fabrics in the Early Palaeozoic, as in Point Peak cones, columns and domes (see *Fabric development*, below). These examples of Cambrian–Early Ordovician microstromatolites may resemble some Proterozoic examples, but are generally much more irregular in overall form, typically occurring as short columns with disjunct branches, and largely consist of peloidal to microclotted irregularly laminated fabrics (Fig. 6). The authors interpret them as likely essentially biogenic in origin. It remains to be seen whether middle Cambrian–Early Ordovician examples mark a final significant development of microstromatolites as fabric-modellers and sediment producers, or whether they represent a novel Early Palaeozoic development, distinct from that of the Proterozoic.

Sponges

Lithistids, and possible keratosans, in and on the stable substrates provided by Point Peak columns, and particularly in column interiors, reflect the environmental resilience of sponges and their ability to interact with microbes (Brunton & Dixon, 1994; Zhuravlev, 2001). Keratosans have been reported in the Proterozoic (Turner, 2021), archaeocyaths were locally volumetrically important in lower Cambrian reefs (James & Debrenne, 1980), and lithistids were present in the mid–late Cambrian (Hamdi *et al.*, 1995; Zhuravlev, 1996, 2001; Lee *et al.*, 2015; Lee & Riding, 2018). Stromatolite–keratolite forms the ragged columns that characterize the interiors of Lower Biostrome large rimmed columns. This association, which also occurs in maceriate forms in Shandong (Lee *et al.*, 2014) (see *Maceriate fabric*, above), has been described in detail in late Cambrian *Cryptozoön* domes (Lee &

Riding, 2021b) and Cambrian–Ordovician branched columns (Lee & Riding, 2021a) in north-eastern Laurentia. Its approximately coeval occurrence in the Wilberns Formation reinforces the likelihood that stromatolite–keratolite was a widespread consortial – even mutualistic – association (Lee & Riding, 2021a).

However, fossilized keratosan spongin network can readily be overlooked. The difficulty of its confident recognition is mainly due to its simplicity and small size, as well as the ease with which it can be confused with a variety of clotted ('grumous') microfabrics (Cayeux, 1935, p. 271; Bathurst, 1976, p. 511; Flügel, 2004, p. 373; Grey & Awramik, 2020, p. 213, 224), such as those that occur in microbial and fenestral carbonates (Lee & Riding, 2022). Nonetheless, well-preserved keratolite fabric is distinctive. It was described by Hall (1883), in Cambrian *Cryptozöon*, as "minute, irregular canaliculi which branch and anastomose without regularity"; by Gürich (1906) in Mississippian *Spongiostroma* as 'canaux du tissu'; and by Walter (1972), in Cambrian *Madiganites*, as 'vermiform fabric'. It was identified as "demosponge ('bath sponge') spongin network" in Devonian reefs by Reitner *et al.* (2001, fig. 1). Luo & Reitner (2016) and Luo *et al.* (2022) proposed criteria to assist recognition of "Keratosa'-type demosponges in carbonates". Key features include: (i) anastomose tubes of (ii) relatively constant diameter in (iii) homogeneous micrite, that occupy (iv) delimited areas. Comparison of Point Peak samples with variably preserved upper Cambrian keratolite fabric from Newfoundland (Fig. 24A to C) illustrates how diagenetic alteration can obscure the primary fabric through irregular tube enlargement that ultimately destroys the distinctive branching pattern. By comparison, the fabric of the Point Peak example in Fig. 24D appears less altered than that in Fig. 16A. Further work is required to determine the extent of keratosan fabric in Point Peak deposits; particularly within Lower Biostrome columns.

These considerations also draw attention to the pitfall of relying solely on field appearance to identify stromatolites; confirming the perceptive studies of Luo & Reitner (2014, 2016) which show that interlayered stromatolite–keratolite can so closely resemble stromatolite in the field, and even in slabs, that these fabrics can be difficult to confidently distinguish without the aid of thin-sections. Lithistid sponges can also be hard to recognize in the field (Figs 10 and 11F)

(e.g. Pham *et al.*, 2021). As well as occupying similar environmental requirements, co-occurring sponges and microbial mats may have cooperated in sharing substrates, and even bacteria and nutrients (Lee & Riding, 2021b). The variety, long history, and substantial role of sponge–microbial carbonates in reef formation (Hartman *et al.*, 1980; Wood, 1990; Reitner & Keupp, 1991; Brunton & Dixon, 1994; Zhuravlev, 2001; Wulff, 2016) continues to offer fruitful opportunities for research.

Fabric development

Relatively good preservation of Point Peak cones, domes and rimmed columns reveals connections between microfabric components and macrofabric. In order of abundance, the main *in situ* components are microstromatolite, stromatolite–keratolite consortium and calcimicrobes (mainly *Razumovskia*, *Renalcis* and *Tarthinia*) (Fig. 3). Substantial amounts of grainy sediment incorporated into the interiors of columns and macerate domes delimit and define the *in situ* components, thereby contributing significantly to overall microfabric formation. This is evident in Honey Creek dendrolite/thrombolite and Lower Biostrome ragged stromatolite–keratolite, column interiors.

Several insights emerge from study of these fabrics (Fig. 25):

- 1 Arrangement of a small component of one type, together with allochthonous matrix, can build a variety of distinctive macrofabrics (Fig. 19). Microstromatolite, the only component present in all four structures (cones, small and large rimmed columns, macerate domes) is a prime example. On its own, microstromatolite constructed isolated cones at Honey Creek, and also formed stromatolitic rims around Honey Creek and Lower Biostrome columns. Mixed with grainy sediment, microstromatolite creates dendrolite (in vertical section) in Honey Creek column interiors which appears distinctly thrombolitic in plan view (Fig. 25) (Riding, 2000, p. 192–193). Similarly, individual microstromatolite columns form thrombolite mesoclots in the middle Cambrian of Inner Mongolia (Lee *et al.*, 2016, fig. 3). Combinations of components are also common, for example where microstromatolite locally incorporates minor volumes of calcimicrobes in laminated column rims (Lower Biostrome) and also in macerate fabric (Upper Biostrome). Similarly, together,

fine-grained stromatolite and keratolite form laminated columns within matrix in Lower Biostrome column cores and laminated domes in the Upper Biostrome.

2 Column interior fabrics often appear distinctly different in plan and vertical view. Microstromatolites in Honey Creek column interior matrix are dendrolitic in vertical section and thrombolitic in plan view. Irregularly ragged stromatolite–keratolite columns observed in vertical sections of Lower Biostrome column interiors display complex network patterns in plan view (Fig. 25) and vertically anastomose microstromatolite–calcimicrobe columns with matrix in Upper Biostrome domes are meandri-form (macerate) in plan view.

3 Deposits that superficially resemble ‘microbial carbonate’ in the field, can contain intimately associated animal fossils, such as sponges, as in Lower Biostrome stromatolite–keratolite column

interiors and in Upper Biostrome laminated domes. These are broadly comparable with fabrics in *Cryptozoön* at its type-locality in New York State (Lee & Riding, 2021b).

4 The two types of stromatolite-rimmed column identified here (Honey Creek and Lower Biostrome) both have grainy interiors hosting complex fabrics (dendrolitic and lobate at Honey Creek, laminated and patterned in the Lower Biostrome). In both cases the rims are essentially composed of layers of densely juxtaposed microstromatolite. It remains to be seen whether ‘rimmed thrombolites’ elsewhere also consist of microstromatolite.

5 Mottled fabrics associated with layered stromatolite–keratolite consortia and grainy matrix, as in Lower Biostrome column interiors, can be further complicated by burrows that localize secondary dolomitization (Fig. 25). In contrast, with less dolomitization, similar small

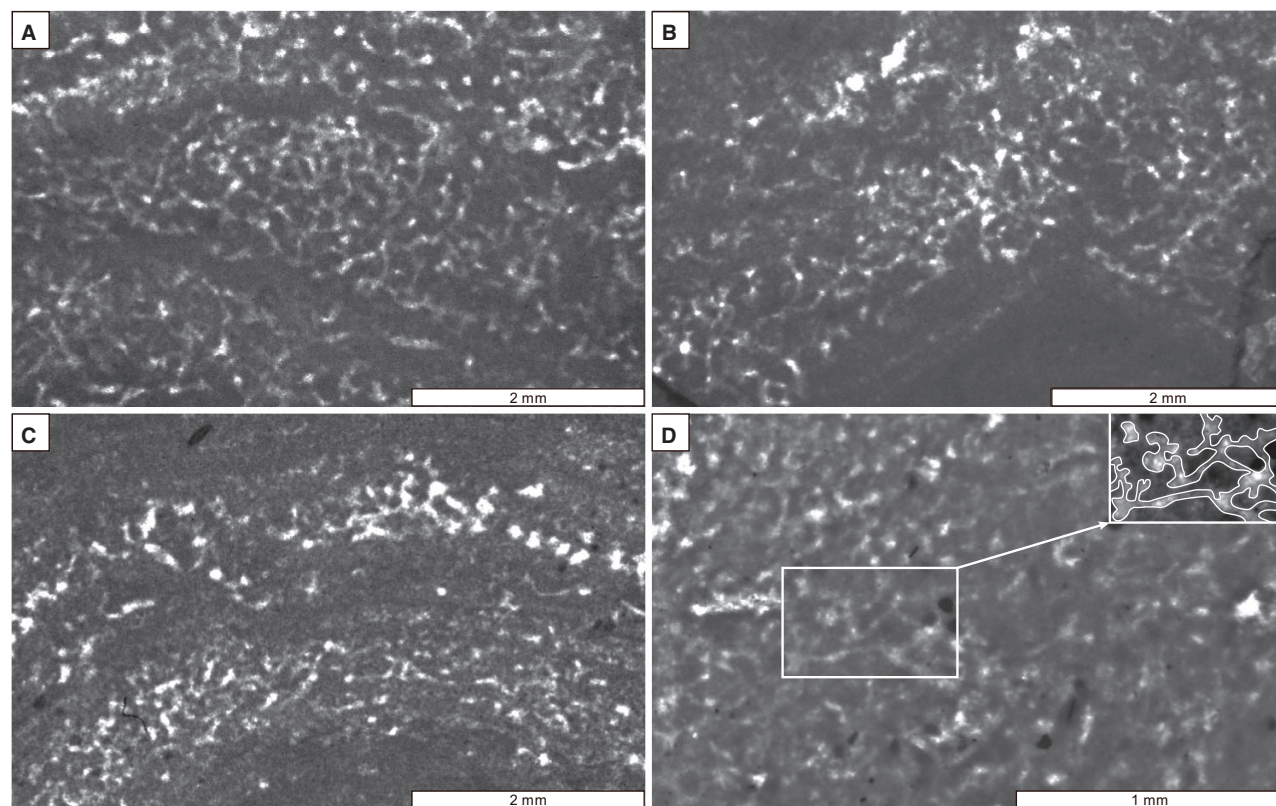


Fig. 24. Various preserved examples of keratolite. (A) to (C) Upper Cambrian keratolite from Newfoundland, Canada (for locality information, see Lee & Riding, 2021a). (A) Relatively well-preserved keratolite (after Lee & Riding, 2021a, fig. 5D). (B) Transition from well (lower left, lower right) to poorly (centre, top) preserved keratolite. Note local diagenetic enlargement of tubules. (C) Contrast between better (lower part) and less well (upper part) preserved keratolite layers intercalated within stromatolite (detail of Lee & Riding, 2021a, fig. 5B). (D) Poorly preserved keratolite from the Lower Biostrome (detail of Fig. 11B). Line drawing of vermiform fabric (inset, upper right) shows characteristic anastomose branching network.

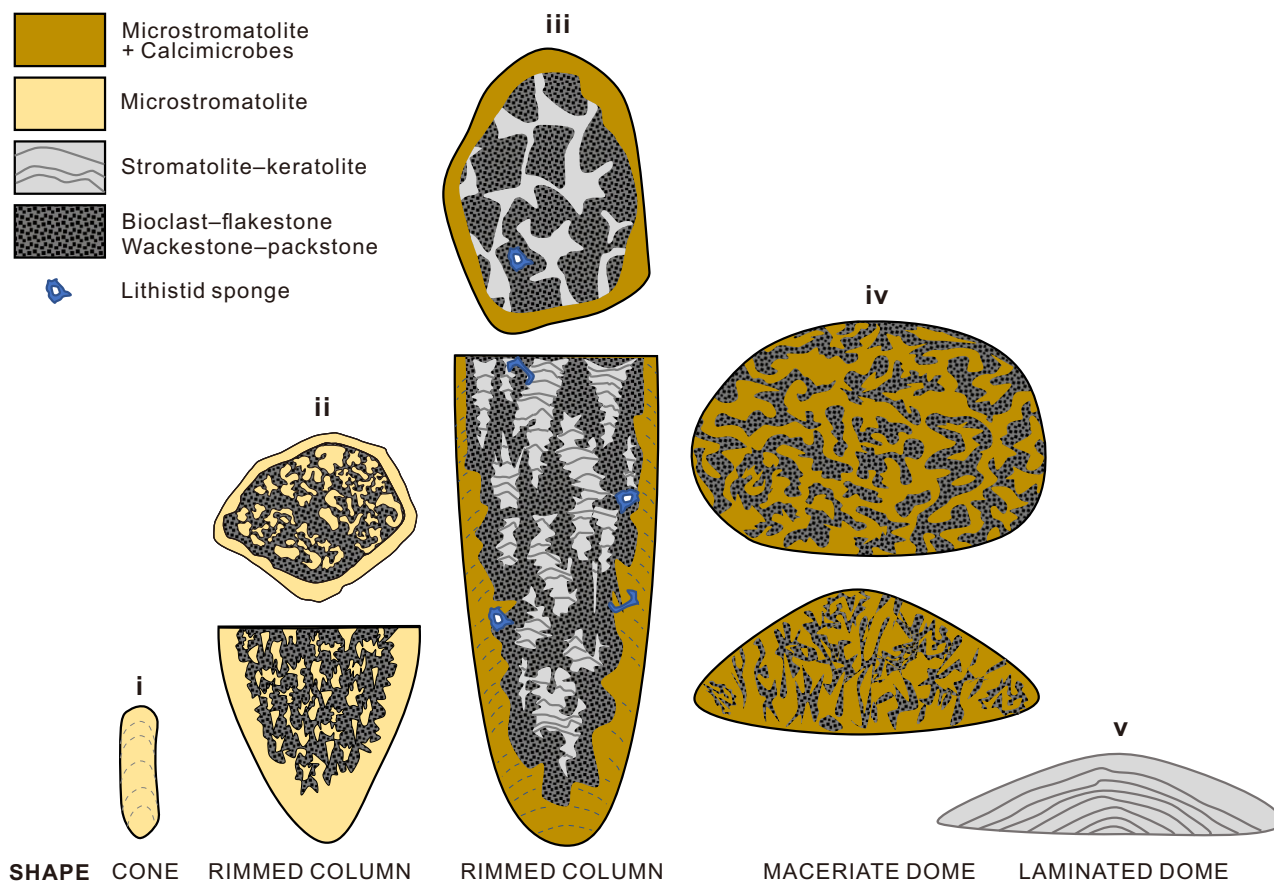


Fig. 25. Comparative summary of Honey Creek and San Saba Bridge cone-column-dome shapes, fabrics and components. (i) Honey Creek cones are stromatolitic macrofabrics virtually entirely composed of innumerable juxtaposed and aligned microstromatolites. (ii) Honey Creek rimmed columns have layered microstromatolite rims surrounding grainy interiors with abundant dendrolitic microstromatolites, that in plan view appear thrombolitic and are often arranged in large lobate patterns. (iii) San Saba Bridge Lower Biostrome columns have microstromatolite rims locally incorporating calcimicrobes. The column interiors consist of ragged stromatolite-keratolite columns surrounded by poorly sorted micro-burrowed matrix, both of which are partly dolomitized. In cross-section, column interiors show irregular netlike to polygonal patterns. Lithistid sponges (for example, *Wilbernicyathus*) are locally common in rims and interiors. (iv) San Saba Bridge Upper Biostrome maceriate domes composed of microstromatolite with small scattered clusters of calcimicrobes. The maceriate fabric is anastomose in vertical section and meandriform in cross-section, with matrix-filled interspaces. (v) San Saba Bridge Upper Biostrome laminated domes consist of stromatolite with interlayered keratolite.

burrows did not significantly modify primary macrofabrics formed by stromatolite-keratolite consortia, as in Upper Biostrome layered domes (Figs 15 and 16).

6 Maceriate fabric, composed of microstromatolite with subordinate calcimicrobes in the Upper Biostrome, might provide the first documented example of well-preserved *Favosamaceria*. However, it would be premature to infer that this example provides a unique model for these still poorly understood structures that are thought to be typically late Cambrian–Early Ordovician in age (Shapiro & Awramik, 2006).

Depositional environment

Thick rims surrounding Honey Creek and Lower Biostrome columns suggest that current movement (Lehrmann *et al.*, 2020), indicated by surrounding coarse sediment (Fig. 4), and localized column elongation and orientation (Figs 7 and 8), favoured precipitative growth of dense layers of microstromatolite. These appear to have been fundamental for the development of strong erect columns with grainy cores that provided stable substrates for keratosan and, locally, lithistid sponges within otherwise wave and current-swept

environments. These columns therefore provided stable elevated substrates well-suited to colonization in current-swept locations. This supports the supposition by Tarhan *et al.* (2013) that “microbialites may have provided havens from harsh environmental conditions for early metazoans”. In the Upper Biostrome, amelioration of these conditions appears instead to have favoured formation of maceriate domes that lack preferred orientation and show lower relief than either Honey Creek or Lower Biostrome columns.

Khanna *et al.* (2020a) compared Point Peak columns with present-day Exuma and Shark Bay examples. They describe small circular microbial columns, each with its own ‘rind’, clustered into progressively larger circular to oblong groups, also surrounded by their own micritic ‘rind’, even when 100 m or more in length. Their detailed morphometric analysis of upper Point Peak microbial buildups at the James River outcrop demonstrates that, as their size increased, column shapes evolved from circular to oblong in plan view, and that north-east/south-west (present-day) alignment progressively increased. Khanna *et al.* (2020b) infer that this paralleled late Cambrian palaeo-trade wind and tidal current directions.

Honey Creek columns are small and rounded, whereas those in the Lower Biostrome at San Saba Bridge are larger and much more varied in plan view, ranging from elongate to ovoid, and also show complex merging patterns (Fig. 9B). These Lower Biostrome columns also commonly exhibit generally north-east/south-west orientation, as noted by Portnoy (1987) and Ruppel & Kerans (1987, fig. 13), similar to those observed by Khanna *et al.* (2020a,b) at the Llano River and James River localities *ca* 50 km to the south. Extensive outcrops of Early Ordovician “inner shelf margin buildups” exposed *ca* 4 km east of Hawker Bay on the Grinnell Peninsula (north-west Devon Island, Nunavut, Canada) (de Freitas & Mayr, 1995) show large-scale clusters and mounds of numerous coalescent rimmed columns. These appear to closely resemble Lower Biostrome columns, and support the suggestion (Khanna *et al.*, 2020b) that relatively unoriented individual columns can form groups of elongate current-oriented mounds.

CONCLUSIONS

1 Biostromes in shallow grainy current-swept normal marine environments at Honey Creek

and San Saba Bridge in the upper Cambrian Point Peak Member of the Wilberns Formation, central Texas, contain well-preserved cones, two types of rimmed column, and laminated and maceriate domes. These were constructed by various combinations of microstromatolite, calcimicrobes (*Razumovskia*, *Renalcis* and *Tarthinia*) and stromatolite–keratolite (keratolite sponge carbonate). In addition, they locally contain common lithistid sponges and rare crinoids, and are surrounded by grainy sediment dominated by trilobite, brachiopod and gastropod bioclasts.

2 These examples show how microbial and sponge components combined to form the stromatolite, dendrolite, thrombolite and maceriate macrofabrics observed in cones, rimmed columns and domes. Microstromatolite – arranged in layers – created macroscale stromatolite fabric and – as dendritic clusters in matrix – created macroscale dendrolite fabric (for example, Honey Creek). Microstromatolite with subordinate calcimicrobe clusters created thrombolitic mesofabric within maceriate domes (Upper Biostrome) and the rims of large columns (Lower Biostrome). Irregularly ragged stromatolite–keratolite consortia dominate patterned cores of large current-oriented columns (for example, Lower Biostrome, San Saba Bridge) and formed laminated domes (Upper Biostrome, San Saba Bridge). Overall, thrombolite fabrics in these samples were formed by both vertical and horizontal sections of microstromatolite, locally with clusters of calcimicrobes. These examples therefore show that a single component, microstromatolite, on its own or with minor amounts of calcimicrobes, could construct a variety of fabrics including stromatolite, dendrolite–thrombolite and maceriate.

3 Rimmed columns reflect persistent current-swept conditions that may have promoted microstromatolite and calcimicrobe precipitation. Upwardly expanding microstromatolite cones created columns with slightly depressed interiors that accumulated poorly sorted grainy sediment through a ‘bucket effect’. These were colonized by dendrolitic microstromatolites at Honey Creek, and by stromatolite–keratolite consortia – that also provided substrates for lithistid sponges – in the Lower Biostrome. Continued upward growth created decimetre to metre-scale rimmed columns with centimetre-thick steep-sided rims. The patterned interiors of Lower Biostrome columns largely reflect primary arrangement of biolithite in grainy matrix

followed by fabric selective dolomitization. Small burrows in column interiors had a minor effect on the primary fabric, but significantly influenced dolomitization. Similar laminated rimmed columns with mottled interiors ('thrombolites with stromatolite rims') have been widely reported from Cambrian–Early Ordovician shallow marine carbonates.

4 *Favosamaceria*-like maceriate domes (Upper Biostrome) with relatively low synoptic relief primarily consist of microstromatolite and subordinate calcimicrobes. They formed in less grainy environments than rimmed columns in the same succession, and may have experienced less wave and current action. Point Peak maceriate domes help to elucidate the origins of these enigmatic widely distributed and probably time-specific structures.

5 Dolomitization preferentially affects grainy fabrics and locally obscures interpretation of associated microbial carbonates, as in Lower Biostrome column interiors. It is likely that this effect has significantly hindered interpretation of Cambrian–Ordovician column and maceriate dome fabrics generally.

6 To parallel stromatolite definition, the authors define thrombolite as *macroscopically clotted benthic microbial carbonate*. Thrombolite recognition requires discrimination between primary microbial clots and secondarily produced clot-like fabrics. Although burrowing has been suggested as a major factor in the formation of thrombolite fabric, this is not supported by well-preserved Point Peak examples.

ACKNOWLEDGEMENTS

We are grateful to two anonymous reviewers and Associate Editor Ying Zhou for detailed and perceptive comments that helped to improve the manuscript. This study was supported by a National Research Foundation of Korea grant to JHL (2022R1A2B5B02001184). We thank Yeoncheol Ha for rock preparation, and Liyuan Liang for help in the field. The authors declare no conflict of interest.

DATA AVAILABILITY STATEMENT

The data that support the findings of this study are available from the corresponding author upon reasonable request.

REFERENCES

- Adachi, N., Ezaki, Y., Liu, J. and Cao, J. (2009) Early Ordovician reef construction in Anhui Province, South China: a geobiological transition from microbial- to metazoan-dominant reefs. *Sediment. Geol.*, **220**, 1–11.
- Ahr, W.M. (1971) Paleoenvironment, algal structures, and fossil algae in the Upper Cambrian of central Texas. *J. Sediment. Petrol.*, **41**, 205–216.
- Aitken, J.D. (1967) Classification and environmental significance of cryptalgal limestones and dolomites, with illustrations from the Cambrian and Ordovician of southwestern Alberta. *J. Sediment. Petrol.*, **37**, 1163–1178.
- Aitken, J.D. and Narbonne, G.M. (1989) Two occurrences of Precambrian thrombolites from the Mackenzie Mountains, northwestern Canada. *Palaios*, **4**, 384–388.
- Allwood, A.C., Rosing, M.T., Flannery, D.T., Hurowitz, J.A. and Heirwegh, C.M. (2018) Reassessing evidence of life in 3,700-million-year-old rocks of Greenland. *Nature*, **563**, 241–244.
- Alsalem, O.B., Fan, M., Zamora, J., Xie, X. and Griffin, W.R. (2018) Paleozoic sediment dispersal before and during the collision between Laurentia and Gondwana in the Fort Worth Basin, USA. *Geosphere*, **14**, 325–342.
- Álvarez, J.J., Ahlberg, P., Babcock, L.E., Bordonaro, O.L., Choi, D.K., Cooper, R.A., Ergaliev, G.K., Gapp, I.W., Pour, M.G., Hughes, N.C., Jago, J.B., Korovnikov, I., Laurie, J.R., Lieberman, B.S., Paterson, J.R., Pegel, T.V., Popov, L.E., Rushton, A.W.A., Sukhov, S.S., Tortello, M.F., Zhou, Z. and Zylinska, A. (2013) Global Cambrian trilobite palaeobiogeography assessed using parsimony analysis of endemism. In: *Early Palaeozoic Biogeography and Palaeogeography* (Eds Harper, D.A.T. and Servais, T.), *Geological Society, London, Memoirs*, **38**, 273–296.
- Armella, C. (1994) Thrombolitic-stromatolitic cycles of the Cambro-Ordovician boundary sequence, Precordillera Oriental basin, Western Argentina. In: *Phanerozoic Stromatolites II* (Eds Bertrand-Sarfati, J. and Monty, C.L.V.), pp. 421–441. Kluwer Academic, Dordrecht.
- Arp, G. (1995) Lacustrine bioherms, spring mounds, and marginal carbonates of the Ries-impact-crater (Miocene, southern Germany). *Facies*, **33**, 35–89.
- Awramik, S.M. (1971) Precambrian columnar stromatolite diversity: reflection of metazoan appearance. *Science*, **174**, 825–827.
- Awramik, S.M., Corsetti, F.A. and Shapiro, R.S. (1994) *Pre-Symposium Excursion: Death Valley Region. Death Valley International Stromatolite Symposium Guidebook*, p. 43. Department of Geological Sciences, University of California, Santa Barbara.
- Barlow, E., Van Kranendonk, M.J., Yamaguchi, K.E., Ikehara, M. and Lepland, A. (2016) Lithostratigraphic analysis of a new stromatolite-thrombolite reef from across the rise of atmospheric oxygen in the Paleoproterozoic Turee Creek group, Western Australia. *Geobiology*, **14**, 317–343.
- Barnes, V.E. and Bell, W.C. (1977) The Moore Hollow Group of Central Texas. *The University of Texas at Austin, Bureau of Economic Geology, Report of Investigations*, **88**, 169 pp.
- Bathurst, R.G.C. (1976) *Carbonate Sediments and their Diagenesis. Developments in Sedimentology*, **12**, Elsevier, 658 pp.
- Bernhard, J.M., Edgcomb, V.P., Visscher, P.T., McIntyre-Wressnig, A., Summons, R.E., Bouxsein, M.L., Louis, L.

- and Jęglinski, M. (2013) Insights into foraminiferal influences on microfabrics of microbialites at Highborne Cay, Bahamas. *Proc. Natl. Acad. Sci.*, **110**, 9830–9834.
- Black, M.** (1933) The algal sedimentation of Andros Island Bahamas. *Philos. Trans. R. Soc. London B Biol. Sci.*, **222**, 165–192.
- Bornemann, J.G.** (1886) Die Versteinerungen des Cambrischen Schichtensystems der Insel Sardinien nebst vergleichenden Untersuchungen über analoge Vorkommnisse aus anderen Ländern. *Verhandlungen der Kaiserlichen Leopoldinisch-Carolinischen-Deutschen Akademie der Naturforscher*, **51**, 1–148 (in German).
- Boyle, R.A., Dahl, T.W., Dale, A.W., Shields-Zhou, G.A., Zhu, M., Brasier, M.D., Canfield, D.E. and Lenton, T.M.** (2014) Stabilization of the coupled oxygen and phosphorus cycles by the evolution of bioturbation. *Nat. Geosci.*, **7**, 671–676.
- Bridge, J., Barnes, V.E. and Cloud, P.E.J.** (1947) Stratigraphy of the Upper Cambrian, Llano Uplift, Texas. *Geol. Soc. Am. Bull.*, **58**, 109–124.
- Brunton, F.R. and Dixon, O.A.** (1994) Siliceous sponge-microbe biotic associations and their recurrence through the Phanerozoic as reef mound constructors. *Palaios*, **9**, 370–387.
- Buick, R., Dunlop, J.S.R. and Groves, D.I.** (1981) Stromatolite recognition in ancient rocks: an appraisal of irregularly laminated structures in an early Archaean chert-barite unit from North Pole, Western Australia. *Alcheringa*, **5**, 161–181.
- Burne, R.V. and Moore, L.S.** (1993) Microatoll microbialites of Lake Clifton, Western Australia: morphological analogues of *Cryptozoön proliferum* Hall, the first formally-named stromatolite. *Facies*, **29**, 149–168.
- Cayeux, L.** (1935) *Les Roches Sédimentaires de France: Roches Carbonatées*, p. 463. Masson et Cie, Paris.
- Chafetz, H.S.** (1973) Morphological evolution of Cambrian algal mounds in response to a change in depositional environment. *J. Sediment. Petrol.*, **43**, 435–446.
- Chen, J., Lee, J.-H. and Woo, J.** (2014) Formative mechanisms, depositional processes, and geological implications of Furongian (late Cambrian) reefs in the North China Platform. *Palaeogeogr. Palaeoclimatol. Palaeoecol.*, **414**, 246–259.
- Cloud, P.E.J.** (1942) Notes on stromatolites. *Am. J. Sci.*, **240**, 363–379.
- Cloud, P.E. and Barnes, V.E.** (1948) The Ellenburger Group of Central Texas. *University of Texas, Bureau of Economic Geology Publication*, **4621**, 473 pp.
- Cloud, P.E., Barnes, V.E. and Bridge, J.** (1945) *Stratigraphy of the Ellenburger Group in Central Texas—A Progress Report*, Vol. **4301**, pp. 133–161. University of Texas, Austin, Bureau of Economic Geology Publication, Austin.
- Cocks, L.R.M. and Torsvik, T.H.** (2011) The Palaeozoic geography of Laurentia and western Laurussia: a stable craton with mobile margins. *Earth-Sci. Rev.*, **106**, 1–51.
- Comstock, T.B.** (1889) A preliminary report on the central mineral region of Texas. In: *First Annual Report of the Geological Survey of Texas*. (Ed. Dumble, E.T.), pp. 239–378. Department of Agriculture, Insurance, Statistics, and History, Austin, TX.
- Coulson, K.P.** (2016) Microbialite elongation by means of coalescence: an example from the middle Furongian (upper Cambrian) Notch Peak Formation of western Utah. *Facies*, **62**, 20.
- Coulson, K.P. and Brand, L.R.** (2016) Lithistid sponge-microbial reef-building communities construct laminated, upper Cambrian (Furongian) ‘stromatolites’. *Palaios*, **31**, 358–370.
- Crowley, A.J. and Hendricks, L.** (1945) Lower Ordovician and Upper Cambrian subsurface subdivisions in north-central Texas. *AAPG Bulletin*, **29**, 413–425.
- Dake, C.L. and Bridge, J.** (1932) Faunal correlation of the Ellenburger Limestone of Texas. *Geol. Soc. Am. Bull.*, **43**, 725–748.
- Doemel, W.N. and Brock, T.D.** (1974) Bacterial stromatolites: origin of laminations. *Science*, **184**, 1083–1085.
- Donaldson, J.A.** (1963) *Stromatolites in the Denault Formation, Marion Lake, Coast of Labrador, Newfoundland*. *Geological Survey of Canada Bulletin*, **102**, 33 pp.
- Donovan, R.N. and Ragland, D.A.** (1986) Paleozoic stratigraphy of the Slick Hills, southwestern Oklahoma. In: *The Slick Hills of Southwestern Oklahoma - Fragments of an Aulacogen?* (Ed. Donovan, R.N.), *Oklahoma Geological Survey Guidebook*, **24**, 13–16.
- Drosdova, N.A.** (1975) Algae in Lower Cambrian deposits of western Mongolia. *Joint Soviet Mongolian Paleontol. Exped. Trans.*, **2**, 302–303 (in Russian).
- Fagerstrom, J.A.** (1987) *The Evolution of Reef Communities*, John Wiley and Sons, New York, NY, 600 pp.
- Feldmann, M. and McKenzie, J.A.** (1997) Messinian stromatolite-thrombolite associations, Santa Pola, SE Spain: an analogue for the Palaeozoic? *Sedimentology*, **44**, 893–914.
- Feldmann, M. and McKenzie, J.A.** (1998) Stromatolite-thrombolite association in a modern environment, Lee Stocking Island, Bahamas. *Palaios*, **13**, 201–212.
- Flügel, E.** (2004) *Microfacies of Carbonate Rocks: Analysis, Interpretation and Application*, p. 976. Springer, Berlin.
- de Freitas, T. and Mayr, U.** (1995) Kilometre-scale microbial buildups in a rimmed carbonate platform succession, Arctic Canada: new insight on Lower Ordovician reef facies. *Bull. Canadian Petrol. Geol.*, **43**, 407–432.
- Fritz, R.D., Medlock, P., Kuykendall, M.J. and Wilson, J.L.** (2012) The geology of the Arbuckle Group in the midcontinent: sequence stratigraphy, reservoir development, and the potential for hydrocarbon exploration. In: *The Great American Carbonate Bank: The Geology and Economic Resources of the Cambrian-Ordovician Sauk Megasequence of Laurentia* (Eds Derby, J.R., Fritz, R.D., Longacre, S.A., Morgan, W.A. and Sternbach, C.A.), *AAPG Memoir*, **98**, 203–273.
- Garrett, P.** (1970) Phanerozoic stromatolites: noncompetitive ecologic restriction by grazing and burrowing animals. *Science*, **169**, 171–173.
- Geyer, G.** (2019) A comprehensive Cambrian correlation chart. *Episodes*, **42**, 321–332.
- Ginsburg, R.N. and Lowenstam, H.A.** (1958) The influence of marine bottom communities on the depositional environment of sediments. *J. Geol.*, **66**, 310–318.
- Glumac, B. and Walker, K.R.** (1997) Selective dolomitization of Cambrian microbial carbonate deposits: a key to mechanisms and environments of origin. *Palaios*, **12**, 98–110.
- Grey, K. and Awramik, S.M.** (2020) *Handbook for the Study and Description of Microbialites*. *Geological Survey of Western Australia Bulletin*, **147**, 278 pp.
- Grey, K. and Thorne, A.M.** (1985) Biostratigraphic significance of stromatolites in upward shallowing

- sequences of the early Proterozoic Duck Creek Dolomite, Western Australia. *Precambrian Res.*, **29**, 183–206.
- Griffin, K.M.** (1988) *Sedimentology and Paleontology of Thrombolites and Stromatolites of the Upper Cambrian Nopah Formation and their Modern Analog on Lee Stocking Island, Bahamas*. M.S. thesis, p. 131. University of California, Santa Barbara.
- Grotzinger, J.P.** (1986) Evolution of early Proterozoic passive-margin carbonate platform, Rocknest Formation, Wopmay Orogen, Northwest Territories, Canada. *J. Sediment. Petrol.*, **56**, 831–847.
- Grotzinger, J.P.** and **James, N.P.** (2000) Precambrian carbonates: evolution of understanding. In: *Carbonate Sedimentation and Diagenesis in the Evolving Precambrian World* (Eds Grotzinger, J.P. and James, N.P.), *SEPM Special Publication*, **67**, 3–20.
- Grotzinger, J.P.** and **Read, J.F.** (1983) Evidence for primary aragonite precipitation, lower Proterozoic (1.9 Ga) Rocknest dolomite, Wopmay orogen, Northwest Canada. *Geology*, **11**, 710–713.
- Grotzinger, J.P.**, **Watters, W.A.** and **Knoll, A.H.** (2000) Calcified metazoans in thrombolite-stromatolite reefs of the terminal Proterozoic Nama Group, Namibia. *Paleobiology*, **26**, 334–359.
- Guppy, H.B.** (1886) Notes on the characters and mode of formation of the coral reefs of the Solomon Islands. *Proc. R. Soc. Edinburgh*, **13**, 857–904.
- Gürich, G.** (1906) Les spongiostromides du Viséen de la Province de Namur. *Musée royal d'histoire naturelle de Belgique, Mémoires*, **3**, 1–55 (in French).
- Hall, J.** (1883) *Cryptozoön*, n.g.; *Cryptozoön proliferum*, nsp. In: *New York State Museum of Natural History, 36th Annual Report of the Trustees*.
- Ham, W.E.** (1952) Algal origin of the “birdseye” limestone in the McLish formation. *Proc. Oklahoma Acad. Sci.*, **33**, 200–203.
- Hamdi, B.**, **Roazanov, A.Y.** and **Zhuravlev, A.Y.** (1995) Latest Middle Cambrian metazoan reef from northern Iran. *Geol. Mag.*, **132**, 367–373.
- Hartman, W.D.**, **Wendt, J.W.** and **Wiedenmayer, F.** (1980) *Living and fossil sponges (Notes for a short course)*. *Sedimentia*, **8**, University of Miami, 274 pp.
- Harwood, C.L.** and **Sumner, D.Y.** (2012) Origins of microbial microstructures in the Neoproterozoic Beck Spring Dolomite: variations in microbial community and timing of lithification. *J. Sediment. Res.*, **82**, 709–722.
- Harwood Theisen, C.** and **Sumner, D.Y.** (2016) Thrombolite fabrics and origins: influences of diverse microbial and metazoan processes on Cambrian thrombolite variability in the Great Basin, California and Nevada. *Sedimentology*, **63**, 2217–2252.
- Hintze, L.F.**, **Taylor, M.E.** and **Miller, J.F.** (1988) *Upper Cambrian-Lower Ordovician Notch Peak Formation in Western Utah*. *U.S. Geological Survey Professional Paper*, **1393**, 30 pp.
- Hoffman, P.** (1972) Proterozoic stromatolites of cyclic shelf, mounded shelfedge and turbidite offshelf facies, northwestern Canadian shield: ABSTRACT. *AAPG Bull.*, **56**, 627–628.
- Hofmann, H.J.** (1969a) *Stromatolites from the Proterozoic Animikie and Sibley Groups, Ontario*. *Geological Survey of Canada Paper*, **68-69**, 77 pp.
- Hofmann, H.J.** (1969b) *Attributes of Stromatolites*. *Geological Survey of Canada Paper*, **69-39**, 58 pp.
- Hofmann, H.J.** (1973) Stromatolites: characteristics and utility. *Earth-Sci. Rev.*, **9**, 339–373.
- Hofmann, H.J.** (1975) Stratiform Precambrian stromatolites, Belcher Islands, Canada; relations between silicified microfossils and microstructure. *Am. J. Sci.*, **275**, 1121–1132.
- Hofmann, H.J.** (1977) On Aphebian stromatolites and Riphean stromatolite stratigraphy. *Precambrian Res.*, **5**, 175–205.
- Hofmann, H.J.** and **Jackson, G.D.** (1987) Proterozoic ministromatolites with radial-fibrous fabric. *Sedimentology*, **34**, 963–971.
- Hong, J.**, **Choh, S.-J.** and **Lee, D.-J.** (2015) Untangling intricate microbial–sponge frameworks: the contributions of sponges to Early Ordovician reefs. *Sediment. Geol.*, **318**, 75–84.
- Illing, L.V.** (1959) Deposition and diagenesis of some Upper Palaeozoic carbonate sediments in western Canada. In: *5th World Petroleum Congress, Section 1*, pp. 23–52. Wiley, Chichester.
- Jahnert, R.J.** and **Collins, L.B.** (2012) Characteristics, distribution and morphogenesis of subtidal microbial systems in Shark Bay, Australia. *Mar. Geol.*, **303–306**, 115–136.
- James, N.P.** and **Debrenne, F.** (1980) Lower Cambrian bioherms: pioneer reefs of the Phanerozoic. *Acta Palaeontol. Polonica*, **25**, 655–668.
- James, N.P.** and **Gravestock, D.I.** (1990) Lower Cambrian shelf and shelf margin buildups, Flinders Ranges, South Australia. *Sedimentology*, **37**, 455–480.
- Johns, R.A.**, **Dattilo, B.F.** and **Spincer, B.** (2007) Neotype and redescription of the Upper Cambrian anthaspidellid sponge, *Wilbernicyathus donegani* Wilson, 1950. *J. Paleol.*, **81**, 435–444.
- Kah, L.C.** and **Grotzinger, J.P.** (1992) Early Proterozoic (1.9 Ga) thrombolites of the Rocknest Formation, Northwest Territories, Canada. *Palaios*, **7**, 305–315.
- Kalkowsky, E.** (1908) Oolith und Stromatolith im norddeutschen Buntsandstein. *Zeitschrift der Deutschen Geologischen Gesellschaft*, **60**, 68–125 (in German).
- Karlstrom, K.**, **Hagadorn, J.**, **Gehrels, G.**, **Matthews, W.**, **Schmitz, M.**, **Madronich, L.**, **Mulder, J.**, **Pecha, M.**, **Giesler, D.** and **Crossey, L.** (2018) Cambrian Sauk transgression in the Grand Canyon region redefined by detrital zircons. *Nat. Geosci.*, **11**, 438–443.
- Karlstrom, K.E.**, **Mohr, M.T.**, **Schmitz, M.D.**, **Sundberg, F.A.**, **Rowland, S.M.**, **Blakey, R.**, **Foster, J.R.**, **Crossey, L.J.**, **Dehler, C.M.** and **Hagadorn, J.W.** (2020) Redefining the Tonto Group of Grand Canyon and recalibrating the Cambrian time scale. *Geology*, **48**, 425–430.
- Kennard, J.M.** and **James, N.P.** (1986) Thrombolites and stromatolites: two distinct types of microbial structures. *Palaios*, **1**, 492–503.
- Kerans, C.** (1990) Depositional Systems and Karst Geology of the Ellenburger Group (Lower Ordovician), Subsurface West Texas. *The University of Texas at Austin, Bureau of Economic Geology Report of Investigations*, **193**, 63 pp.
- Khanna, P.**, **Hopson, H.H.**, **Droxler, A.W.**, **Droxler, D.A.**, **Lehrmann, D.**, **Kubik, B.**, **Proctor, J.**, **Singh, P.** and **Harris, P.M.** (2020a) Late Cambrian microbial build-ups, Llano area, Central Texas: a three-phase morphological evolution. *Sedimentology*, **67**, 1135–1160.
- Khanna, P.**, **Pyrcz, M.**, **Droxler, A.W.**, **Hopson, H.H.**, **Harris, P.M.** and **Lehrmann, D.J.** (2020b) Implications for controls on upper Cambrian microbial build-ups across multiple-

- scales, Mason County, Central Texas, USA. *Marine Petrol. Geol.*, **121**, 104590.
- Korde, K.B.** (1958) On aspects of fossil blue-green algae. *Mater Princ Palaeontol*, **2**, 112–119 (in Russian).
- Kornicker, L.S.** and **Boyd, D.W.** (1962) Shallow-water geology and environments of Alacran reef complex, Campeche Bank, Mexico. *AAPG Bulletin*, **46**, 640–673.
- Krasnopeeva, P.S.** (1937) Vodorosli i arkhetsiaty drevneyshikh tolshch Potekhinskogo rayona Khakassii. In: *Materialy po geologii Krasnoyarskogo kraya 3* (Ed. Usov, M.A.), pp. 1–51. West Siberian Geological Trust (in Russian), Tomsk.
- Kröger, B.** and **Penny, A.** (2020) Early–Middle Ordovician seascape-scale aggregation pattern of sponge-rich reefs across the Laurentia Paleocoast. *Palaios*, **35**, 524–542.
- Lanier, W.P.** (1986) Approximate growth rates of early Proterozoic microstromatolites as deduced by biomass productivity. *Palaios*, **1**, 525–542.
- Lee, J.-H., Chen, J., Choh, S.-J., Lee, D.-J., Han, Z.** and **Chough, S.K.** (2014) Furongian (late Cambrian) sponge-microbial maze-like reefs in the North China Platform. *Palaios*, **29**, 27–37.
- Lee, J.-H., Chen, J.** and **Chough, S.K.** (2010) Paleoenvironmental implications of an extensive maceriate microbialite bed in the Furongian Chaomidian Formation, Shandong Province, China. *Palaeogeogr. Palaeoclimatol. Palaeoecol.*, **297**, 621–632.
- Lee, J.-H., Chen, J.** and **Chough, S.K.** (2015) The middle–late Cambrian reef transition and related geological events: a review and new view. *Earth-Sci. Rev.*, **145**, 66–84.
- Lee, J.-H., Dattilo, B.F., Mrozek, S., Miller, J.F.** and **Riding, R.** (2019) Lithistid sponge-microbial reefs, Nevada, USA: filling the late Cambrian ‘reef gap’. *Palaeogeogr. Palaeoclimatol. Palaeoecol.*, **520**, 251–262.
- Lee, J.-H., Kim, B.-J., Liang, K., Park, T.-Y., Choh, S.-J., Lee, D.-J.** and **Woo, J.** (2016) Cambrian reefs in the western North China Platform, Wuhai, Inner Mongolia. *Acta Geol. Sin.*, **90**, 1946–1954.
- Lee, J.-H., Lee, H.S., Chen, J., Woo, J.** and **Chough, S.K.** (2014) Calcified microbial reefs in the Cambrian Series 2 of the North China Platform: implications for the evolution of Cambrian calcified microbes. *Palaeogeogr. Palaeoclimatol. Palaeoecol.*, **403**, 30–42.
- Lee, J.-H.** and **Riding, R.** (2018) Marine oxygenation, lithistid sponges, and the early history of Paleozoic skeletal reefs. *Earth-Sci. Rev.*, **181**, 98–121.
- Lee, J.-H.** and **Riding, R.** (2021a) Keratolite–stromatolite consortia mimic domical and branched columnar stromatolites. *Palaeogeogr. Palaeoclimatol. Palaeoecol.*, **571**, 110288.
- Lee, J.-H.** and **Riding, R.** (2021b) The ‘classic stromatolite’ *Cryptozoön* is a keratose sponge-microbial consortium. *Geobiology*, **19**, 189–198.
- Lee, J.-H.** and **Riding, R.** (2022) Recognizing sponge in *Spongiostroma* Gürich, 1906 from the Mississippian of Belgium. *J. Paleol.*, in press, 1–12.
- Lehrmann, D.J., Droxler, A.W., Harris, P., Minzoni, M., Droxler, D.A., Hopson, H.H., Kelleher, C., Khanna, P., Lehrmann, A.A., Lhemann, A., Mabry, G., Mercado, L., Proctor, J.M., Singh, P.** and **Yazbek, L.** (2020) Controls on microbial and oolitic carbonate sedimentation and stratigraphic cyclicity within a mixed carbonate-siliciclastic system: Upper Cambrian Wilberns Formation, Llano Uplift, Mason County, Texas, USA. *Deposit. Rec.*, **6**, 276–308.
- Li, F., Deng, J., Kershaw, S., Burne, R., Gong, Q., Tang, H., Lu, C., Qu, H., Zheng, B., Luo, S., Jin, Z.** and **Tan, X.** (2021) Microbialite development through the Ediacaran–Cambrian transition in China: distribution, characteristics, and paleoceanographic implications. *Global Planet. Change*, **205**, 103586.
- Logan, B.W.** (1961) *Cryptozoon* and associate stromatolites from the recent, Shark Bay, Western Australia. *J. Geol.*, **69**, 517–533.
- Loucks, R.G.** (2003) *Review of the Lower Ordovician Ellenburger Group of the Permian Basin, West Texas*. Bureau of Economic Geology, The University of Texas at Austin, Austin. https://www.beg.utexas.edu/files/content/beg/research/pbSyn/writ_synth/Ellenburger%20report.pdf.
- Luchinina, V.A.** (1975) Palaeoalgal characteristics of the Early Cambrian of the Siberian Platform. *Trans. Instit. Geol. Geophys. Siberian Branch, Novosibirsk*, **216**, 1–99 (in Russian).
- Luo, C., Pei, Y., Richoz, S., Li, Q.** and **Reitner, J.** (2022) Identification and current palaeobiological understanding of ‘Keratosa’-type nonspicular demosponge fossils in carbonates: with a new example from the lowermost Triassic, Armenia. *Life*, **12**, 1348.
- Luo, C.** and **Reitner, J.** (2014) First report of fossil ‘keratose’ demospores in Phanerozoic carbonates: preservation and 3-D reconstruction. *Naturwissenschaften*, **101**, 467–477.
- Luo, C.** and **Reitner, J.** (2016) ‘Stromatolites’ built by sponges and microbes - a new type of Phanerozoic bioconstruction. *Lethaia*, **49**, 555–570.
- Macintyre, I.G., Reid, R.P.** and **Steneck, R.S.** (1996) Growth history of stromatolite in Holocene fringing reef, Stocking Island, Bahamas. *J. Sediment. Res.*, **66**, 231–242.
- Maslov, V.P.** (1954) On the lower Silurian of eastern Siberia. In: *Voprosy Geologii Azii* (Ed. Shatskiy, N.S.), pp. 495–529. Akademii Nauk SSSR, Moskva (in Russian).
- Middleton, L.T.** (2001) Middle Cambrian offshore microbialites and shoaling successions, western Wyoming: implications for regional paleogeography. *Rocky Mount. Geol.*, **36**, 81–98.
- Miller, J.F., Evans, K.R.** and **Dattilo, B.F.** (2012) The Great American Carbonate Bank in the miogeocline of western Central Utah: tectonic influences on sedimentation. In: *The Great American Carbonate Bank: The Geology and Economic Resources of the Cambrian-Ordovician Sauk Megasequence of Laurentia* (Eds Derby, J.R., Fritz, R.D., Longacre, S.A., Morgan, W.A. and Sternbach, C.A.), *AAPG Memoir*, **98**, 769–854.
- Miller, J.F., Loch, J.D.** and **Taylor, J.F.** (2012) Biostratigraphy of Cambrian and Lower Ordovician strata in the Llano Uplift, Central Texas. In: *The Great American Carbonate Bank: The Geology and Economic Resources of the Cambrian-Ordovician Sauk Megasequence of Laurentia* (Eds Derby, J.R., Fritz, R.D., Longacre, S.A., Morgan, W.A. and Sternbach, C.A.), *AAPG Memoir*, **98**, 187–202.
- Monty, C.L.V.** (1973) Precambrian background and Phanerozoic history of stromatolitic communities, an overview. *Annales de la Société géologique de Belgique*, **96**, 585–624.
- Monty, C.L.V.** (1976) The origin and development of cryptalgal fabrics. In: *Stromatolites* (Ed. M.R. Walter), *Developments in Sedimentology*, **20**, 193–249.
- Morgan, W.A.** (2012) Sequence stratigraphy of the Great American Carbonate Bank. In: *The Great American Carbonate Bank: The Geology and Economic Resources of the Cambrian-Ordovician Sauk Megasequence of Laurentia*

- (Eds Derby, J.R., Fritz, R.D., Longacre, S.A., Morgan, W.A. and Sternbach, C.A.), *AAPG Memoir*, **98**, 37–82.
- Mosher, S.** (1998) Tectonic evolution of the southern Laurentian Grenville orogenic belt. *Geol. Soc. Am. Bull.*, **110**, 1357–1375.
- Mosher, S., Levine, J.S.F. and Carlson, W.D.** (2008) Mesoproterozoic plate tectonics: a collisional model for the Grenville-aged orogenic belt in the Llano Uplift, Central Texas. *Geology*, **36**, 55–58.
- Newell, D.L., Jensen, J.L., Frantz, C.M. and Vanden Berg, M.D.** (2017) Great Salt Lake (Utah) microbialite $\delta^{13}\text{C}$, $\delta^{18}\text{O}$, and $\delta^{15}\text{N}$ record fluctuations in lake biogeochemistry since the late Pleistocene. *Geochem. Geophys. Geosyst.*, **18**, 3631–3645.
- Nicholson, H.A. and Etheridge, R.** (1878) *A Monograph Of The Silurian Fossils Of The Girvan District In Ayrshire, With Special Reference To Those Contained In The 'Gray Collection'*, Blackwood, Edinburgh, 341 pp.
- Nomchong, B.J. and Van Kranendonk, M.J.** (2020) Diverse thrombolites from the c. 2.4 Ga Turee Creek Group, Western Australia. *Precambrian Res.*, **338**, 105593.
- Oliver, L.K. and Rowland, S.M.** (2002) Microbialite reefs at the close of the Proterozoic Eon: the Middle Member Deep Spring Formation at Mt. Dunfee, Nevada. In: *Proterozoic-Cambrian of the Great Basin and Beyond* (Ed. Corsetti, F.A.), *SEPM (Society for Sedimentary Geology) Pacific Section Book*, **93**, 97–122.
- Peng, S.C., Babcock, L.E. and Ahlberg, P.** (2020) The Cambrian Period. In: *Geologic Time Scale 2020* (Eds Gradstein, F.M., Ogg, J.G., Schmitz, M.D. and Ogg, G.M.), pp. 565–629, Elsevier, Amsterdam.
- Peters, S.E. and Gaines, R.R.** (2012) Formation of the 'Great Unconformity' as a trigger for the Cambrian explosion. *Nature*, **484**, 363–366.
- Pham, D., Hong, J. and Lee, J.-H.** (2021) Keratose sponge-microbial consortia in stromatolite-like columns and thrombolite-like mounds of the Lower Ordovician (Tremadocian) Mungok Formation, Yeongwol, Korea. *Palaeogeogr. Palaeoclimatol. Palaeoecol.*, **572**, 110409.
- Planavsky, N. and Ginsburg, R.N.** (2009) Taphonomy of modern marine Bahamian microbialites. *Palaio*, **24**, 5–17.
- Portnoy, M.B.** (1987) *A Study of Two Isolated Cambrian Stromatolitic Outcrops, Mason and McCulloch Counties, Texas*. M.S. thesis, p. 126. Texas Tech University, Lubbock.
- Pratt, B.R.** (1984) *Epiphyton and Renalcis* - diagenetic microfossils from calcification of coccooid blue-green algae. *J. Sediment. Petrol.*, **54**, 948–971.
- Pratt, B.R. and James, N.P.** (1982) Cryptalgal-metazoan bioherms of Early Ordovician age in the St George Group, western Newfoundland. *Sedimentology*, **29**, 543–569.
- Pratt, B.R. and James, N.P.** (1989) Coral-*Renalcis*-thrombolite reef complex of Early Ordovician age, St. George Group, western Newfoundland. In: *Reefs: Canada and Adjacent Areas* (Eds Geldsetzer, H.H.J., James, N.P. and Tebbutt, G.E.), *Canadian Society of Petroleum Geologists Memoir*, **13**, 224–230.
- Proctor, J.M., Droxler, A.W., Derzhi, N., Hopson, H.H., Harris, P., Khanna, P. and Lehrmann, D.J.** (2019) Upscaling lithology and porosity-type fractions from the micro- to the core-scale with thin-section petrography, dual-energy computed tomography, and rock typing: creation of diagenesis and porosity-type logs. *Interpretation*, **7**, B9–B32.
- Raaben, M.E.** (1980) Microstromatolites – a characteristic element of the lower Proterozoic stromatolite assemblage. *Doklady Akademia Nauk SSSR*, **250**, 734–737 (in Russian).
- Raviolo, M.M., Bordonaro, O.L. and Pratt, B.R.** (2010) Thrombolites (microbial reefs) of the form-genus *Favosamaceria* in the Upper Cambrian of the Eastern Precordillera, San Juan, Argentina. *Ameghiniana*, **47**, 331–341 (in Spanish with English abstract).
- Reid, R.P., Macintyre, I.G., Browne, K.M., Steneck, R.S. and Miller, T.** (1995) Modern marine stromatolites in the Exuma Cays, Bahamas: uncommonly common. *Facies*, **33**, 1–18.
- Reitner, J., Hühne, C. and Thiel, V.** (2001) Porifera-rich mud mounds and microbialites as indicators of environmental changes within the Devonian/Lower Carboniferous critical interval. *Terra Nostra*, **4**, 60–65.
- Reitner, J. and Keupp, H.** (1991) *Fossil and Recent Sponges*, Springer-Verlag, Berlin Heidelberg, 595 pp.
- Riding, R.** (1979) Origin and diagenesis of lacustrine algal bioherms at the margin of the Ries crater, Upper Miocene, southern Germany. *Sedimentology*, **26**, 645–680.
- Riding, R.** (1991a) Classification of microbial carbonates. In: *Calcareous Algae and Stromatolites* (Ed. Riding, R.), pp. 21–51. Springer-Verlag, Berlin.
- Riding, R.** (1991b) Calcified cyanobacteria. In: *Calcareous Algae and Stromatolites* (Ed. Riding, R.), pp. 55–87. Springer-Verlag, Berlin.
- Riding, R.** (1999) The term stromatolite: towards an essential definition. *Lethaia*, **32**, 321–330.
- Riding, R.** (2000) Microbial carbonates: the geological record of calcified bacterial-algal mats and biofilms. *Sedimentology*, **47**, 179–214.
- Riding, R.** (2001) Calcified algae and bacteria. In: *Ecology of the Cambrian Radiation* (Eds Zhuravlev, A.Y. and Riding, R.), pp. 445–473. Columbia University Press, New York, NY.
- Riding, R.** (2008) Abiogenic, microbial and hybrid authigenic carbonate crusts: components of Precambrian stromatolites. *Geologia Croatica*, **61**, 73–103.
- Riding, R.** (2011a) The nature of stromatolites: 3,500 million years of history and a century of research. In: *Advances in Stromatolite Geobiology* (Eds Reitner, J., Quéric, N.-V. and Arp, G.), *Lecture Notes in Earth Sciences*, **131**, 29–74.
- Riding, R.** (2011b) Microbialites, stromatolites, and thrombolites. In: *Encyclopedia of Geobiology* (Eds Reitner, J. and Thiel, V.), pp. 635–654. Springer, Heidelberg.
- Riding, R. and Awramik, S.M.** (2000) *Microbial Sediments*, Springer, Berlin, 331 pp.
- Riding, R., Awramik, S.M., Winsborough, B.M., Griffin, K.M. and Dill, R.F.** (1991) Bahamian giant stromatolites: microbial composition of surface mats. *Geol. Mag.*, **128**, 227–234.
- Riding, R., Braga, J.C. and Martin, J.M.** (1991) Oolite stromatolites and thrombolites, Miocene, Spain: analogues of recent giant Bahamian examples. *Sediment. Geol.*, **71**, 121–127.
- Riding, R. and Virgone, A.** (2020) Hybrid Carbonates: *in situ* abiotic, microbial and skeletal co-precipitates. *Earth-Sci. Rev.*, **208**, 103300.
- Riding, R. and Voronova, L.** (1985) Morphological groups and series in Cambrian calcareous algae. In: *Paleoalgology* (Eds Toomey, D.F. and Hitecki, M.H.), pp. 56–78. Springer, Berlin.
- Roddy, H.J.** (1915) Concretions in streams formed by the agency of blue green algae and related plants. *Proc. Am. Philos. Soc.*, **54**, 246–258.

- Romberg, F. and Barnes, V.E.** (1944) Correlation of gravity observations with the geology of the Smoothingiron granite mass, Llano County, Texas. *Geophysics*, **9**, 79–93.
- Ross, R.J.J.** (1976) Ordovician sedimentation in the western United States. In: *The Ordovician System: Proceedings of a Palaeontological Association Symposium, Birmingham, September 1974* (Ed. Bassett, M.G.), pp. 73–105. University of Wales Press, Cardiff.
- Rowland, S.M. and Shapiro, R.S.** (2002) Reef patterns and environmental influences in the Cambrian and earliest Ordovician. In: *Phanerozoic Reef Patterns* (Eds Kiessling, W., Flügel, E. and Golonka, J.), *SEPM Special Publication*, **72**, 95–128.
- Runnegar, B., Pojeta, J., Taylor, M.E. and Collins, D.** (1979) New species of the Cambrian and Ordovician chitons *Matthevia* and *Chelodes* from Wisconsin and Queensland: evidence for the early history of polyplacophoran mollusks. *J. Paleol.*, **53**, 1374–1394.
- Ruppel, S.C. and Kerans, C.** (1987) Paleozoic buildups and associated facies, Llano Uplift, Central Texas. *Austin Geol. Soc. Guidebook*, **10**, 33 pp.
- Sásáran, E., Bucur, L.L., Pleş, G. and Riding, R.** (2014) Late Jurassic *Epiphyton*-like cyanobacteria: indicators of long-term episodic variation in marine bioinduced microbial calcification? *Palaeogeogr. Palaeoclimatol. Palaeoecol.*, **401**, 122–131.
- Schopf, W.J.** (2000) Solution to Darwin's dilemma: discovery of the missing Precambrian record of life. *Proc. Natl. Acad. Sci.*, **97**, 6947–6953.
- Scoffin, T.P. and Stoddart, D.R.** (1978) The nature and significance of microatolls. *Philos. Transac. R. Soc. B: Biol. Sci.*, **284**, 99–122.
- Semikhatov, M.A. and Raaben, M.E.** (2000) Proterozoic stromatolite taxonomy and biostratigraphy. In: *Microbial Sediments* (Eds Riding, R.E. and Awramik, S.M.), pp. 295–306. Springer, Berlin, Heidelberg.
- Shapiro, R.S.** (1991) Morphological variations within a modern stromatolite field: Lee Stocking Island, Exuma Cays, Bahamas. In: *Proceedings of the Fifth Symposium on the Geology of the Bahamas* (Ed. Bain, R.J.), pp. 209–219, Bahamian Field Station, San Salvador.
- Shapiro, R.S.** (2000) A comment on the systematic confusion of thrombolites. *Palaios*, **15**, 166–169.
- Shapiro, R.S., Aalto, K.R. and Dill, R.F.** (1992) Zonation in the Bock Cay microbialite field, Bahamas. In: *Geological Society of America Cordilleran Section Meeting*, pp. 80.
- Shapiro, R.S., Aalto, K.R., Dill, R.F. and Kenny, R.** (1995) Stratigraphic setting of a subtidal stromatolite field, Iguana Cay, Exumas, Bahamas. In: *Terrestrial and Shallow Marine Geology of The Bahamas and Bermuda* (Eds Curran, H.A. and White, B.), *Geological Society of America Special Paper*, **300**, 139–155.
- Shapiro, R.S. and Awramik, S.M.** (2000) Microbialite morphostratigraphy as a tool for correlating Late Cambrian–Early Ordovician sequences. *J. Geol.*, **108**, 171–180.
- Shapiro, R.S. and Awramik, S.M.** (2006) *Favosamaceria cooperi* new group and form: a widely dispersed, time-restricted thrombolite. *J. Paleol.*, **80**, 411–422.
- Shapiro, R.S. and Wilmeth, D.T.** (2020) Part B, Volume 1, Chapter 8: Microbialites. *Treatise Online*, **134**, 1–24.
- Shinn, E.A.** (1968) Practical significance of birdseye structures in carbonate rocks. *J. Sediment. Petrol.*, **38**, 215–223.
- Sloss, L.L.** (1963) Sequences in the cratonic interior of North America. *Geol. Soc. Am. Bull.*, **74**, 93–114.
- Spencer, C.J., Prave, A.R., Cawood, P.A. and Roberts, N.M.W.** (2014) Detrital zircon geochronology of the Grenville/Llano foreland and basal Sauk sequence in West Texas, USA. *Geol. Soc. Am. Bull.*, **126**, 1117–1128.
- Straccia, F.G., Wilkinson, B.H. and Smith, G.R.** (1990) Miocene lacustrine algal reefs—southwestern Snake River Plain, Idaho. *Sediment. Geol.*, **67**, 7–23.
- Tang, D., Shi, X., Jiang, G., Pei, Y. and Zhang, W.** (2013) Environment controls on Mesoproterozoic thrombolite morphogenesis: a case study from the North China Platform. *J. Paleogeogr.*, **2**, 275–296.
- Tarhan, L.G., Droser, M.L., Planavsky, N.J. and Johnston, D.T.** (2015) Protracted development of bioturbation through the early Palaeozoic era. *Nat. Geosci.*, **8**, 865–869.
- Tarhan, L.G., Planavsky, N.J., Laumer, C.E., Stolz, J.F. and Reid, R.P.** (2013) Microbial mat controls on infaunal abundance and diversity in modern marine microbialites. *Geobiology*, **11**, 485–497.
- Taylor, J.F., Repetski, J.E., Loch, J.D. and Leslie, S.A.** (2012) Biostratigraphy and chronostratigraphy of the Cambrian–Ordovician Great American Carbonate Bank. In: *The Great American Carbonate Bank: The Geology and Economic Resources of the Cambrian–Ordovician Sauk Megasequence of Laurentia* (Eds Derby, J.R., Fritz, R.D., Longacre, S.A., Morgan, W.A. and Sternbach, C.A.), *AAPG Memoir*, **98**, 15–35.
- Tosti, F. and Riding, R.** (2014) Are Dendrolite and Thrombolite Macrofabrics Always Primary? Examples from the Cambrian of Shandong, China. In: *19th International Sedimentological Congress*, Geneva, 696.
- Turner, E.C.** (2021) Possible poriferan body fossils in early Neoproterozoic microbial reefs. *Nature*, **596**, 87–91.
- Turner, E.C., James, N.P. and Narbonne, G.M.** (2000) Taphonomic control on microstructure in early Neoproterozoic reefal stromatolites and thrombolites. *Palaios*, **15**, 87–111.
- Turner, E.C., Narbonne, G.M. and James, N.P.** (1993) Neoproterozoic reef microstructures from the little dal Group, northwestern Canada. *Geology*, **21**, 259–262.
- Turner, E.C., Narbonne, G.M. and James, N.P.** (2000) Framework composition of early Neoproterozoic calcimicrobial reefs and associated microbialites, Mackenzie Mountains, NWT, Canada. In: *Carbonate Sedimentation and Diagenesis in the Evolving Precambrian World* (Eds Grotzinger, J.P. and James, N.P.), *SEPM Special Publication*, **67**, 179–205.
- Vologdin, A.G.** (1932) *Archaeocyaths of Siberia, Part 2. Cambrian Fauna of Altai Limestones*, p. 106. State of Science and Technology in Geology, Leningrad. (in Russian).
- Vologdin, A.G.** (1939) Archaeocyaths and algae of the middle Cambrian of the southern Urals. *Prob. Paleontol.*, **5**, 210–245 (in Russian).
- Vologdin, A.G.** (1962) *The Oldest Algae of the USSR*, p. 657. Academy of Sciences of the USSR, Moscow (in Russian).
- Walker, N.** (1992) Middle Proterozoic geologic evolution of Llano Uplift, Texas: evidence from U–Pb zircon geochronometry. *Geol. Soc. Am. Bull.*, **104**, 494–504.
- Walter, M.R.** (1972) *Stromatolites and the Biostratigraphy of the Australian Precambrian and Cambrian. Special papers in Palaeontology*, Vol. **11**, p. 256. The Palaeontological Association, London.
- Walter, M.R. and Heys, G.R.** (1985) Links between the rise of the metazoa and the decline of stromatolites. *Precambrian Res.*, **29**, 149–174.

- Wilson, J.L.** (1950) An Upper Cambrian pleospongid (?). *J. Paleo.*, **24**, 591–593.
- Wood, R.** (1990) Reef-building sponges. *Am. Sci.*, **78**, 224–235.
- Wulff, J.** (2016) Sponge contributions to the geology and biology of reefs: past, present, and future. In: *Coral Reefs at the Crossroads* (Eds Hubbard, D.K., Rogers, C.S., Lipps, J.H. and Stanley, G.D.), *Coral Reefs of the World*, **6**, 103–126.
- Xiao, C.-T., Wei, G.-Q., Song, Z.-Y., Xiao, Y.-P., Yang, W., Dong, M., Huang, Y.-F. and Gao, D.** (2019) Petrography and origin of the Lower Ordovician microbial carbonates in the Songzi area of Hubei Province, middle Yangtze region, China. *Petrol. Sci.*, **16**, 956–971.
- Zhang, X.-Y., Li, Y., Wang, G. and Yang, H.-Q.** (2021) Different accretion and diagenetic patterns within the fabrics of the Permian–Triassic boundary microbialites on the Leye isolated carbonate platform, South China Block. *J. Palaeogeogr.*, **10**, 11.
- Zhuravlev, A.Y.** (1996) Reef ecosystem recovery after the Early Cambrian extinction. In: *Biotic Recovery from Mass*

Extinction Events (Ed. Hart, M.B.), *Geological Society of London Special Publications*, **102**, 79–96.

Zhuravlev, A.Y. (2001) Paleocology of Cambrian reef ecosystems. In: *The History and Sedimentology of Ancient Reef Systems* (Ed. Stanley, G.D.), pp. 121–157. Kluwer Academic/Plenum Publishers, New York.

Manuscript received 24 March 2022; revision accepted 30 September 2022

Supporting Information

Additional information may be found in the online version of this article:

Appendix S1 Stratigraphic setting and early research.